2022

Geological Survey Paper 10:

Mega-sheath fold core of the Southern Tyennan Domain - the De Witt-Propsting and South West Cape sheath-fold systems, Tasmania

Author: D. R. Gray and M. J. Vicary
Date: 14/09/2022
Email: info@mrt.tas.gov.au
Website: www.mrt.tas.gov.au

REPORT No.: GSP10

Cover description: View of the complexly deformed, quartzite ridgeline south of Davey River Gorge. The start of Davey River gorge is the cleft (bottom right of photo) with the Davey River meandering towards Payne Bay and Port Davey (photo top left). The photo is looking towards Davey Head (hill top left of photo) with the De Witt Range on the far-right horizon under cloud. The ridgeline consists of refolded macro-isoclinal folds of the Davey River fold system. This fold-system is interpreted as the nose of the east-closing De Witt-Propsting mega-sheath fold.

Tasmanian Government
Mineral Resources Tasmania
mrt

CONTENTS

Abstract

The Southern Tyennan Domain of southwest Tasmania is dominated structurally by two regional-scale sheath-folds that have 25 km length scales (sheath 'y' dimension). These folds control the stacking order and distribution of the litho-tectonic units that comprise the Southern Tyennan domain. They are the east-closing De Witt-Propsting mega-sheath fold and the west-closing South West Cape mega-sheath fold, that together form a complementary isoclinal fold pair within quartzite and platy quartzite/quartzite respectively. The mega-sheath folds are north-south trending and are bisected by a broadly west-south west trending mineral lineation Lm. The associated mesoscopic isoclinal folds have variable orientation and geometry but overall reflect position in the mega-sheath folds.

A younger, co-planar, Devonian north-south trending, open anticline folds the De Witt-Propsting mega-sheath fold into two outcrop parts that give two oblique sections in map view through the mega-fold. The map-view sections result from tilting on the limbs of the younger anticline. The western, west-dipping anticline limb exposes the largest section as the De Witt-Propsting sheath profile. The eastern, east-dipping limb provides the Davey River profile as the nose or eastern termination of the mega-sheath fold. Unfolding or removing the effects of the younger fold enables reconstruction of the mega-sheath fold to give a projected sheath length ('x' dimension) of ~20km, a maximum width ('y' dimension) of ~29km, an apical angle of 50° and an interlimb angle of 10°.

The De Witt-Propsting mega-sheath fold consists of three shells, an outer 1.5km thick shell of alternating intensely banded So/Sm and platy to mylonitic quartzite with Sm dominant, a middle shell ~3.5km in thickness constituting a folded domain of asymmetric isoclinal fold pairs in compositional layering So/Sm, and an inner shell or core of ~1.7km thickness consisting of refolded isoclinal folds and multiple fabrics reflecting successive overprinting in progressive deformation. The inner shell projects across the younger anticline as the complexly deformed Davey River nose to the mega-sheath fold. The outer and middle shells do not have uniform character and thickness around the mega-sheath and appear discontinuous southwards along the De Witt Range. They show transitions from banded So/Sm to zones of platy quartzite due to braided development of high-strain zones.The outer quartzite is isoclinally in-folded with, and therefore interdigitates with, the overlying low-grade pelite and high-grade schist to form an isoclinal fold-stack as carapace to the mega-fold.

The De Witt-Propsting mega-sheath fold has cats-eye-fold sheath geometry indicative of folding within a simple or general shear deformation. The ellipticity ratio (R') of the outer ellipse (Ryz) to the inner ellipse (Ry'z') is 0.81 (i.e. R'<1) where Ryz=2.57 and Ry'z'=2.97 such that Ry'z'>Ryz. The shell thickness ratio (Tyz=Ty/Tz) varies from 2 to 2.6.

The Davey River sheath-nose consists of an elongated, S-shaped, sinuous ridgeline in quartzite that defines a closed loop form with pinched, lateral fold-nose terminations typical of a sheath-like 'tectonic fish'. It has an unfolded length ('y' dimension) of ~12.5 km and a maximum map width of 1.7km with a thickness ('z' dimension) of ~0.7km. The macro-geometry consists of two major, north-south trending, inclined plunging F2 folds that coaxially refold isoclinal F1 macro-folds with sheath-like form that are bounded by zones of platy to mylonitic quartzite. Curved hingelines and intersection lineations at the outcrop scale reflect sheath-fold initiation at the meso-scale. An X/Y strain of 3.2:1 within the foliation Sm is recorded by ovoid skeletal opaque-meshworks after framboidal pyrite?

The South West Cape mega-sheath fold is en echelon with the De Witt-Propsting mega-sheath fold as part of a regional-scale oppositely closing fold-pair. It has a minimum length ('y' sheath dimension) of 25km and a half-width ('z' sheath dimension) of 8km. By closing out a possible oval or eye-shaped form of the inner shell it is likely that half of the mega-fold is offshore. Map geometry is typical of a regional-scale mushroom-style Type 2 fold interference pattern where F1 macro-isoclinal folds are coaxially refolded by upright, north-south trending, isoclinal F2 macro-folds. These are the same geometrical relationships seen in the inner shell of the De-Witt-Propsting fold and the Davey River sheath nose. Component folds in the South West Cape mega-fold have inclined plunging to reclined geometry with west-plunge in contrast to the northeast plunge in the Davey sheath nose, a plunge-change related to the younger Devonian refolding.

The lower limb of the South West Cape mega-sheath fold transitions into the south-closing and west-plunging Red Point macro-fold within high-grade schist (Red Point Metamorphic Complex) and low-grade pelite. This macro-fold structurally overlies a recumbent isoclinal fold pair relationship holds for the entire region east of Bathurst Harbour to the Arthur Range, including the Ray Range, Mt Norold and the Spiro Range with an areal extent of 450-500 square kilometres.

The complex refolding and overprinting fabrics at the meso-scale within the inner shell and nose of the De Witt-Propsting mega-fold, as well as within the body of the South West Cape mega-fold require decoupling of zones or shells within these developing mega-sheath folds. The Southwest Tyennan domain mega-sheath folds suggest that this internal decoupling and translation relative to the outer shells results in macro-isoclinal refolding and complex fabric development as part of progressive regional-scale sheath-fold development.

The development of these mega-sheath folds within the Southern Tyennan domain, in contrast to other parts of the nucleus, potentially relates to an anomalous quartz sand wedge in this part of the margin. Both mega-sheath folds are developed within quartzite and platy quartzite. A similar stratigraphic mound or wedge was postulated for the initiation of the Seidlwinkl sheath fold nappe in the Austrian Alps (Gross et al., 2020).

Tasmanian Government

Mineral Resources Tasmania

Department of State Growth
www.mrt.tas.gov.au

Mega-sheath fold core of the Southern Tyennan Domain - the De Witt-Propsting and South West Cape sheath-fold systems, Tasmania

David R. Gray[1] and Michael J. Vicary[2]
[1] *Consultant Structural Geologist to Mineral Resources Tasmania*
[2] *Geological Survey Branch - Mineral Resources Tasmania*

ARTICLE INFO

Published: xx September 2022
Publisher: Mineral Resources Tasmania
Report No.: GSP10

KEYWORDS

Structural Geology
Mega-sheath folds
Southern Tyennan

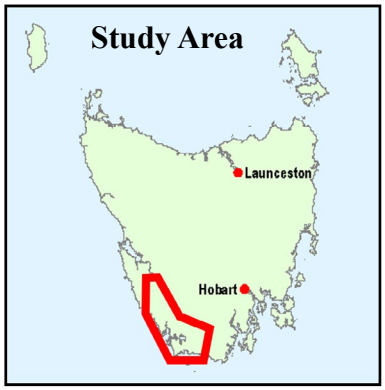

1.0 INTRODUCTION

The Southern Tyennan domain represents the southernmost extent of the Tyennan nucleus (Figure 1), the geological "core" of Tasmania. It is a structurally complex, litho-tectonic sequence of high-grade garnet schists with intercalated low-grade phyllite and quartzite. These units represent shear zone-bounded slabs of Neoproterozoic age former continental margin deposits that were subducted to depths of 20 to 60km beneath an advancing ophioloite sheet during a Cambrian obduction event along the margin of Gondwana (see Berry and Crawford, 1988; Berry, 2014, Figure 4.10). The Tyennan Structural Geology Series of publications aims to investigate the structures that develop in these rocks during the subduction-obduction process.

In map projection the Southern Tyennan domain has a ~100 km length and ~50 km width representing an oblique crustal view of complex structures within the subducted and obducted Neoproterozoic continental margin sequence (Figure 2). The major structural elements of this crustal-scale architecture (Figures 2 and 3) include:

1. Nye Bay-Charles Range Fold-nappe: a south-closing, west-plunging macro-isoclinal fold with reclined geometry.

2. High-grade isoclinal macro-fold stack: in-folded sequence of high-grade schist, low-grade pelite and low-grade quartzite.

3. De Witt-Propsting mega-sheath fold: a closed macro-fold outcrop pattern within the low-grade quartzite sequence.

4. Davey River sheath-fold nose: the east-closing nose of the De Witt-Propsting mega-sheath fold exposed on the eastern limb of a Devonian anticline.

5. South West Cape mega-sheath fold, a partially preserved, west-closing mega-sheath fold.

6. Eastern isoclinal fold domain, including the Arthur Range.

7. Red Point macro-isocline: an interpreted south-closing, west-plunging macro-fold cored by low-grade pelite enveloped by high-grade schist.

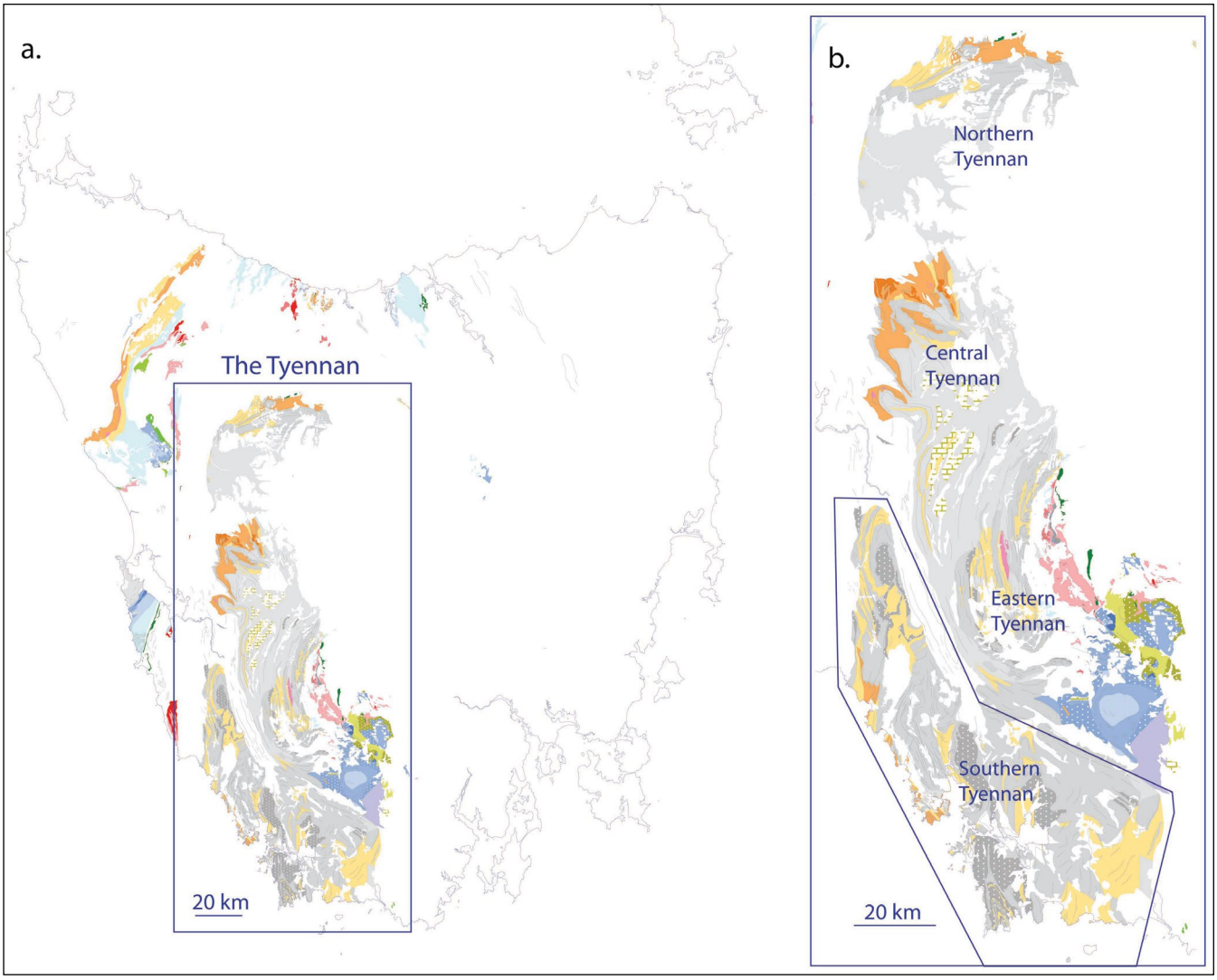

Figure 1. The Tyennan Proterozoic region of Tasmania shown in a). Map base is Mineral Resources Tasmania 1:25000 and 1:250000 digital geological atlas. b) Enlarged map with the location of the Southern Tyennan region. The divisions within the Tyennan are after Berry (2014). The approximate Southern Tyennan map sheet polygon boundaries are 5345400mN (northern boundary), 5165000mN (southern boundary), 467000mE (eastern boundary) and 386000mE (western boundary).

This paper defines and investigates the mega-sheath-fold elements 3, 4 and 5 (Figure 2) that comprise the core of the Southern Tyennan domain, and control the overall stacking and distribution of the low-grade quartzite, platy quartzite, and phyllite, and high-grade schist litho-tectonic units.

The Nye Bay-Charles Range fold-nappe (element 1) is the structurally highest part of the crustal stack with transition along the lower limb into the high-grade isoclinal fold stack (element 2). Both elements involve the high-grade schist sequence of the Southwest high-grade coastal belt discussed in Mineral Resources Tasmania Geological Survey Paper 9 (Gray et al., 2022). The fold-nappe and isoclinal fold-stack form a structural carapace to the mega-sheath folds within the quartzite sequence (Figure 3). A reversal in stacking order occurs from the fold nappe into the isoclinal fold stack (Figure 3). This is across an inferred high-strain zone at the Mulcahy River mouth (Figure 47 in Gray et al., 2022).

The dominant De Witt-Propsting and South West Cape mega-sheath folds appear en echelon to each other (Figures 2 and 3) and form a complementary sheath-fold pair (Figure 4). Critical to the sheath-fold interpretation are 1) the ovoid to eye-shaped outcrop patterns seen in map view as oblique sections due to tilting of these structures by the younger Devonian folding, and 2) the approximately orthogonal relationship between the mineral-stretching lineation Lm and the long dimensions of the oval outcrop patterns (Figure 4a). In the Southern Tyennan domain the lineation Lm is broadly west-southwest trending at high angle (~90°) to the long dimensions ('y' dimension of the inferred sheath folds) that are broadly north-south trending to west-northwest-trending (Figure 4a). Noses of the sheath folds will be elongated sub-parallel to the L stretch (thick blue arrows, Figure 4a). All of these relationships are the geometric requirements of sheath-folds (Figures 4b and c) as part of their progressive shear-related evolution (see Section 2).

Each mega-sheath fold will be investigated and their internal structural relationships defined in Sections 3, 4 and 5. A background to the definition of, the analysis of and understanding the significance of sheath folds is presented in Section 2.

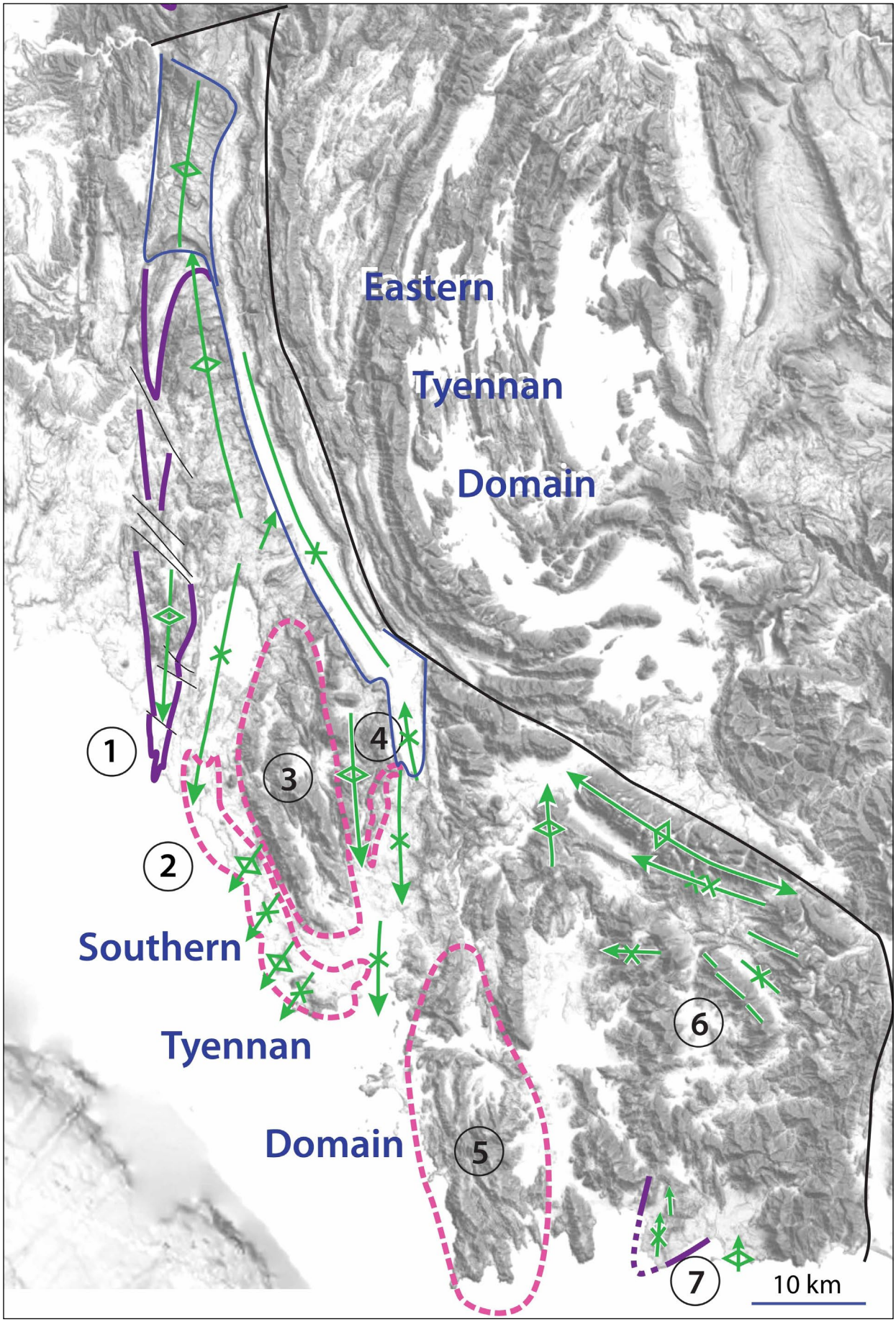

Figure 2. Major structural elements of the Southern Tyennan domain with ListMap greyscale digital elevation model as base map. Purple lines are So/Sm formlines that outline the Nye Bay-Charles Range fold-nappe (element 1) and the Red Point macro-fold (element 7). Pink dashed lines show the approximate extent and positions of the isoclinal fold stack (element 2) and the De Witt-Propsting mega-sheath fold (element 3), the Davey River sheath nose (element 4), the South West Cape mega-sheath (element 5). Element 6 represents the remaining area to the east as the isoclinal macro-fold domain. Element 7 is the Red Point isoclinal macro-fold, part of the isoclinal fold domain. The axial surface traces of younger, Late Cambrian to Devonian folds that fold the older Cambrian macro-structures are shown by the green line traces. The black is the faulted boundary between the Southern and Eastern Tyennan domains.

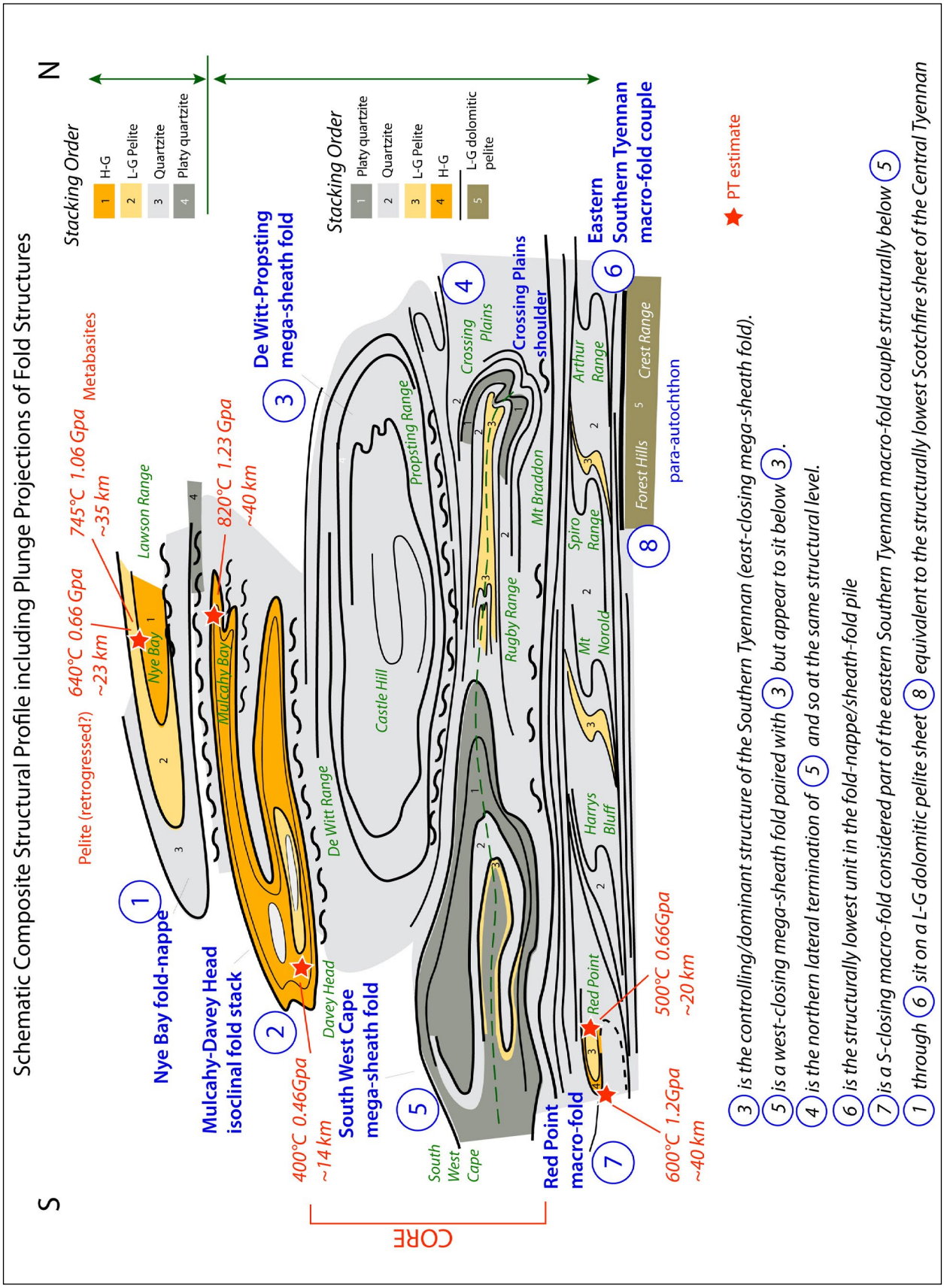

Figure 3. Schematic structural profile of the Southern Tyennan domain showing the major structural elements, the structural stacking and the mega-sheath fold core of the Southern Tyennan crustal stack. This is an approximate down-plunge view of the Southern Tyennan domain map pattern (i.e. as an oblique tilted view looking to the west).

P, T determinations and an estimate of the maximum depth of subduction from the high-grade schists (orange unit) are shown in red text and their approximate positions in the structural stack shown by the red stars. The litho-tectonic units and stacking order are shown for the respective upper and lower limbs of the De Witt-Propsting mega-sheath fold. Unit numbers 1 to 4 are from top of stack to bottom of the stack with an order reversal between the upper and lower limbs. Orange: high-grade (H-G) schist; low-grade (L-G) pelite; light grey: low-grade (L-G) quartzite; dark grey: platy/schistose quartzite; khaki: low-grade dolomitic pelite as element 8 in the far eastern part of the Southern Tyennan domain incorporating the Spiro and Arthur Ranges.

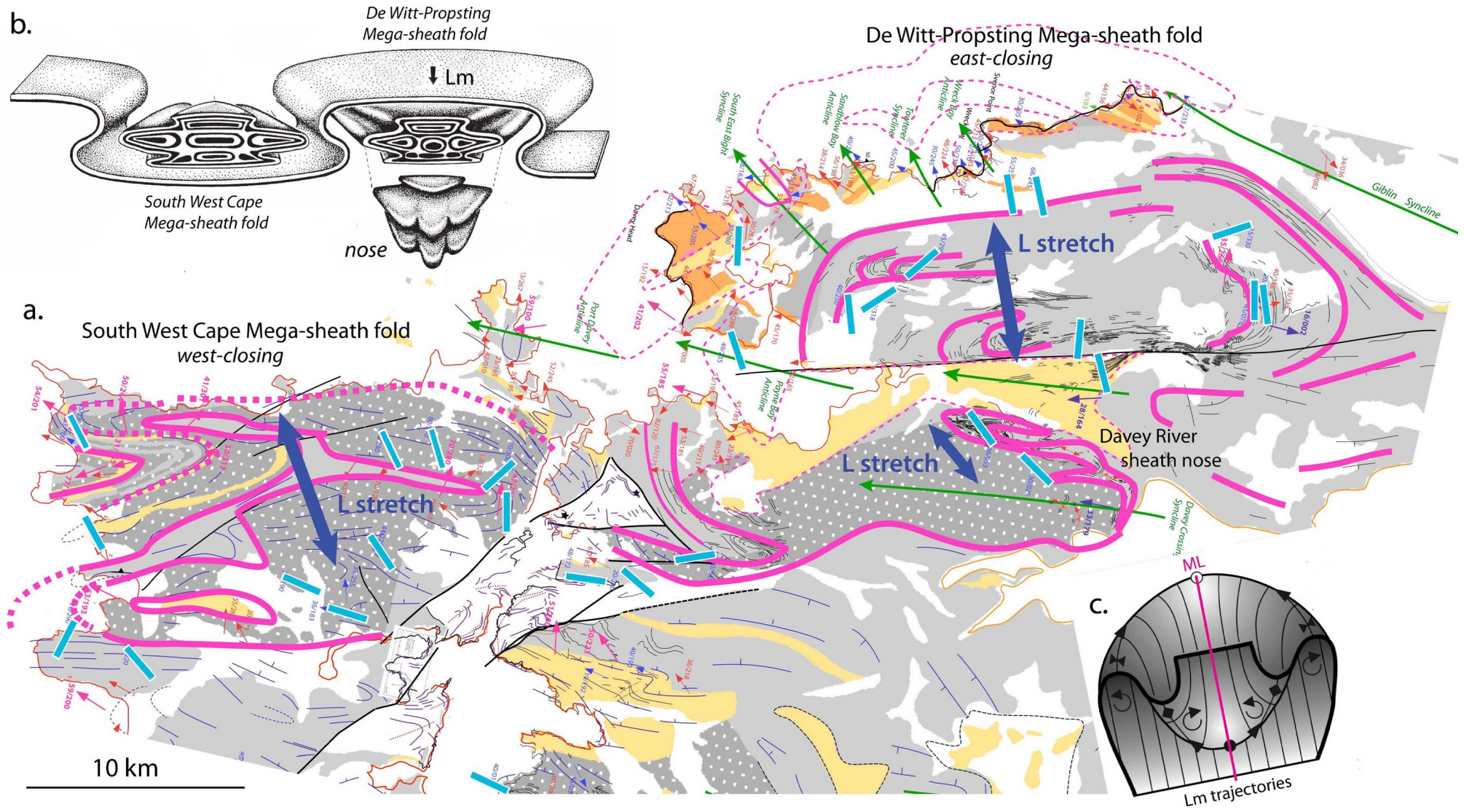

Figure 4. Mega-sheath fold relationships in the central part of the Southern Tyennan domain. a) Simplified structure map of the area showing formlines in So/Sm (pink line traces) defining the outcrop geometry of the mega-folds and structural relationships of the lineation Lm (short light blue lines) to the mega-sheath folds. Green line traces are the axial surface traces of the younger, open Devonian folds that refold the early Cambrian mega-structures. b) Schematic 3D diagram of an oppositely-closing sheath-fold pair with sections showing the inferred internal structural geometry after Alsop and Holdsworth (2004, Figure 2). c) Diagrammatic top-view of oppositely-closing (antithetic) sheath-fold pair showing hingeline curvature, fold-hingeline vergence (clockwise or anti-clockwise arrows), the sheath-fold median line (ML) and the lineation Lm pattern (after Alsop and Carreras, 2007, Figure 10d).

2.0 BACKGROUND

2.1 Sheath Folds and Analysis

Sheath folds reflect progressive and intense shear-related deformation (Alsop & Holdsworth, 2004). They are considered to form by sequential rotation of fold hinges that initiate at high angles to the shear direction during progressive non-coaxial deformation (Cobbold & Quinquis, 1980).

An essential synopsis/summary of sheath fold types, their analysis and implications are provided here as background to the geometry of the macro-folds in the Southern Tyennan domain. Detailed reference to definitions, descriptions and analysis of sheath folds are provided in Alsop & Holdsworth (1999, 2004, 2006 and 2012). The following summary is based on figures and discussions within these papers.

It is important to note that the form and shape of sheath folds (Figure 5) change with increasing shear strain. Developing sheath-folds show increasing hinge curvilinearity along with axial surface rotation towards the shear plane approximated by the foliation Sm (Figure 6).

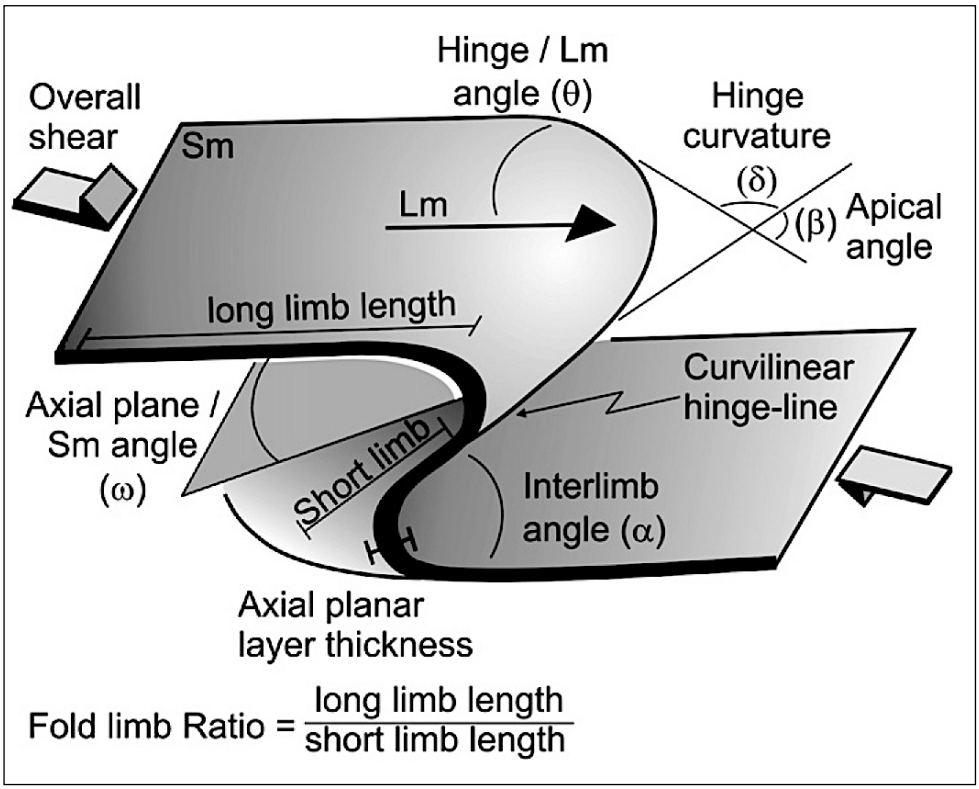

Figure 5 (left). 3D schematic diagram illustrating an asymmetric fold pair developing sheath-form in general shear and showing relationship to Lm. Measurable sheath-fold geometrical parameters include interlimb angle (α), apical angle (ß), hinge curvature (δ) and fold limb ratio. Diagram from Alsop and Carreras (2007, Figure 2).

Figure 6 (below). Schematic evolution of sheath-fold shape and isoclinal sheath form (portrayed diagram left to right) with 1) increasing curvilinearity of fold hinges and 2) accompanying clockwise rotation of fold axial planes (grey shaded planes) towards the generalised Sm plane at the base or lower limb. This plane is highlighted by the transport-parallel mineral lineation Lm. Note the pinched nature of the return hinge. Diagram from Alsop and Carreras (2007, Figure 11).

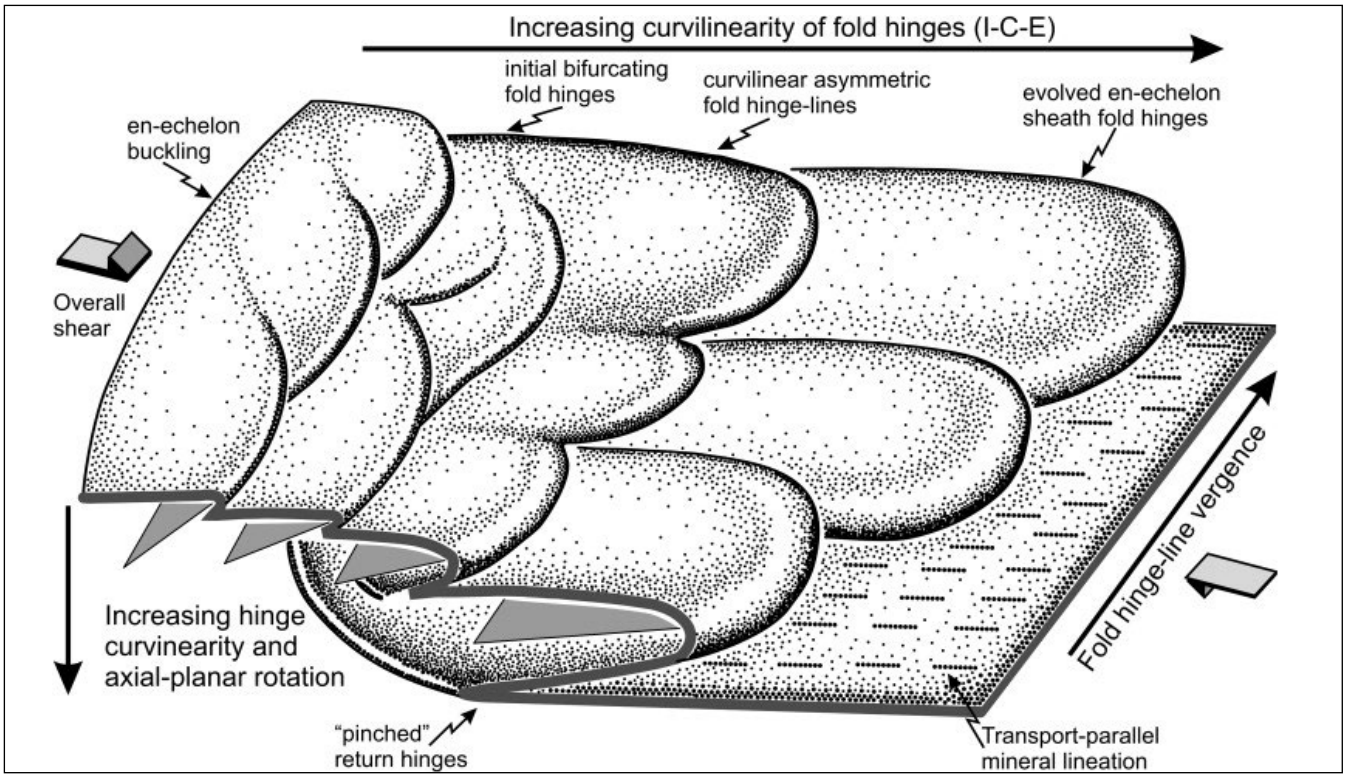

A hypothetical geometry of adjacent, symmetrical, oppositely-closing sheath-fold pairs existing at the same structural level (diagram from Alsop and Holdsworth, 1999, Figure 1) provides methodology to define the existence and form of sheath folds in deformed ancient terrains. The schematic 3D diagram (Figure 7) shows the closeout geometry of doubly-vergent fold pairs that define the sheath folds, a possible macro-sheath fold nose geometry and the patterns of internal nested folds within the sheaths. Relationships of mesoscopic folds to the cone axis of the sheath fold and/or hingeline culmination include 1) fold hingeline vergence towards the hingeline culmination or nose closeout, and 2) different fold axis (FA) to lineation Lm rotations separated by the hingeline culmination. These relationships have been used to define and reconstruct the geometries of interpreted macro-folds for other parts of the Tyennan nucleus (Gray and Vicary, 2021 2022a and Gray et al., 2022).

Typically cross-sections of sheath folds display nested elliptical closures defining y-z sections where z is the minimum elongation, y is the intermediate elongation and x is the maximum elongation (Figure 1, Alsop & Holdsworth, 2006) (Figure 8a). The x, y and z geometric axes of sheath folds are generally considered to lie sub-parallel with or equate to the X, Y and Z axes of the finite strain ellipsoid. In most cases the x-axis or long direction of sheath folds is broadly parallel to the mineral elongation lineation Lm.

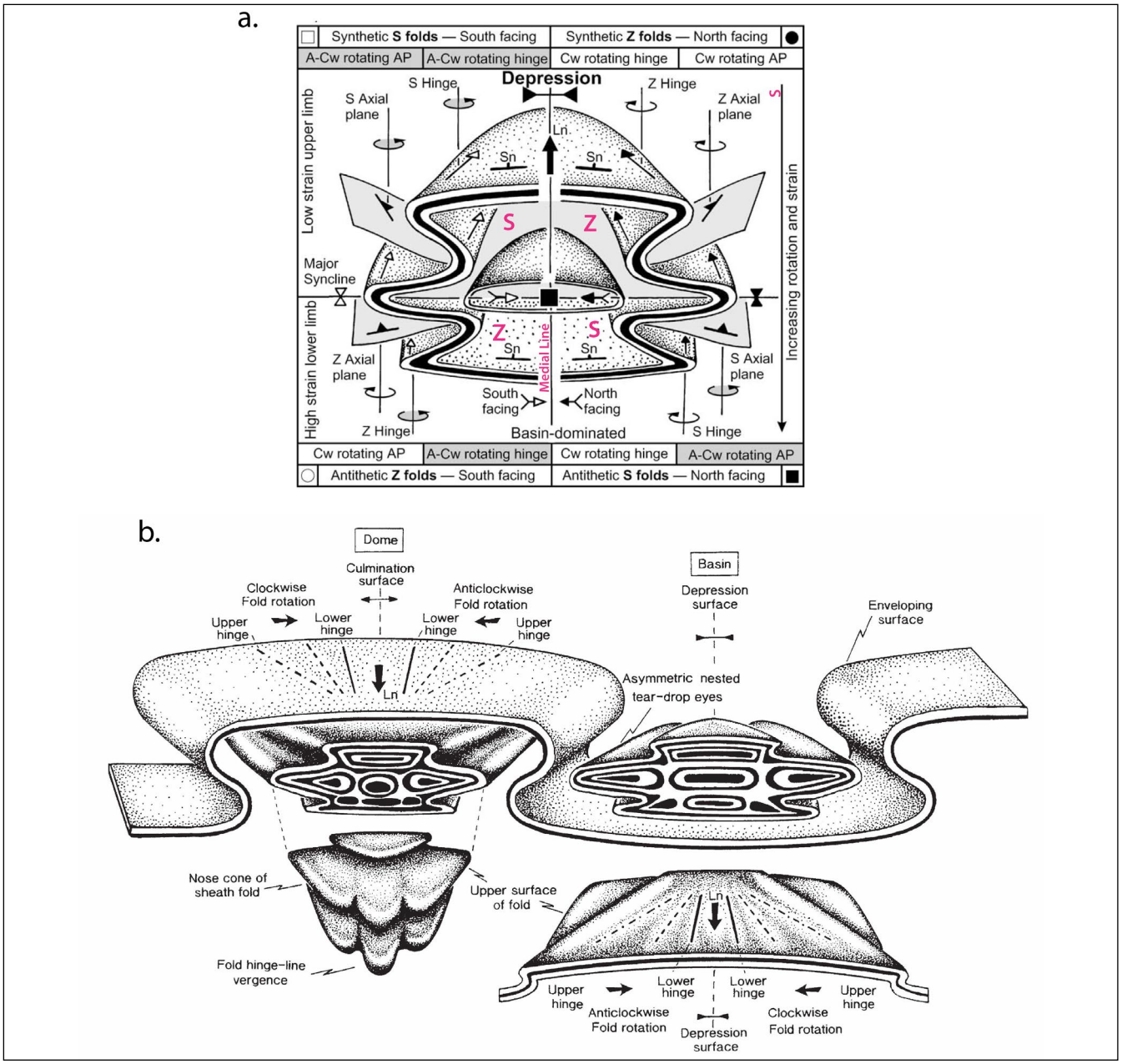

Figure 7. Schematic 3D sketches of sheath-fold geometry and fold-lineation relationships. a) Sheath-fold nose showing geometrical relationships between mesoscopic S and Z fold-vergence/symmetry, as well as fold-hingeline vergence as counter-clockwise and clockwise rotation of the FA to the lineation Lm (Figure 13b from Alsop and Holdsworth, 2004). Note the fold vergence quadrants are designated by the intersecting vertical medial plane and the horizontal xy symmetry plane of the sheath-fold nose. b) Geometry of symmetrical, oppositely-closing sheath-fold pairs (Figure 2. from Alsop and Holdsworth, 2004). Cut-through sections show nested, asymmetric tear-drop eye folds within their cores. A sheath nose cone is shown for the left side sheath fold. General trends of minor folds developed on the upper to lower limbs of the sheath folds are projected as dashed lines on the enveloping surface with the extension lineation Lm. Minor folds show clockwise and counter-clockwise rotations to Ln on opposing flanks of the sheath noses.

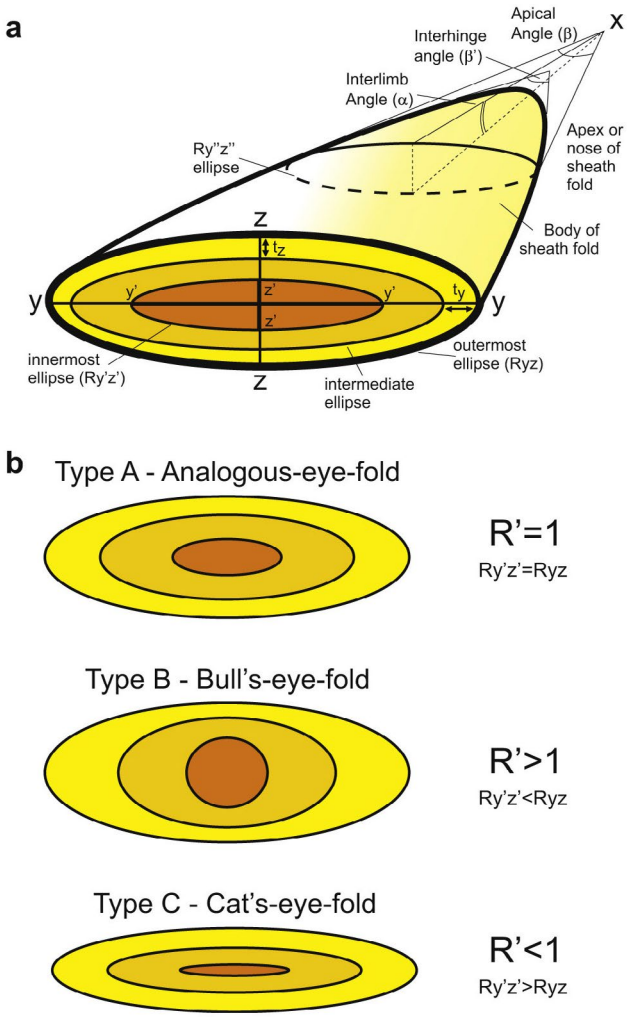

Figure 8. Sheath fold parameters and types from Alsop and Holdsworth (2012, Figure.1). a) Schematic 3D sketch of a sheath fold illustrating the x, y and z-axes as the sheath long, intermediate and short axes respectively. The apical angle β of the curvilinear hinge and the fold interlimb angle α also define the geometry of the sheath fold. b) Schematic sheath y-z profile diagrams illustrating the variation in elliptical ratios (R') with Type A, analogous-eye-fold (R'=1), Type B, bulls-eye-fold (R'>1) and Type C, cats-eye-fold (R'<1).

Parameters used to define sheath folds (Figure 2, Alsop & Holdsworth, 2006) include 1) ellipticity variation (R') and 2) layer thickness variations (Tyz) in nested elliptical closures in y-z cross-sections of sheath-folds (see Figure 8a). Parameters include:

Ryz: ellipticity of the outermost ellipse

Ry'z': ellipticity of the innermost ellipse

R'= Ryz/Ry'z'

ty :thickness of an individual layer measured in the y direction contained within the axial (x-y) surface of the sheath fold

tz :thickness of an individual layer measured in the z direction at 90° to the axial surface plane

Tyz: ty/tz

Ellipse aspect ratios measured from the outermost ellipse (Ryz) to the innermost ellipse (Ry'z') of individual sheaths provide a measure of the nested-eye shape (Alsop & Holdsworth, 2006). Three major sheath geometries have been defined (Figure 8b):

1. *Analogous-eye-fold (R'=1 and Ry'z'=Ryz,*
2. *Bulls-Eye-fold where R'>1 and Ry'z'<Ryz, and*
3. *Cats-eye-fold where R'<1 and Ry'z'>Ryz*

Based on the ratio of the outer and inner ellipse there is an increase in ellipticity (R'>1) for a cats-eye sheath fold to a decrease in ellipticity (R'<1) for a bulls-eye fold.

The layer thickness ratio (Tyz) for individual layers can be determined as a ratio of Ty where thickness is measured along the y-axis direction and Tz as thickness measured along the z axis direction (Figure 8a).

Both ellipticity (Ryz) and thickness variations (Tyz) increase with increasing deformation in both simple- and general-shear dominated deformation and the actual geometry may be used to define the nature of the bulk rock strain (Alsop and Holdsworth, 2006, 2012). In summary, sheath folds formed in simple or general shear have cats-eye geometry (R'<1), whereas sheath folds formed in constriction with shortening along both y and z-axes have bull-eye geometries (R'>1) (Figure 9). Analogous-eye-folds reflect plane strain without change in the y dimension.

Layering rheology and different shear strain rates can influence sheath fold development (Reber et al., 2012) and the final structural relationships within the different shells (Figure 10). Relative rates of flow within individual layers dictate the sheath geometry and whether a sheath fold has passive (Figure 10a) versus active form (Figures 10b and c) (Alsop and Holdsworth, 2012). In active sheath fold development the inner shell and nose of the sheath can translate relative to the outer shell of the sheath (Figures 10b and 10c).

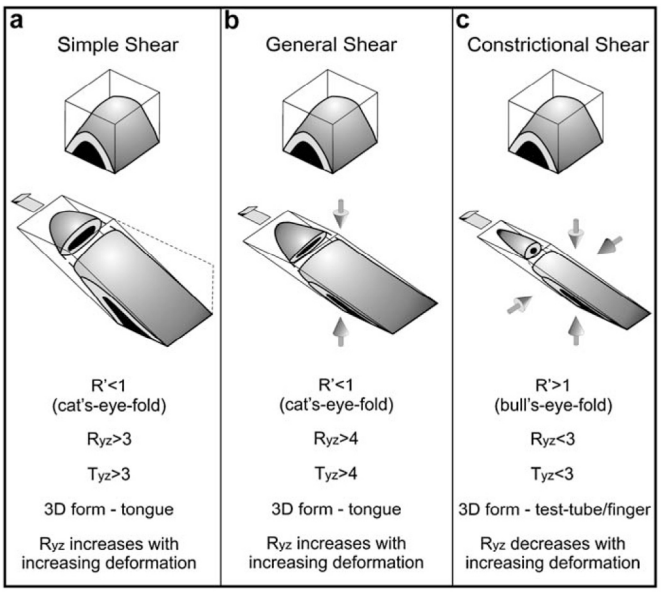

Figure 9. Summary diagram illustrating geometry variations for sheath folds generated in a) simple shear, b) general shear and c) constrictional shear. The geometry of the initial fold is shown (above) in each case. Typical parameters R', Ryz and Tyz are given for the folds generated. Diagram is from Alsop and Holdsworth (2006, Figure 9).

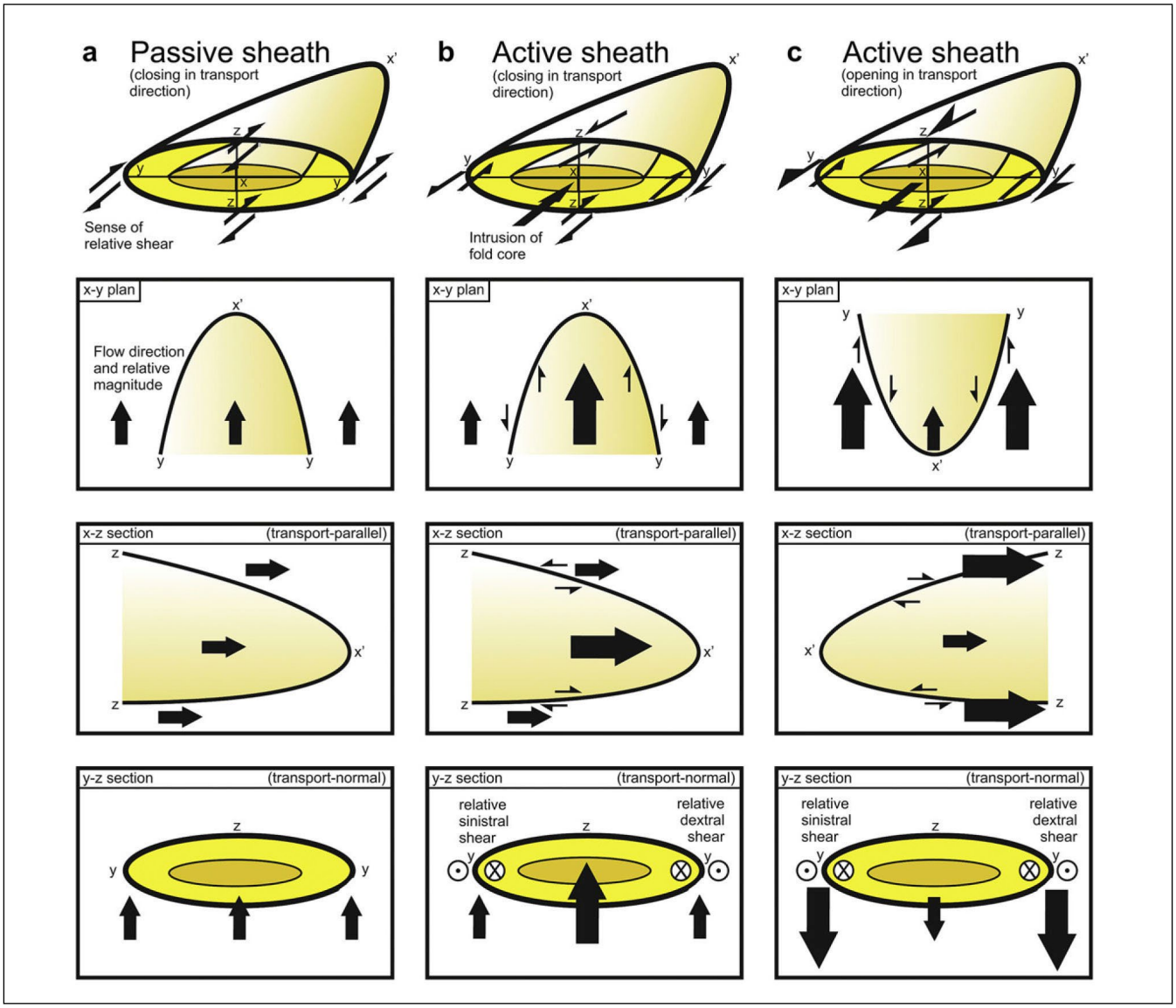

Figure 10. Deformation partitioning within developing sheath folds including separation and detachment of the inner shell relative to the outer shell such the inner and outer shells can deform independently and at different rates of shear strain. a) Passive sheath where all shells deform together and at the same shear strain rate. b) Active sheath fold development where the inner shell deforms at higher shear strain rate relative to the outer shell. c) Active sheath fold development where the outer shell deforms at higher shear strain rate relative to the inner shell. Diagram is from Alsop and Holdsworth (2012, Figure 15).

2.2 Structural Terminology

The following **structural terminology** is used in this paper:

So/Sm	metamorphic foliation parallel to bedding (commonly a transposition layering)
So/Sm env	enveloping surface to folded So/Sm
Sm	dominant or main metamorphic foliation
Sb	shear band (S-C' structure)
AST	fold axial surface trace
AS/Sm	dominant foliation sub-parallel to fold axial surfaces
Sm/Sb	dominant foliation developing from Sb, shear band foliation
Scc:	crenulation cleavage
Scl	Devonian overprinting low-grade cleavage
S1	early slaty cleavage
Lm	dominant lineation
Lstretch	stretching lineation
Lelongation	mineral elongation lineation
TD	transport direction
Lint	intersection lineation
Lrod	rodding lineation developed from deforming Lint
FA	fold axis
F1, F2, F3	local age of fold axes (oldest to youngest)
Lm^FA	angle between Lm and FA
Sm^Sb	angle between Sm and Sb

3.0 GEOMETRY OF THE DE WITT-PROPSTING MEGA-SHEATH FOLD

3.1 Map Relationships and Structural Definition

The De Witt-Propsting Mega-sheath Fold is a large-scale, doubly plunging, mega-sheath fold with elliptical form within the low-grade quartzite sequence of the De Witt-Propsting Ranges (Figures 11 and 12). It is expressed topographically in the quartzite ridges and low hills and has a 29 km length and a map half-width of 6.9 km. The southern flank of the mega-fold is defined by the De Witt Range, whereas the northern flank is defined by the Propsting Range (Figure 11). A north-south-trending, sub-vertical brittle fault cuts the structure into two, with down-drop of the western fault-block. Closed at the north and south ends the mega-fold has a doubly plunging antiformal core in the form of a macro-sheath fold "pod" (Figures 12 and 13).

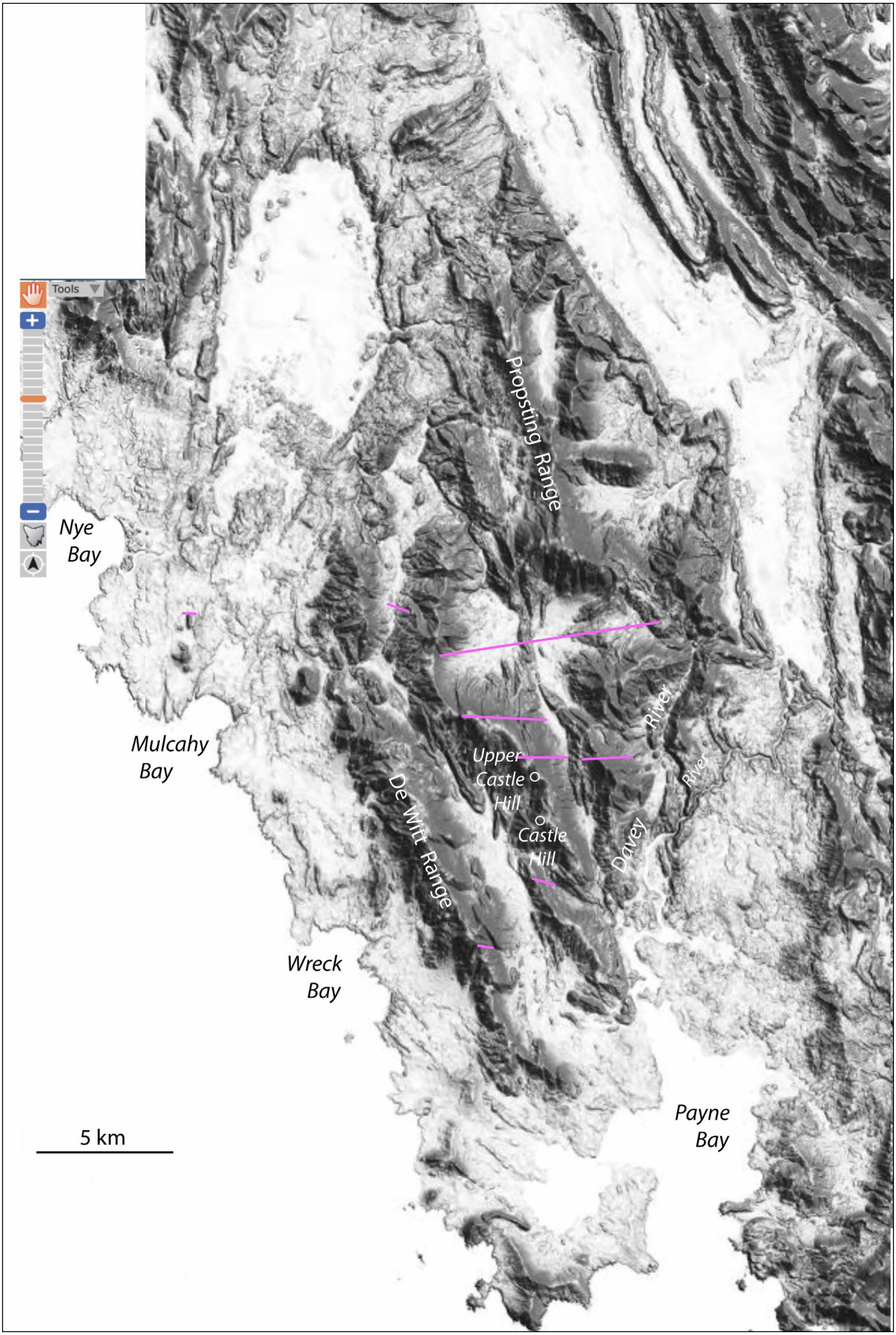

Figure 11. ListMap Digital Elevation Model (DEM) showing topographic expression of the Propsting-De Witt mega-fold structure. It has a closed form and apparent eye-structure within the quartzite ridgelines. The Propsting and De Witt Ranges define the northern and southwestern flanks of the structure.

Positions of the photo profiles are shown by the pink lines. Geographic locations/references are in white text.

Figure 12. Compositional layering So/Sm and foliation Sm formline trace-map for the low-grade quartzite sequence of the De Witt and Propsting Ranges, and intervening hills. The closed, doubly-plunging form gives an elliptical outcrop pattern, transected by a sub-vertical fault that extends from Payne Bay to the Propsting Range. Google satellite image as base. Rectangles show the positions of Figures 29a, 35 and 50 respectively.

The De Witt-Propsting mega-sheath fold has also been refolded, tightened and modified by younger, Devonian, open, north-south-folding approximately coplanar with the sheath long dimension ('y' axis). The north- and south- plunges of the younger superposed folds indicate a pre-existing structural form prior to the younger Devonian age folding. This implies the existence of the mega-sheath fold prior to the Devonian folding.

The De Witt-Propsting mega-sheath fold has a moderately inclined, elliptical form with early, mesoscopic, isoclinal fold plunges at 30°-45° (Figure 13). The western flank has limb dips of 50°-70° to the west and the northern and southern closures dips of 20°-30° to the north and south respectively (Figure 13).

The formline interpretation from Google earth imagery and ListMap air photos (Figure 14) depicts:

1. A modified sheath-geometry with distinct geometrical differences between the northern and southern doubly-vergent fold pair terminations of the elliptical form (Figure 9). In the north the doubly-vergent fold pair is truncated by the Payne Bay-Giblin Valley Fault with an interpreted tighter fold-pinchout in the lower south-closing fold. In the south, the south-closing upper part of the mega-sheath has broad curvature across Port Davey with an extremely tight pinchout in the structurally lower north-closing fold (compare with the "pinched return hinge' of the lower limb Figure 14).
2. A modified sheath-geometry incorporating a wedge of structurally lower, low-grade pelite exposed east of the Payne Bay-Giblin Valley Fault. This occurs within the core of a south-plunging younger Devonian north-south-trending, south-plunging anticline. Inferred scissors movement on the Payne Bay-Giblin Valley Fault led to a pivoting, western-side down movement with the hinge-pivot point located north of Upper Castle Hill.
3. Superposition of the younger north-south folding on the existing sheath structure has created complex fold interference at the northern elliptical close-out. A younger anticline-syncline pair tightens the early formed macro-isocline, north-closing and south-closing pinchouts (Figure 14).
4. The northern south-closing pinchout east of the Payne Bay-Giblin Valley Fault transitions southwards into the south-plunging anticline that exposes the low-grade pelite sequence (Figure 14).
5. The Southwest high-grade coastal sequence (Figure 14) forms a carapace to the quartzite on the western or upper limb of the De Witt-Propsting mega-fold. This high-grade schist sequence interdigitates with and is isoclinally in-folded with the quartzite (Gray et al., 2022, Figure 78). The axial surface traces of the interpreted macro-isoclines are shown as pinked dashed lines folded by a series of southwest plunging open folds (Figure 14). These are folded and swing to an east-west orientation across Port Davey as part of the south-closing hinge of the mega-sheath.
6. The complementary north-closing pinchout appears to have an asymmetric fold-pair augen embedded within the folded Sm in the nose of the pinchout (Figure 14). This antiformal closure represents the inter-digitating, northern projection of the South West Cape mega-sheath fold system.
7. The superposition of the younger open folding (green axial surface traces in Figure 14) and the presence of and inferred movement on the Payne Bay-Giblin Valley Fault (heavy black line trace in Figure 14) give an overall skewed asymmetry and distortion to the mega-sheath profile, unlike the schematic symmetrical sheath folds in Figure 7.

3.1.1 Mineral Lineation Lm and Fold Axis Relationships

Limited early, mesoscopic isocline fold axis and lineation Lm data (Figure 13) show that:

1. The stretching lineation Lm has a predominant west-south-west trend with west plunges approximately orthogonal to the long axis ('y' dimension) of the outcrop-defining elliptical pattern (Figures 4, 13 and 14). The overall Lm trend therefore bisects the elliptical form (eye-closure) of the mega-sheath fold.
2. Some lineation Lm data through the mega-fold shows a different northwest trend (Figure 14). This may reflect folding of the lineation (cf. Alsop & Carreras, 2007) around second- and third-order isoclinal folds within the mega-sheath, where Lm on the lower or short limbs had a northwest trend.
3. Mesocopic F1/F2 isocline fold axes on the south side of the sheath-fold eye show a clockwise obliquity to the lineation, whereas very limited data on the north side suggest counterclockwise obliquity to Lm (Figure 16).
4. The elliptical form of the sheath profile is bounded by double-vergence geometries where the outermost Sm closes around the north and south noses (Figure 15). This reflects the sheath initiation from an asymmetric fold-pair (Alsop & Holdsworth, 2012).

All of the above are characteristics or features typical of all sheath folds (Alsop & Holdsworth, 1999, 2004 and 2006).

The overall fold asymmetry and trends are consistent with an east-closing sheath-form.

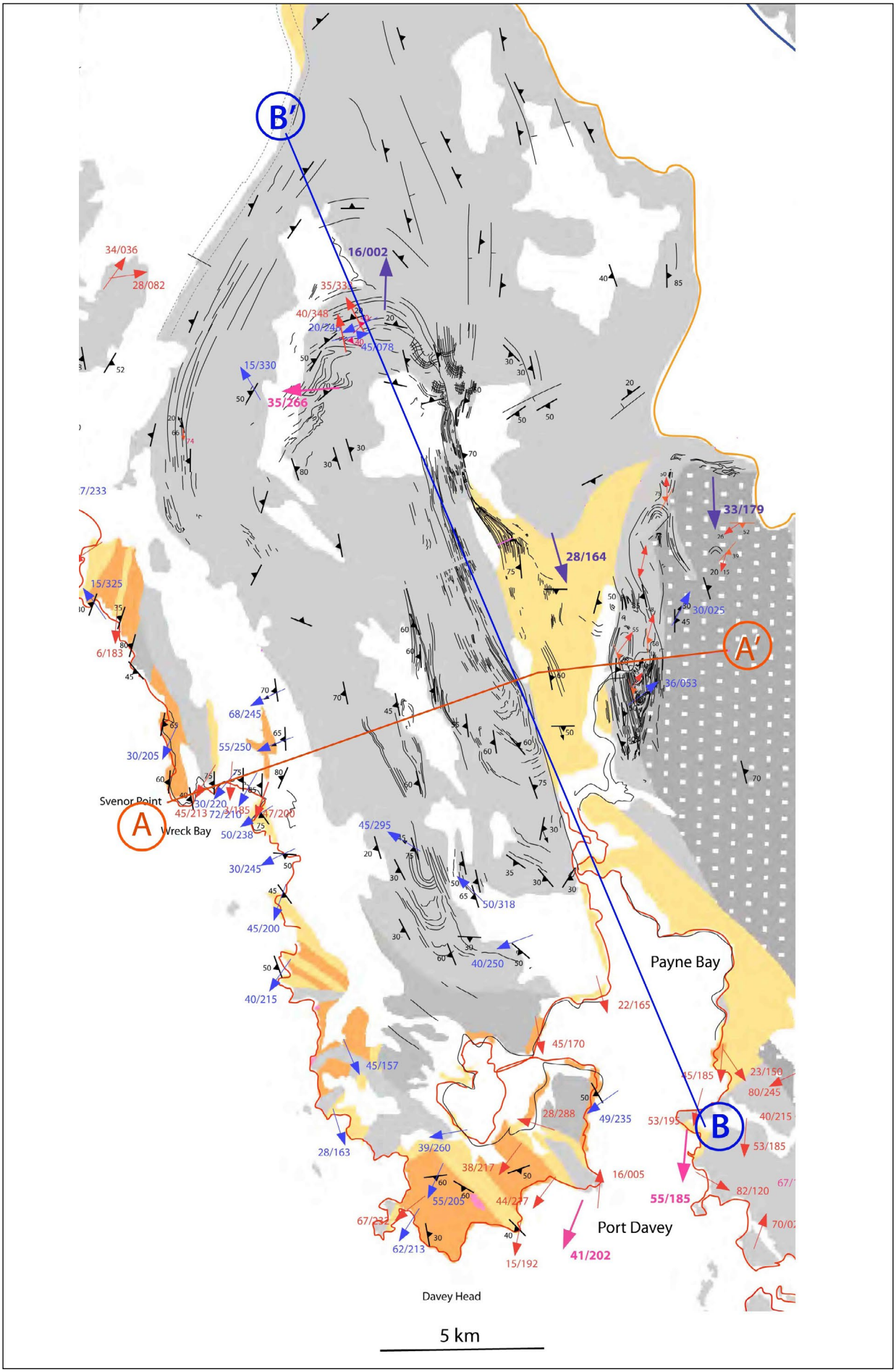

Figure 13. Structure map of the De Witt-Propsting mega-sheath fold with Mineral Resources Tasmania 1:250000 digital atlas litho-tectonic map base. Lineation Lm shown by blue arrows, mesoscopic isocline fold axes shown by the red small arrows and calculated β axis macro-fold axes by the large pink arrows. The positions of section lines A-A' (Figure 19) and B-B' (Figure 20) are shown.

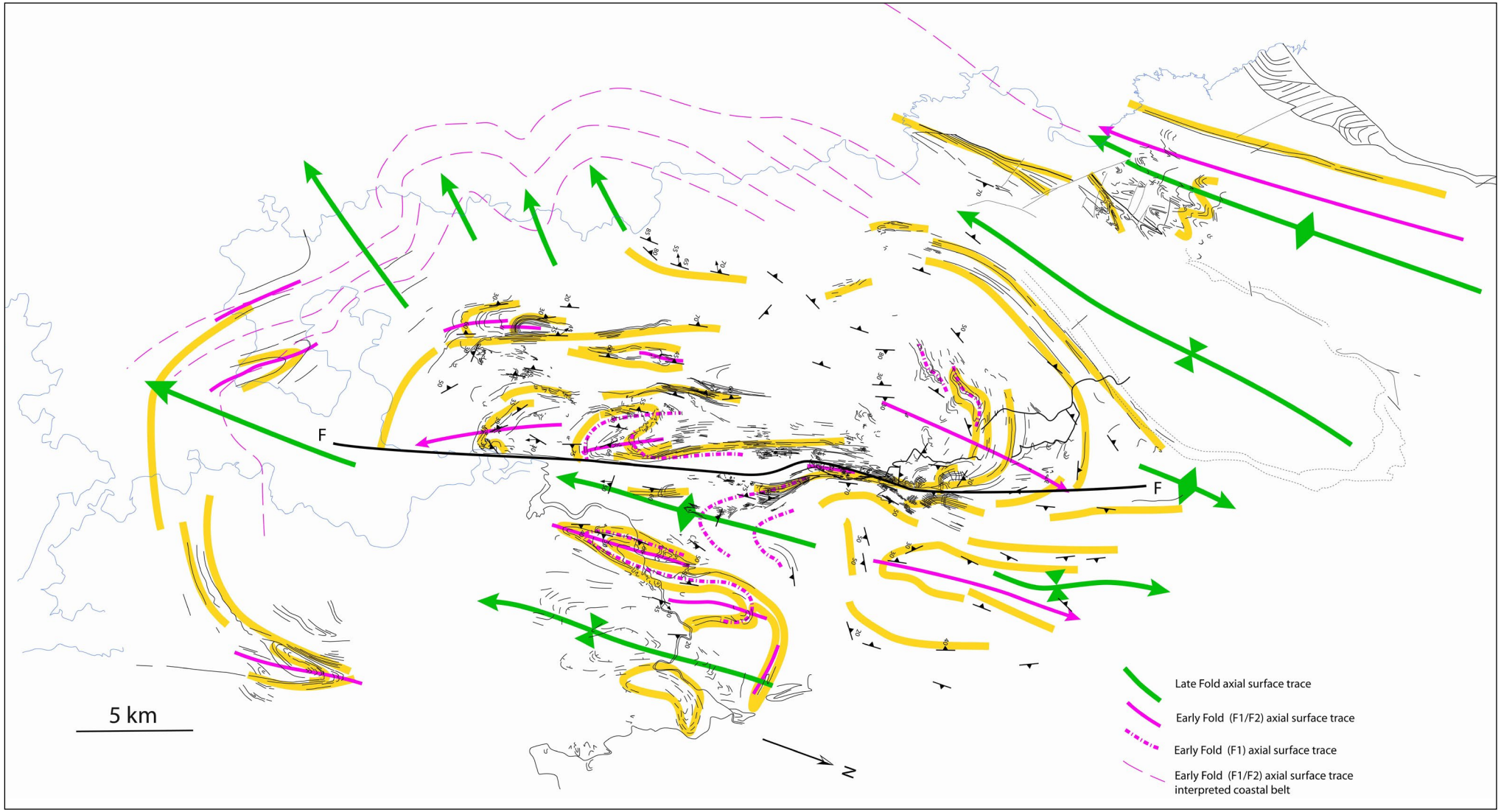

Figure 14. Formline map of the De Witt-Propsting mega-sheath fold showing the northern and southern close-outs, the pinchouts of the lower limb sheath structure and the axial surface traces of the early F1 macro-isoclines (pink dashed line traces), the second generation macro-isoclines (pink line traces) and the younger Devonian folds (green line traces). Interpreted early macro-isocline axial surface traces in the high-grade coastal sequence are shown by the thin, dashed pink line traces from Gray et al. (2022, Figure 78).

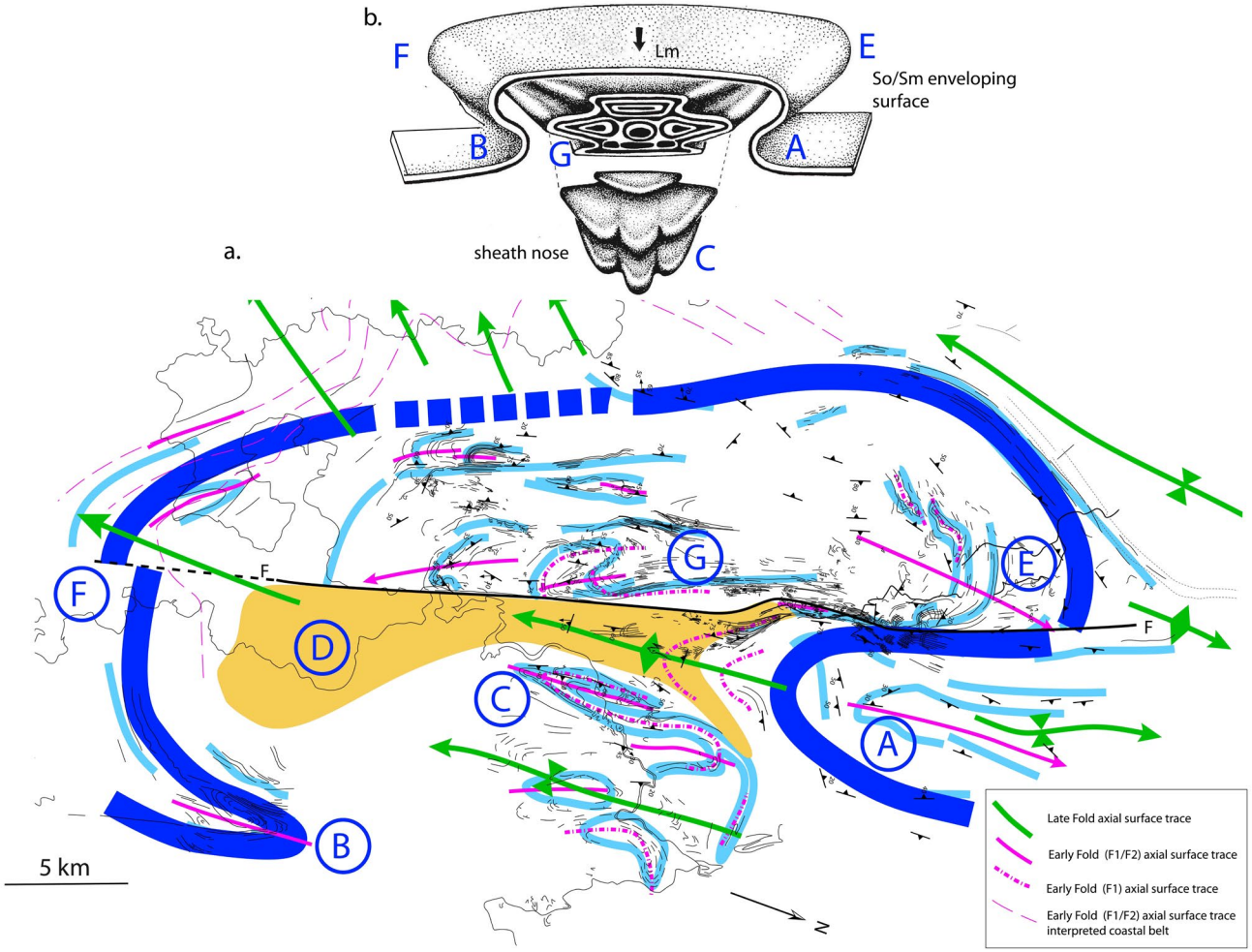

Figure 15. a) Simplified formline map of the De Witt-Propsting mega-sheath fold-enveloping surface showing the northern and southern close-outs, the pinch-outs of the lower-limb sheath structure and the axial surface traces of the early F1 macro-isoclines (pink dashed line traces), the second generation macro-isoclines (pink line traces) and the younger Devonian folds (green line traces). Circled A: northern lower limb pinch-out. Circled B: southern lower limb pinch-out. Circled C: Thick dark blue lines: simplified outline of mega-sheath fold. Thin light blue lines: summary formlines in So/Sm and Sm. Davey River sheath nose of the mega-sheath fold. Circled D: orange area a region of platy quartzite and/or pelite. Circled E: northern close-out of the mega-sheath shell. Circled F: faulted southern close-out of the mega-sheath shell. Circled G: inner shell of the mega-sheath fold.

b) Schematic 3D diagram of sheath-fold form, profile section and nose (modified Figure 2 from Alsop and Holdsworth, 2004) with blue letters corresponding to the structural positions shown in (a).

3.1.2 Structural Architecture and Internal Structure

The mega-sheath (Figure 17) consists of:

1. An outer shell of banded quartzite and platy, schistose to mylonitic quartzite (western high-strain zone carapace),
2. A middle shell of asymmetric fold pairs as pods within variously deformed quartzite and bounded by further banded quartzite and platy quartzite, and
3. A structurally complex inner shell or core (Figures 18 and 19).

The core consists of refolded macro-isoclines with complex, overprinting fabric and structural relationships (Figure 19).

Although elliptical in section the internal structure is not as simple as the eye-sheath forms of Alsop & Holdsworth (2006, Figure 2). These are characterised by simple nested ellipses with varying ellipticities. For the De Witt-Propsting mega-sheath the core, or innermost "ellipse", is structurally more complex with banana-shaped refolds of early second-order macro-isoclines by a second set of macro-isoclines that trend parallel to the intermediate axis ('y' dimension) of the mega-sheath fold (Section 6.3). Similar relationships of refolding of earlier formed sheath-folds by subsequent folding during continuous shear-related deformation have been described by Quinquis et al. (1978), Goscombe (1991, Figure 6c), Henderson (1981) and Srivastava (2011).

The second- and third-order isocline fold pattern within the middle and inner shells is shown in a schematic 3D sketch of the mega-sheath fold in an oblique view looking to the west (Figure 18). The northern and southern closing flanks of the apparent sheath show gentle plunges away from the inner shell or core. Within the core both the mesoscopic and macroscopic folds, particularly along the Castle Hill and Upper Castle Hill ridgeline, show inclined-west-plunging to reclined-west-plunging geometries (Figure 18).

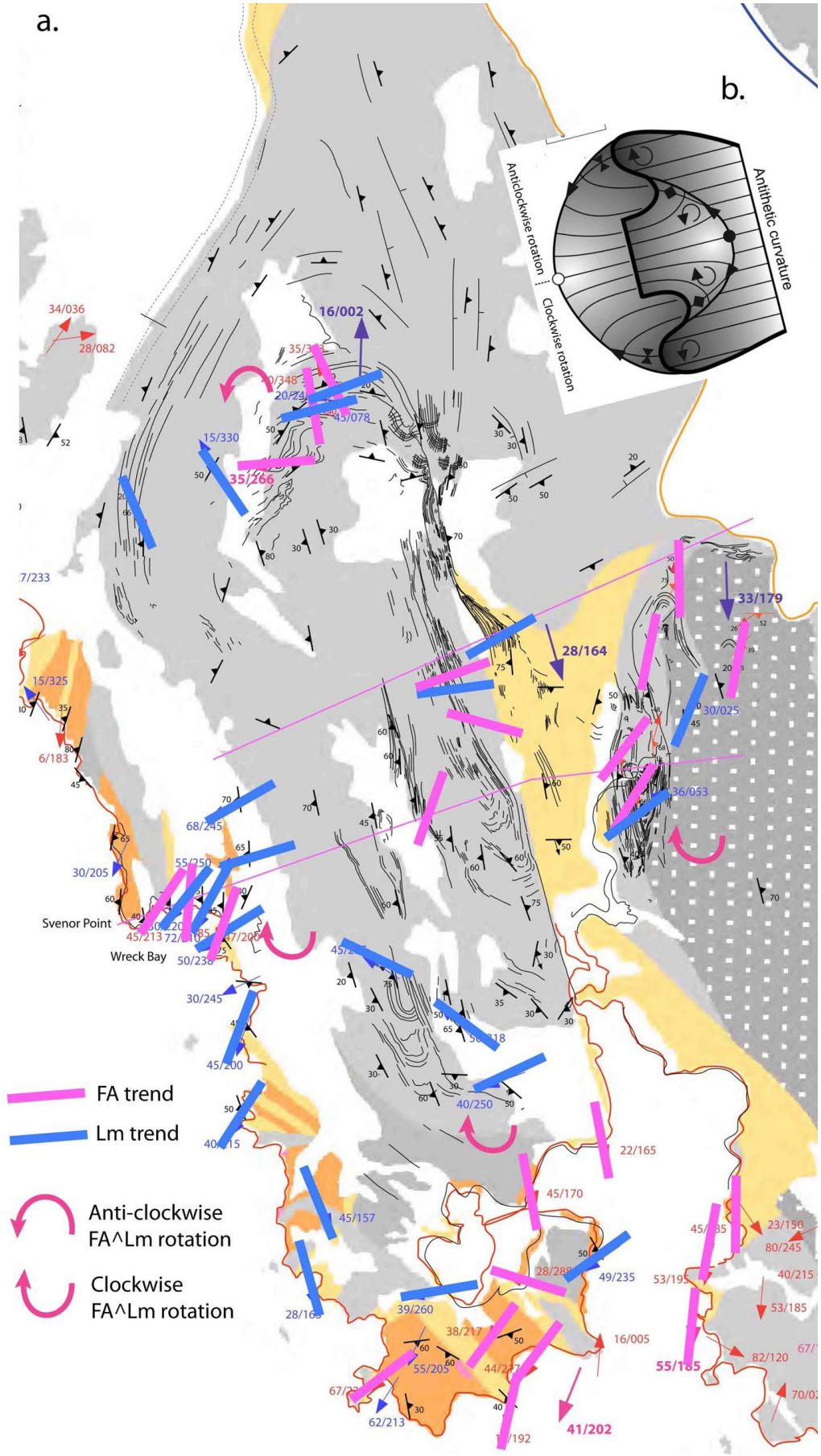

Figure 16. Fold axis FA (pink traces) and mineral stretching lineation Lm (blue traces) trend map for the De Witt-Propsting mega-sheath fold. a) Trend map on Mineral Resources Tasmania 1:250000 digital atlas lithological base. Rotation directions for closing the acute angle between the fold axis trend and the lineation trend are shown by the red arrows. b) Schematic diagram of oppositely-closing sheath fold pair displaying antithetic curvature with FA to Lm rotations shown (from Alsop and Carreras, 2007). Note for the inferred east-closing macro-sheath fold the northern closeout should show anticlockwise rotation of the FA towards Lm with a clockwise rotation on the southern closeout.

Figure 17. Internal structure of the De Witt-Propsting mega-sheath fold showing the three component shells on a Google satellite image base. These shells are internal zones or layers that include 1) the Outer Shell or western high-strain carapace, 2) the Middle Shell or folded zone, and 3) the Inner Shell or core of the mega-fold. An oblique map section close to the nose of the mega-sheath fold is shown as eastern termination (Davey River structure) that has been folded across a younger anticline centred between the two elements. Blue circles are locations of helicopter aerial photographs discussed in the text. Field stations visited by the authors are shown by the yellow pins.

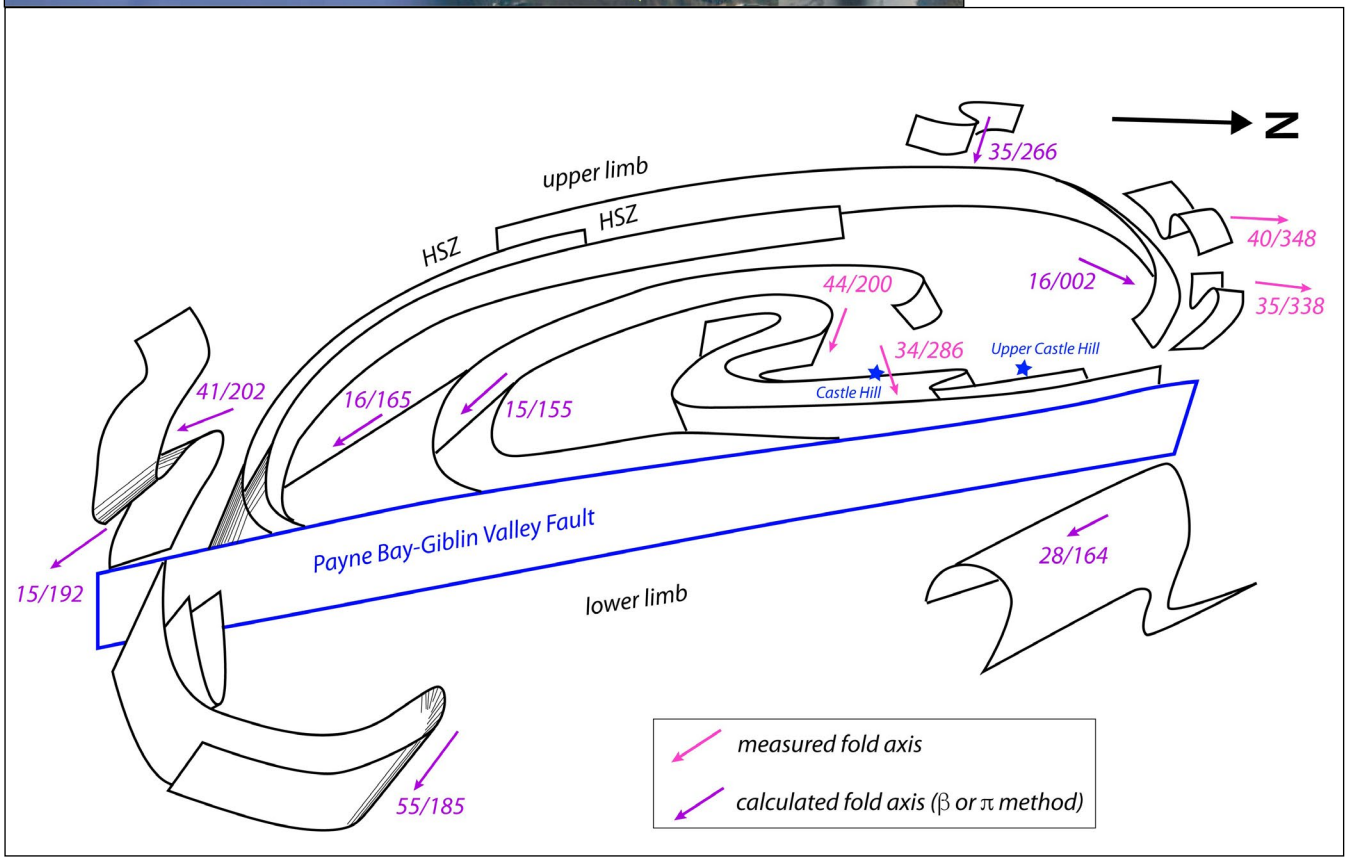

Figure 18. Sketch of the 3D geometry of the De Witt-Propsting mega-sheath fold showing the concentric outer shells, the geometry of the inner structurally complex core and the relationships of the second and third order isoclines within the elliptical form HSZ: high strain zone. of the sheath. The view is to the west. Measured mesoscopic-isocline fold plunges are shown by pink arrows as a plunge/plunge direction and calculated fold axes (β or π method) by the purple arrows. The steep, north-south trending blue outlined, plane represents the Payne Bay-Giblin Valley Fault that cuts or truncates the eastern flank of the elliptical shell. The geographic locations of Castle Hill and Upper Castle Hill within the structure are shown by the blue stars. HSZ: high strain zone.

3.2 Structural Profiles

Two structural profiles were constructed as cross sections through the De Witt-Propsting mega-sheath fold. A vertical east-west section (Section A-B, Figure 13) extending from Svenor Point/Wreck Bay to the Crossing River shows the sheath geometry and fold- and fabric-relationships across the mega-sheath fold (Figure 19). This profile is parallel to the regional lineation Lm and the 'x' direction of the sheath fold. It also shows the arching or anticlinal folding of the sheath fold across the younger Devonian Davey River Anticline and offset along the Payne Bay-Giblin Valley Fault with inferred west side-down movement. The younger anticline essentially cuts the sheath fold into two segments, the main De Witt-Propsting segment and the Davey River segment as the projected nose of the mega-sheath fold. The inner shell exposed in the Castle Hill-Upper Castle Hill ridgeline shows the complex mesoscopic folding and refolding and the multiple fabrics that define rocks of the sheath core of the De Witt Propsting part as well as the inferred Davey River mega-sheath nose (inset sketches, Figure 19).

The other profile is a vertical north-south section extending from Port Davey to the Giblin River Valley (Figure 20). It is approximately orthogonal to the general lineation Lm direction and parallel to the 'y' direction of the mega-sheath fold. This cross section shows the geometry as a broad, gentle arching across the inner shell of the mega-sheath fold with gentle plunges to the north and south on the respective flanks or shoulders of the sheath fold. The section shows a layered internal structure consisting of zones of second- and third-order isoclinal folds bounded by zones of intense foliation Sm.

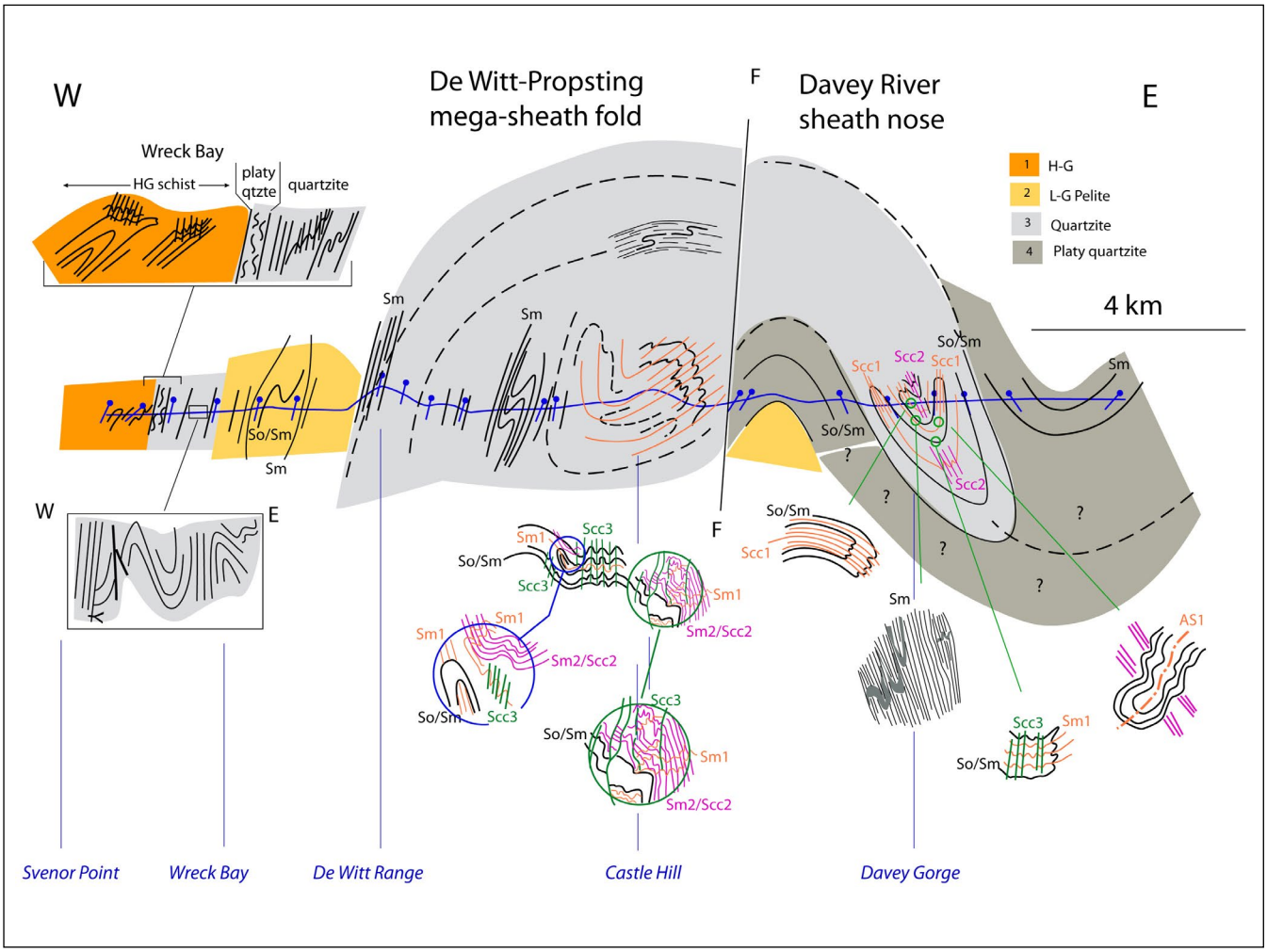

Figure 19. East-west structural section A-A' across the De Witt-Propsting mega-sheath fold (approximating the x-z section of the sheath fold.). For section location see Figure 13. The diagram also shows local structural/fabric relationships within the quartzite containing the mega-sheath fold (grey unit) and the structural relationships for the western, homoclinally west-dipping carapace to the mega-sheath fold. Bright orange: H-G schist; grey: L-G quartzite; yellow-orange: L-G pelite; dark grey: schistose quartzite.

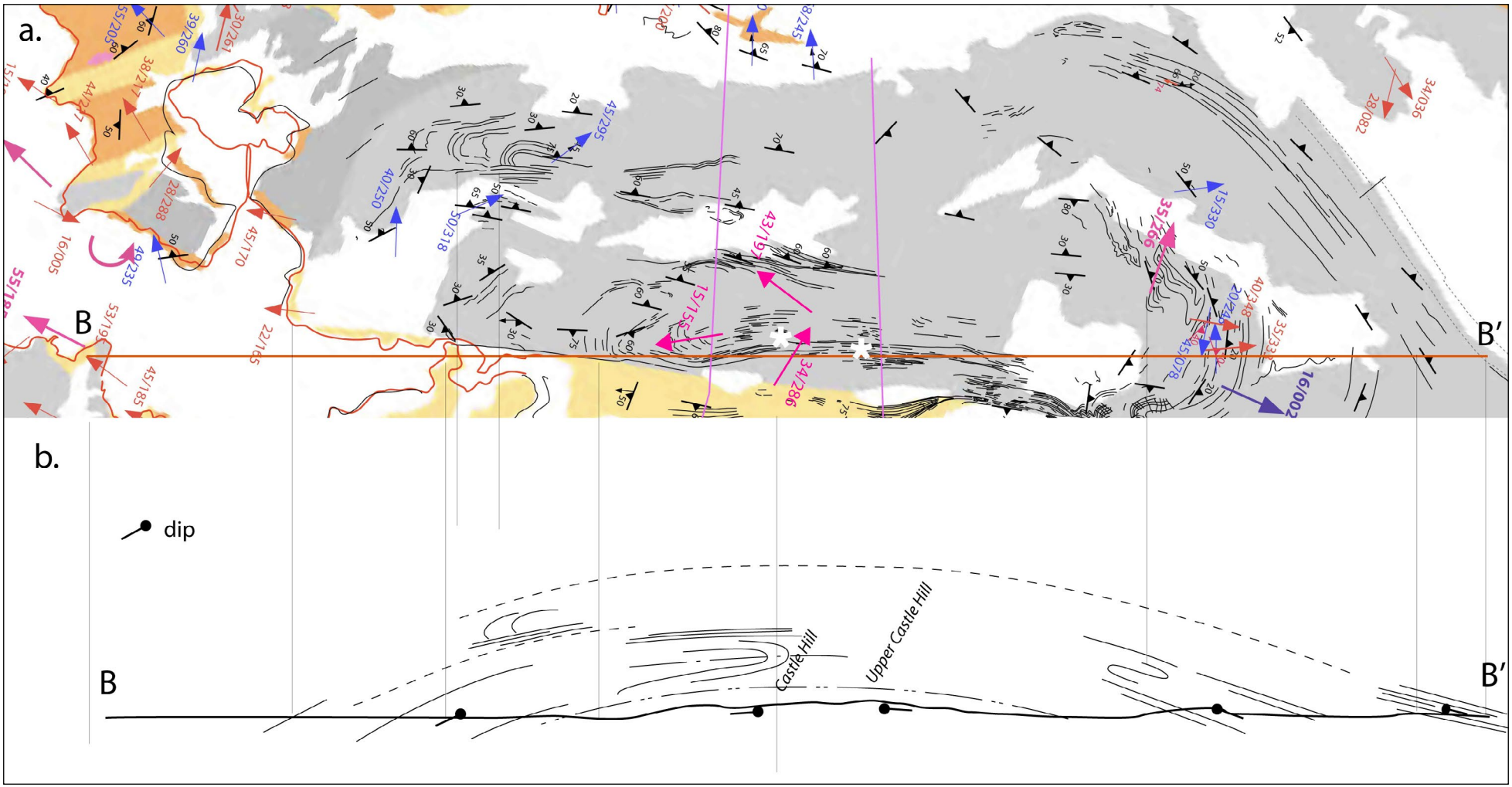

Figure 20. North-south long structural section B-B' from Port Davey to the Giblin River Valley (340° profile alignment) across the De Witt-Propsting mega-sheath fold. For section location see Figure 13. a) Structure map with structural data showing foliation Sm (black strike/dip symbol), lineation Lm (blue arrows), fold axis (red arrows) attitudes. Bright orange: H-G schist. Grey: L-G quartzite. Yellow-orange: L-G pelite.

3.3 Unfolding/Profile Deconstruction

Devonian folding of the mega-sheath about a north-south trending, south-plunging anticline (Figure 14) provides in map pattern two, 2-D slices through the sheath fold (Figures 14 and 17). The major or more centralised "profile" sits on the western limb of the anticline and the nose profile on the eastern limb. Unfolding of the anticline (Figure 21b) shows a reconstructed sheath-fold length (x-direction) of approximately 20km.

Eye-fold shells in the two 2-D (y-z) slices were used to reconstruct the fold geometry along the x-axis (i.e. self-similarity is useful if tracing layering in large sheath folds) (cf. Alsop and Holdsworth, 2012).

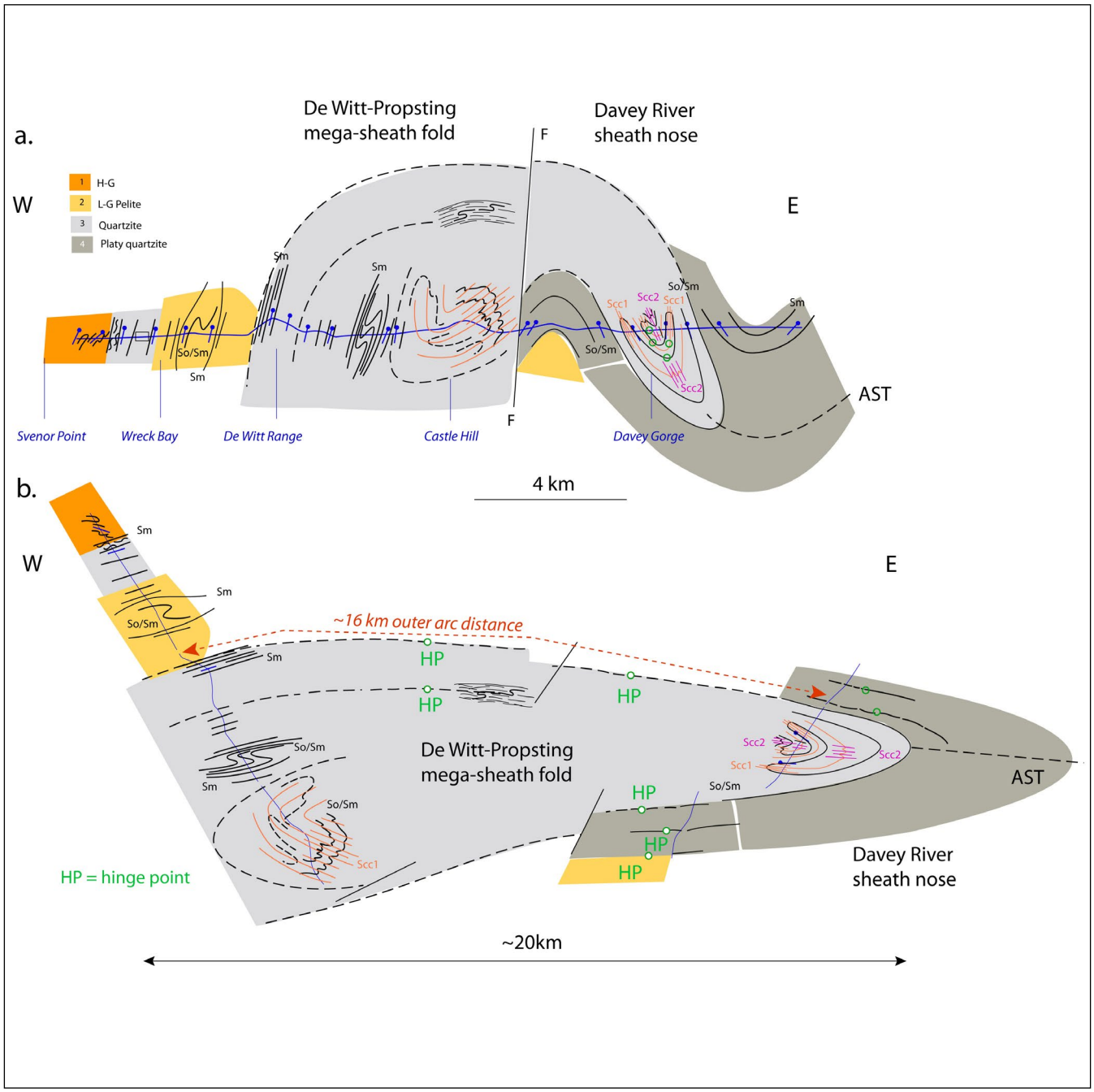

Figure 21. De Witt-Propsting mega-sheath longitudinal (x-z plane) profile restoration. a) East-west cross-section showing the folded and faulted, east-closing Cambrian sheath fold-nappe (deformed-state). Topographic surface in blue with geographic locations in blue text. b) Restored fold-nappe form constructed by removal of the Devonian open folding. Restoration was by hinge rotation at hinge points of the Devonian folds (designated by the green H) accompanied by line-length balancing of the upper quartzite contact (uppermost outer shell). Displacement and movement sense on the Payne Bay-Giblin Valley subvertical fault (F) is unknown, but likely with a west-side component. Separation of the now rotated map views (oblique profiles) along the upper contact is approximately 16km with an approximate x-length dimension of 20 km for the sheath fold-nappe.

3.4 Sheath-fold Shape Analysis and Implications

The De Witt-Propsting sheath fold trends 345°-165° and has a length ('y' direction or sheath width) of 29 km (Figure 22). As the mega-sheath is truncated on the east by a sub-vertical fault the width ('z' direction) can only be estimated by closing the shape as ~14 km (i.e. 2 x 6.9km).

Other parameters include (Figure 22):

1. Elliptical Aspect Ratio (R')

Dimensions for the De Witt-Propsting sheath-fold ellipses are:

Tz1 (MD)= 3.4km with a dip 70° gives a true thickness Tz1=2.6 (i.e. 3.4 x 0.77)

Tz2 (MD)= 3.5km with a dip 60° gives a true thickness Tz2= 3.03 (i.e. 3.5 x 0.88), where MD is the map distance measurement from the plunging shell outcrop trace.

This gives Ryz= 14.5/5.63= 2.57 and Ryz' = 9/3.03= 2.97 such that Ry'z'>Ryz and R'=Ryz/Ryz'= 2.57/2.97= 0.87 equated to **Type C cats-eye-fold** sheath-fold form developed with a flattening component ('z' shortening) to the sheath.

2) Layer Thickness ratio (Tyz)

Thickness ratios vary between the outer and inner ellipses (Figure 22) with the outer ellipse giving Tz1: 2.6km and Ty1: 7.0km where Tyz1=2.06 and the inner ellipse giving Tz2: 2.57km and Ty2: 9km where Tyz2= 3.5. Taking the half dimensions of the complete sheath fold gives Tz3: 6.9km and Ty3: 14.5km where Tyz3= 2.1.

3.5 Reconstructed 3D Sheath Form

The 3D form of the De Witt-Propsting mega-fold was constructed using the unfolded spacing of the map oblique-sections (Figure 21) and the profile dimensions (Figure 22). This enabled construction of a simple sheath-fold outer-shell that gave the approximate length scale, apical angle (β) and hinge curvature (δ) of the macro-fold (Figure 23).

In summary, the reconstructed shell of the De Witt-Propsting mega-sheath fold has a projected length ('x' dimension) of ~20km, a maximum known width ('y' dimension) of 29km, a maximum known shell height ('z' dimension) of ~14km, with an apical angle of 50°, a hinge curvature of 130° and interlimb angle of 10° (Figure 23).

3.6 Structure of the De Witt-Propsting Shells

3.6.1. Outer shell (Zone of banded quartzite and platy quartz mylonite with third-order asymmetric fold pairs as augen bounded by intense Sm)

The western margin appears as banded quartzite with intense Sm/So commonly transitional with, and interfingering with, platy, schistose quartzite with intense Sm (Figure 24). It defines a high-strain carapace to the De Witt-Propsting mega-sheath fold with the outermost part as a high-strain, inter-digitating interface due to isoclinal-infolding of quartzite with the overlying high-grade units (Gray et al., 2022). The structural character of this zone is shown in Figures 24, 25, 26, 27 and 28. Outcrop-scale relict fold hinges and fold-pods (augen) are preserved in places within and bounded by the intense Sm foliation (Figures 24, 25 and 26). The nature of the banded So/Sm to intense Sm foliation is shown in Figures 25 and 26. At the outcrop scale this commonly consists of zones of platy, schistose quartzite (Figures 27 and 28) with rodded to mylonitic character in places (Figure 28).

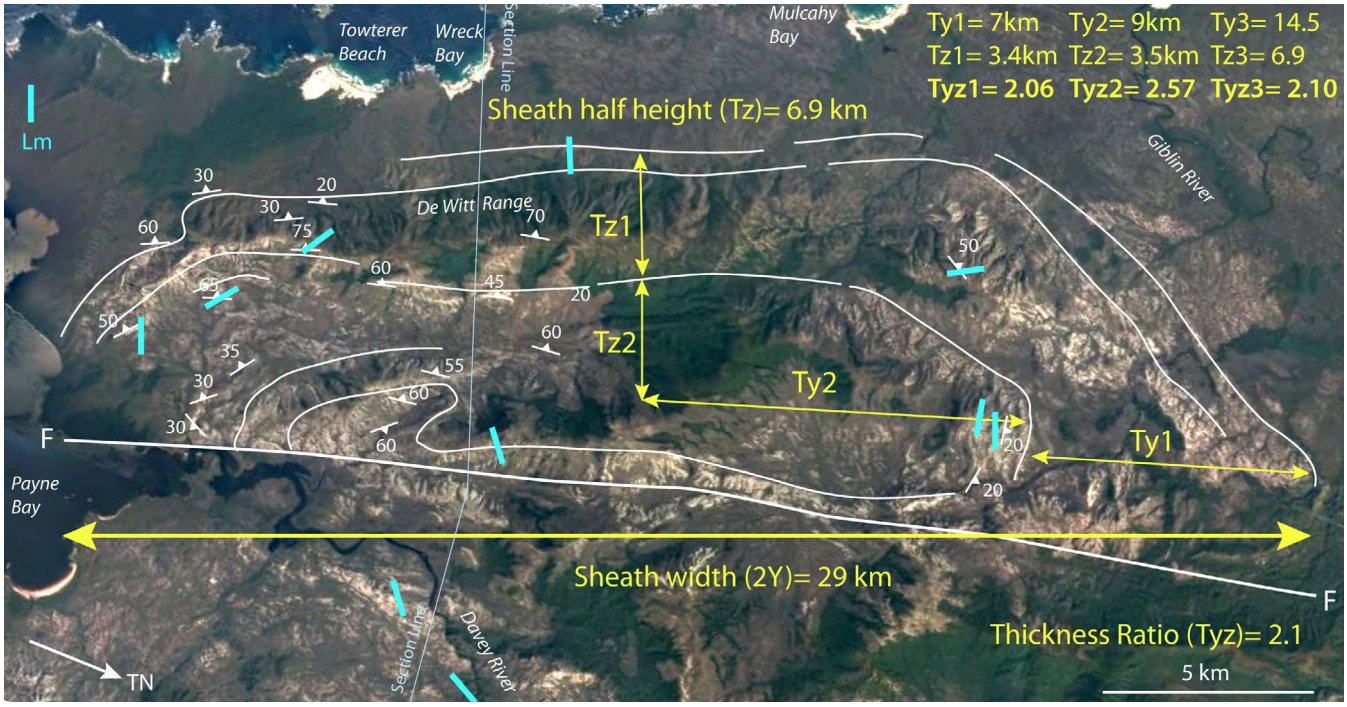

Figure 22. Approximate down-plunge profile view of the De Witt-Propsting mega-sheath fold as a Google Earth image base. Formlines in So/Sm (white line traces) define the shape, sheath geometry and the inner and outer ellipses of the mega-sheath fold. Thickness measurements Ty and Tz are shown for the outer (designated 1) and inner ellipses (designated 2). Note the sheath is cut by a sub-vertical fault on the eastern side (lower part of the Google image) shown by the white line trace near the yellow arrowed length dimension line. Note the Google image has been rotated 105° clockwise to view the sheath in an approximate profile plane. The coast is at the top of the image with beach areas of Mulcahy Bay (top centre right), Wreck Bay and the dunes of Towterer Beach (top centre left) visible.

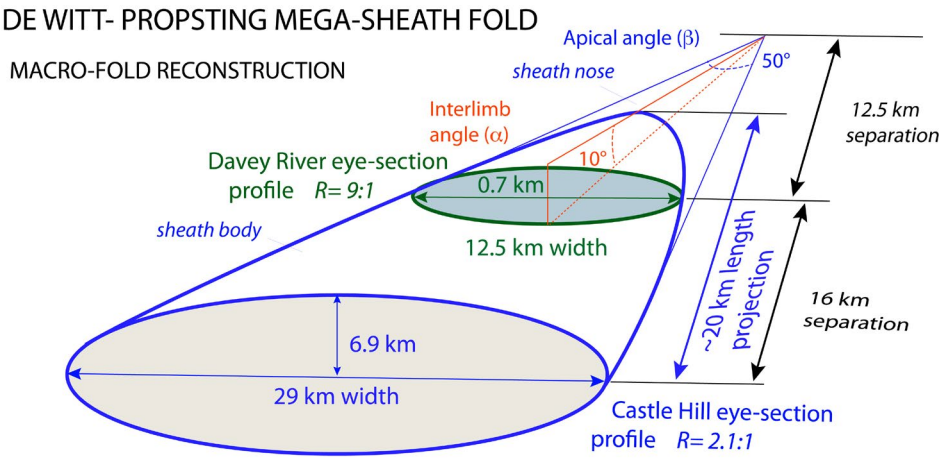

Figure 23. Reconstruction of the shape of the De Witt-Propsting mega-sheath form using 1) the outer shell dimensions from the Castle Hill eye-section (khaki ellipse) and the Davey River "eye"-section (grey ellipse), and 2) the section spacing of ~16 km based on the unfolded longitudinal x-z section in Figure 21. These give a projected length (x direction) of ~20 km, an apical angle of 50° and an interlimb angle of 10° for the proposed mega-sheath fold.

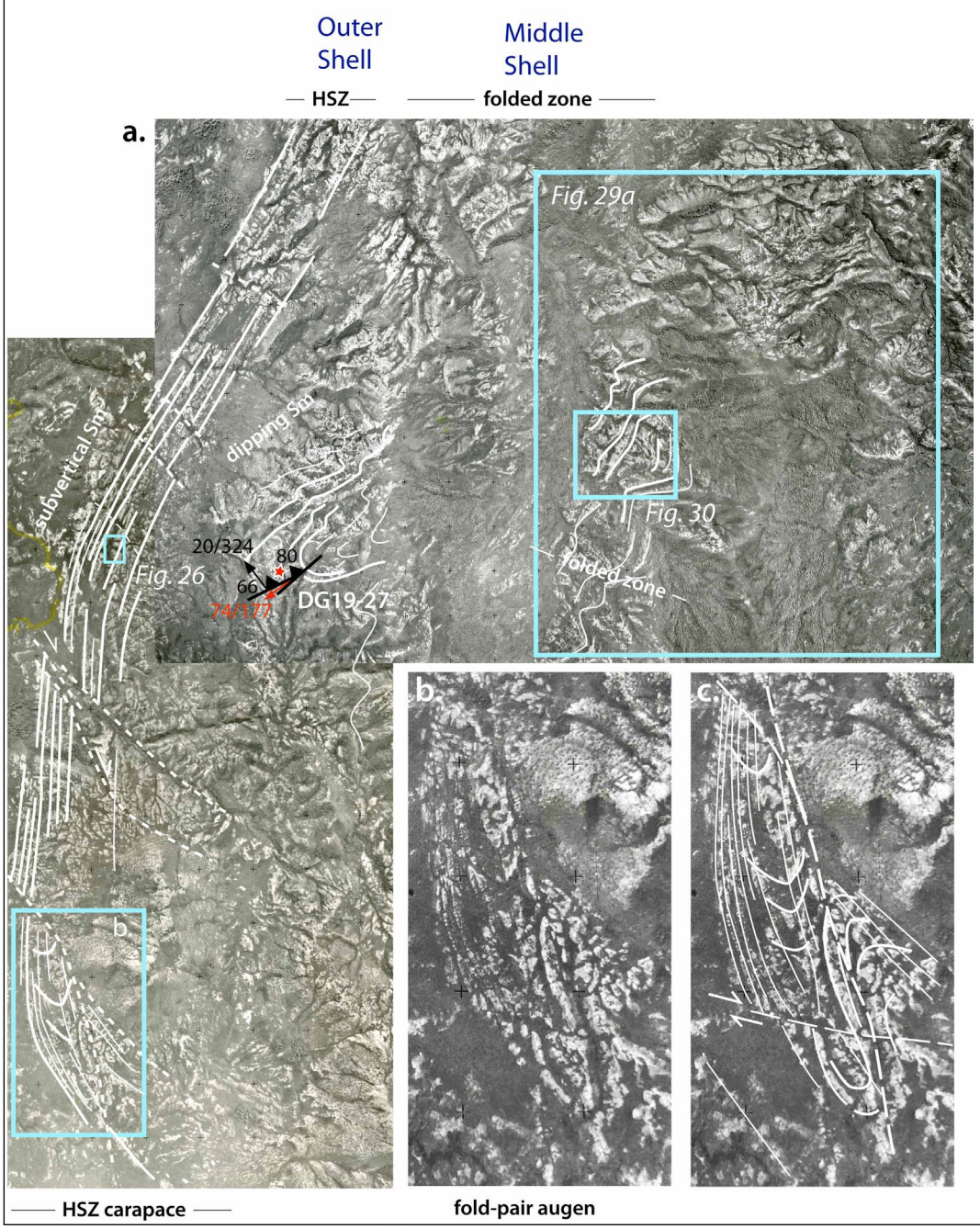

Figure 24. Aerial photograph composite image of part of the Outer Shell high-strain carapace (HSZ: high-strain zone) as the strongly foliated western, upper limb of the De Witt-Propsting mega-fold. This shows transition into the structurally-lower folded zone (Middle Shell). The northern sheath closure sits in the upper right corner of (a). b) Enlarged part of the western margin high-strain zone showing apparent fold closures in weathered quartzite outcrops as asymmetric fold pods/augen within the Sm. c) Formline interpretation of (b) showing interpreted fold-pair augen within this outer intensely foliated high-strain zone

Figure 25 (right). De Witt Range view south towards Davey hills (background centre-left). a) The hillside shows west-dipping, banded quartzite with intense Sm. b) Enlargement of area covered by the rectangle in (a) showing fold closure in So/Sm bounded by the intense Sm layering (see lower left). c) Formline interpretation of photo in (b).

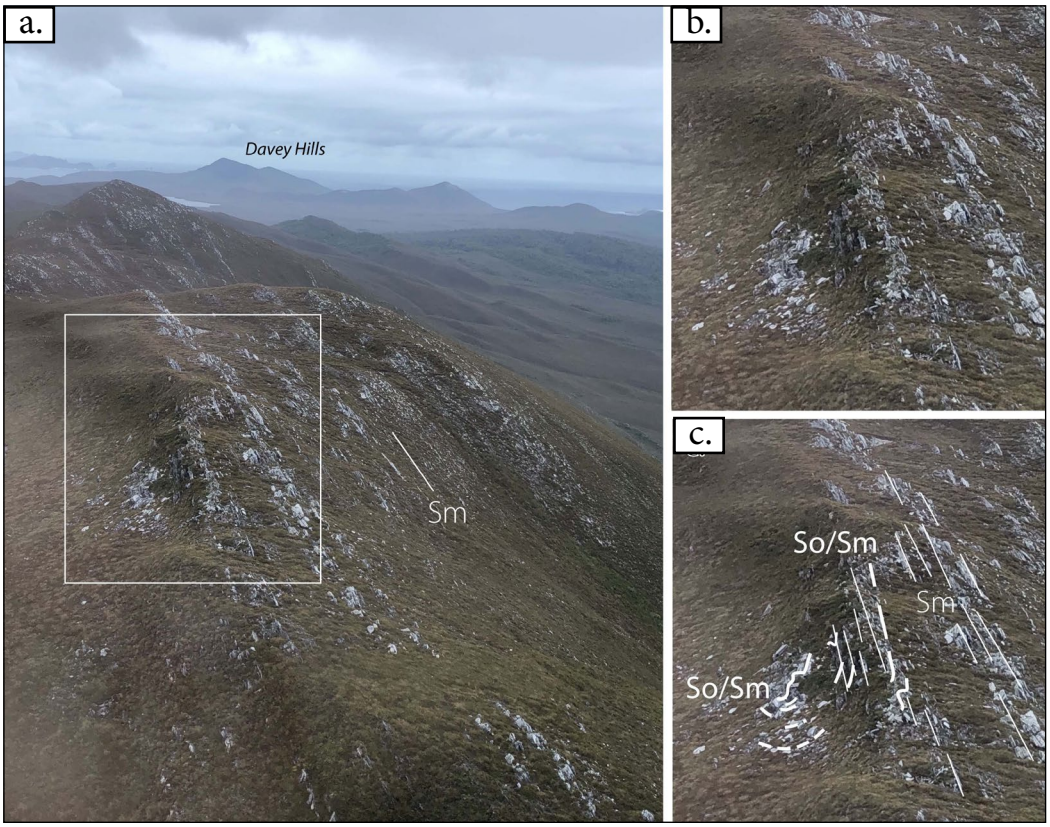

Figure 26 (below). Aerial view of steeply dipping foliation Sm in banded quartzite along the west side of the northern De Witt Range. Relict fold hinges in So/Sm occur within low-strain pods, as augen enveloped by the intense Sm (see b). The steep, west-dipping banding appears to be cut by a younger ~70° east-dipping cleavage (see c.).

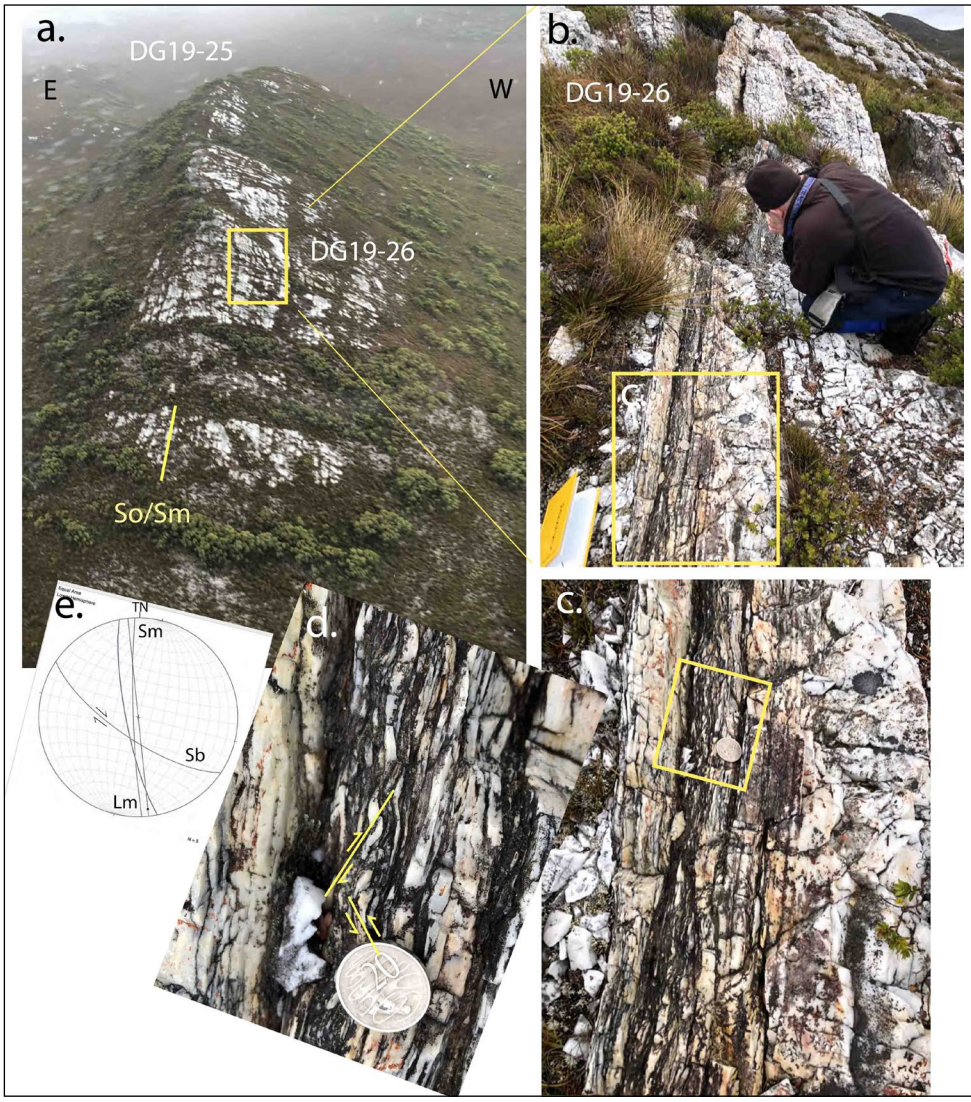

Figure 27. Knoll of banded quartzite (Stations DG19-25 and DG19-26) in coastal belt between Mulcahy Bay and Nye Bay. A steeply west-dipping foliation So/Sm contains Sm parallel zones of higher strain as platy, mylonitic quartzite (see c and d) containing weak antithetic and synthetic shear bands (see d). The stereonet inset (e) shows geometric relations between great circle traces for Sm and the dextral "synthetic" shear band set.

Figure 28. Ridgeline of platy quartzite with partial rodding fabric, relict fold hinges in quartz veins, as well as marked silicification as silica "infiltration". The ridgeline represents the middle part of the De Witt-Propsting mega-sheath fold Outer Shell (see Figure 24).

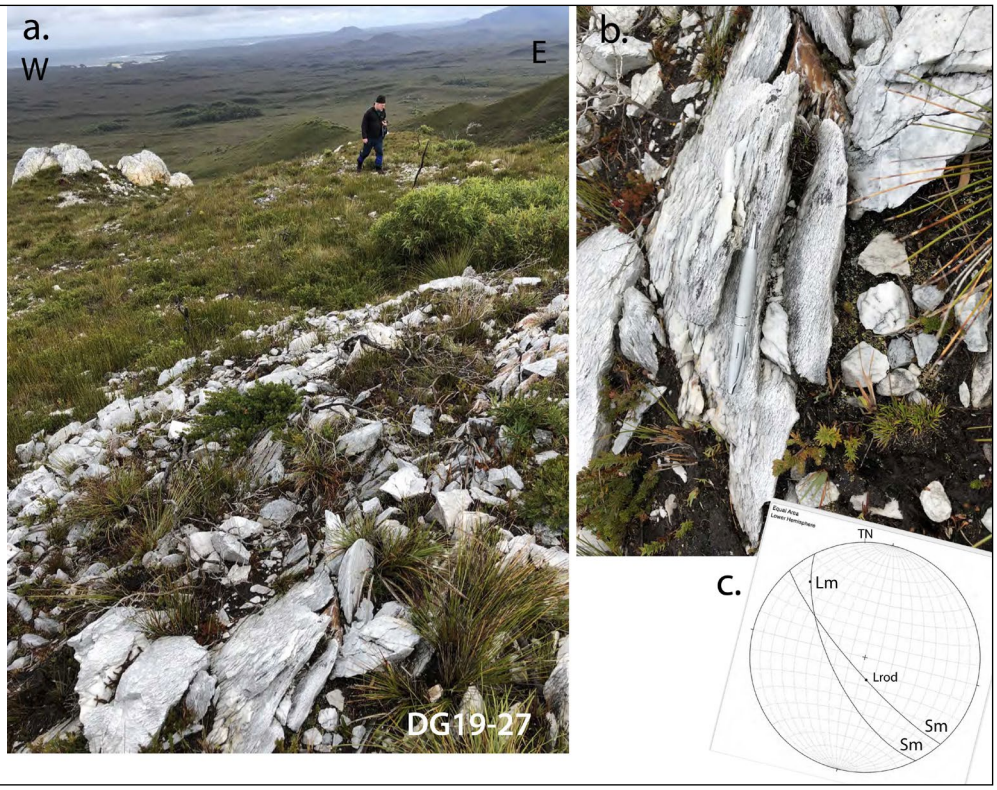

3.6.2 Middle Shell (dominated by second- and third-order asymmetric fold pairs in So/Sm)

The middle shell part of the northern flank or shoulder of the mega-sheath fold (Figure 30a) contains a series of second-order (tens-of-metre scale) (Figures 29a, b) and third-order (metre-scale) reclined, to recumbent isoclinal folds (Figures 29c, d, 31, 32, 33 and 34). Other second-order reclined folds occur further southwest where the middle shell transitions from the north-dipping flank into the west-dipping "roof" of the mega-sheath fold (Figures 29a and 30).

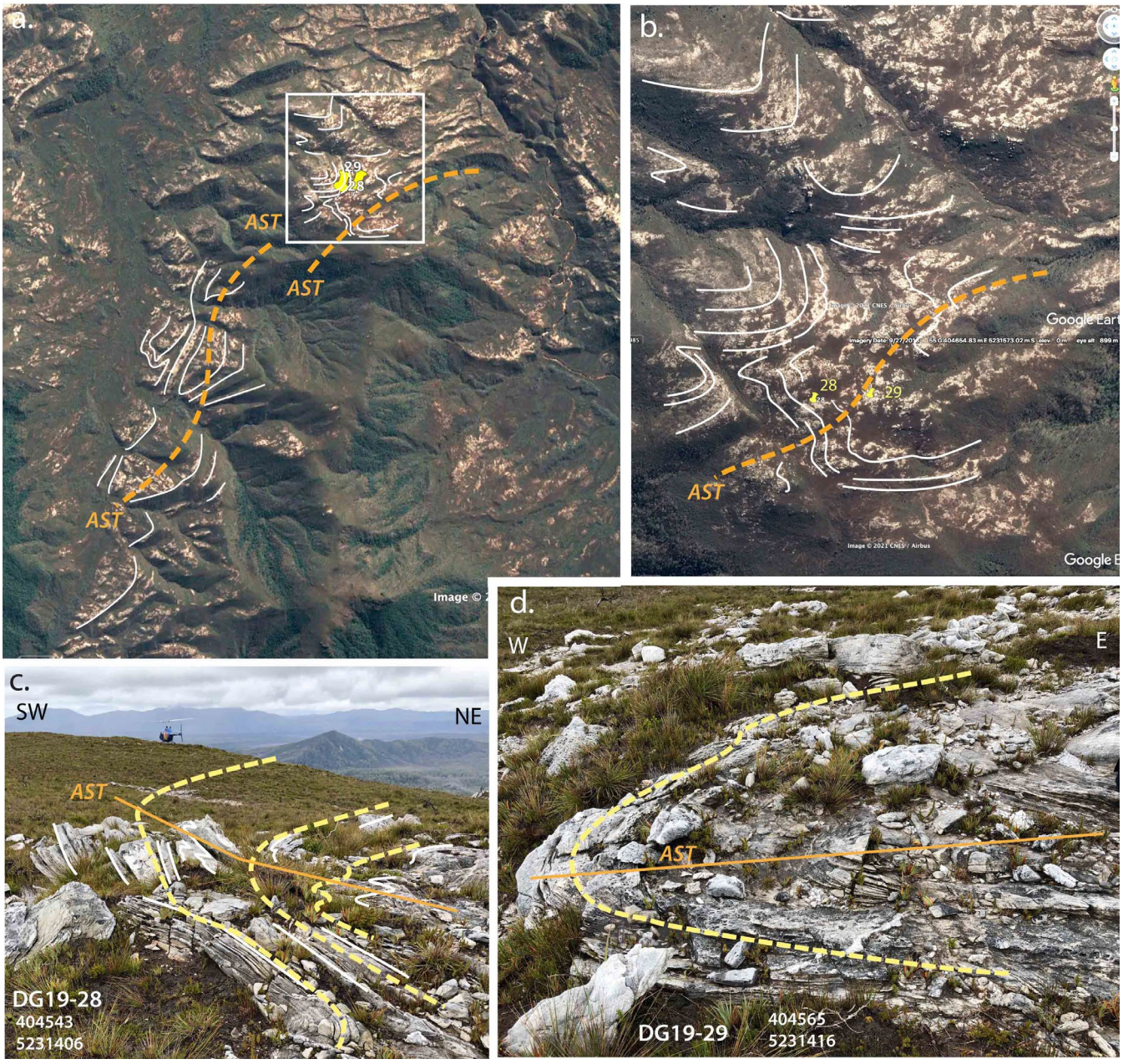

Figure 29. Northern flank or close-out of the Middle Shell (folded zone) of the De Witt-Propsting mega-sheath fold.

a) Google Landsat image with formlines in So/Sm (white line traces). Fold axial surface traces (AST) are shown by the dashed orange lines. The white rectangle outline is area enlargement in (b).

b) Enlarged part of (a) showing a major north-plunging, west-closing recumbent isocline in the So/Sm formline traces. Yellow pins show positions of DG19-28 and DG19-29 field stations. c) Folded So/Sm layering at DG19-28. d) Recumbent isoclinal fold hinge at DG19-29.

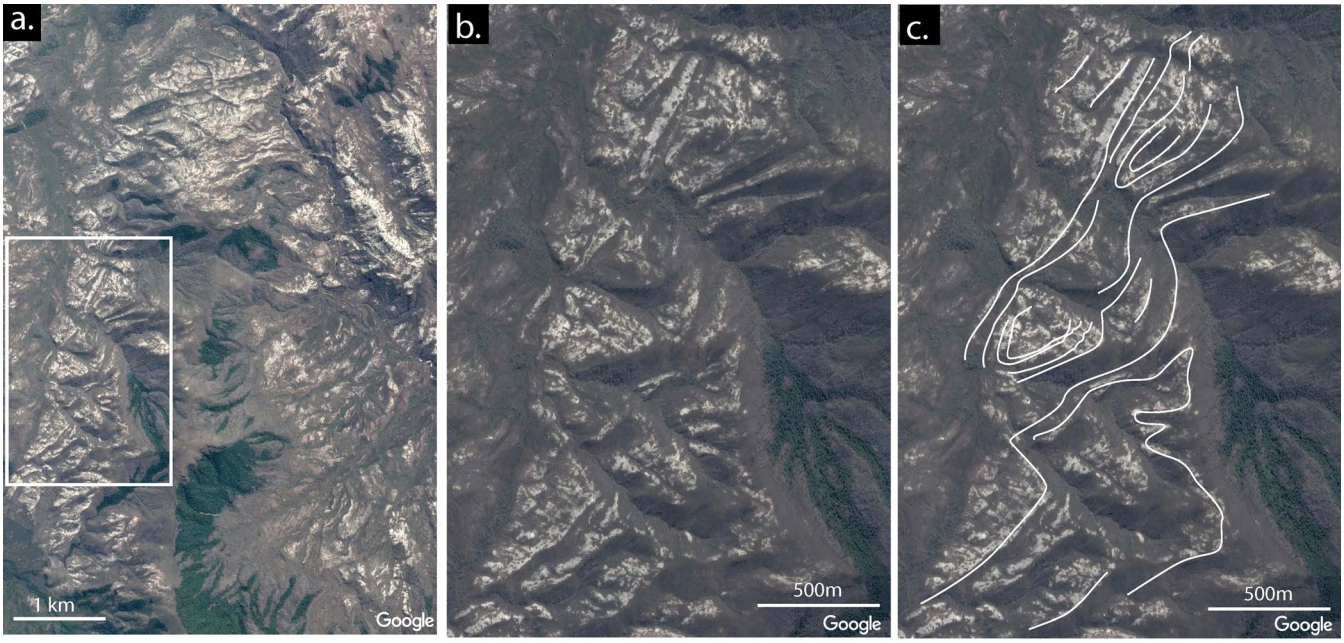

Figure 30. Google satellite images of the west-dipping "roof" or western flank of the De Witt-Propsting mega-sheath fold (a). Outcrop traces in weathered quartzite showing apparent fold closures with a structurally higher south-closing isocline juxtaposed with a structurally lower north-closing fold. These macro-folds are also part of the inner folded zone or Middle Shell (see Figure 29a).

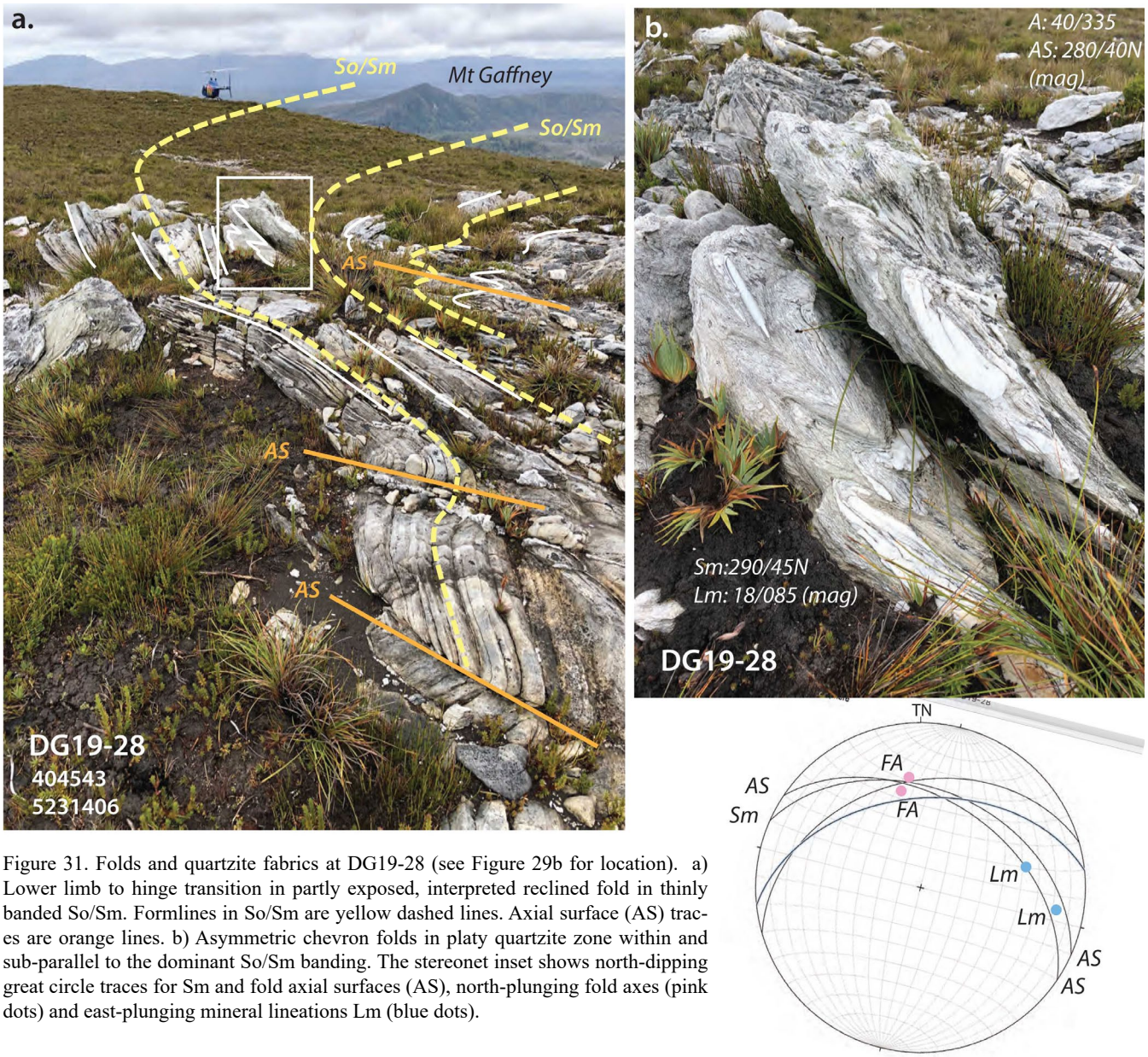

Figure 31. Folds and quartzite fabrics at DG19-28 (see Figure 29b for location). a) Lower limb to hinge transition in partly exposed, interpreted reclined fold in thinly banded So/Sm. Formlines in So/Sm are yellow dashed lines. Axial surface (AS) traces are orange lines. b) Asymmetric chevron folds in platy quartzite zone within and sub-parallel to the dominant So/Sm banding. The stereonet inset shows north-dipping great circle traces for Sm and fold axial surfaces (AS), north-plunging fold axes (pink dots) and east-plunging mineral lineations Lm (blue dots).

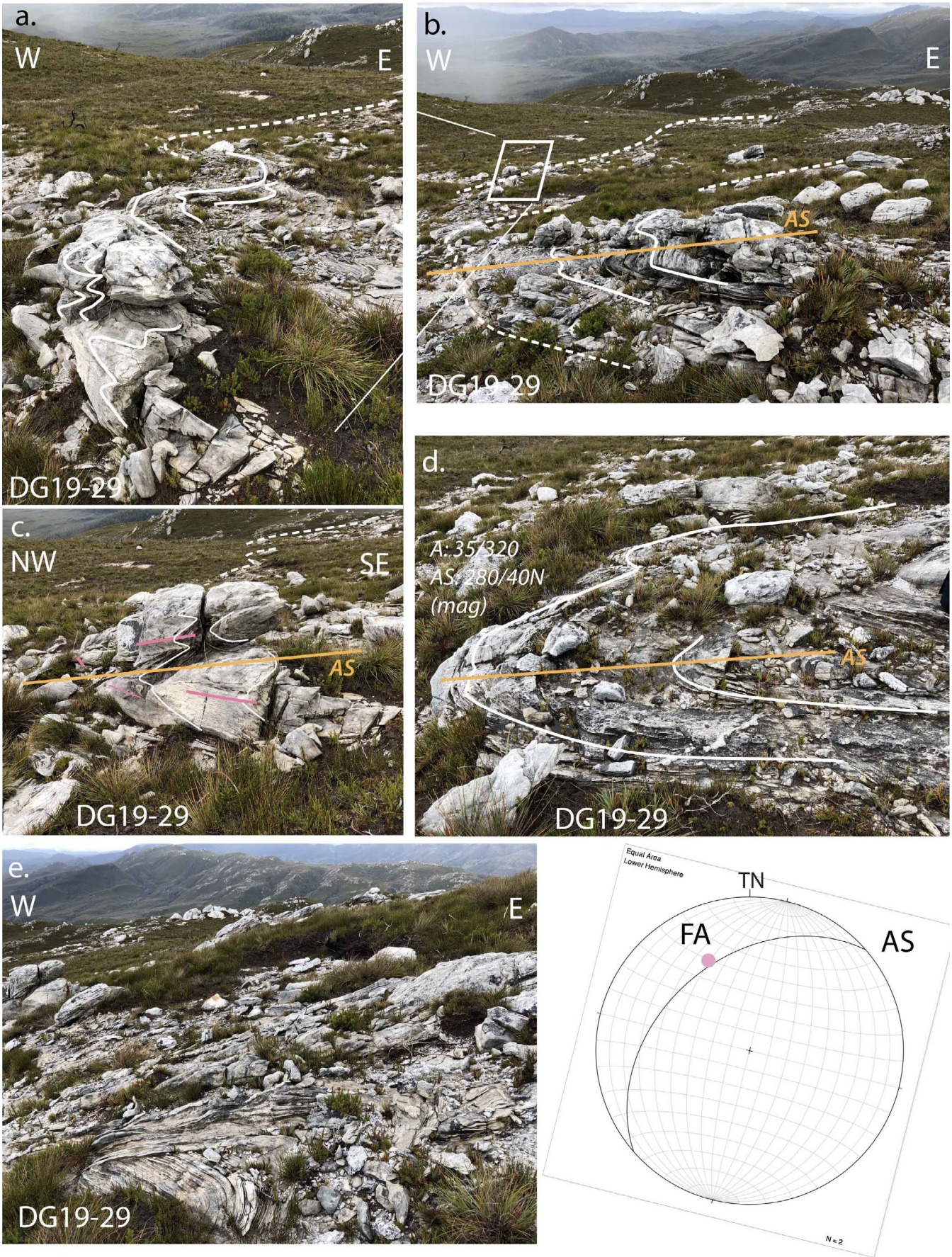

Figure 32. Ridgeline series of northwest-plunging, reclined to recumbent isoclinal folds at DG19-29 within the core of a larger west-closing macro-fold (see Figure 30b). a), b), c) and d) show the hinge geometry of sub-rounded to sub-angular fold noses. Foliation So/Sm formline traces are white and dashed white lines. Fold axial surface traces are orange line traces. The stereonet inset shows axial surface great circle and fold axis FA (pink dot). e) Pseudo cross-bedding created by complex fold form (lower right) with hinge pinch-out to the west (on left) within the core of the fold. These folds are within high-strain platy quartzite.

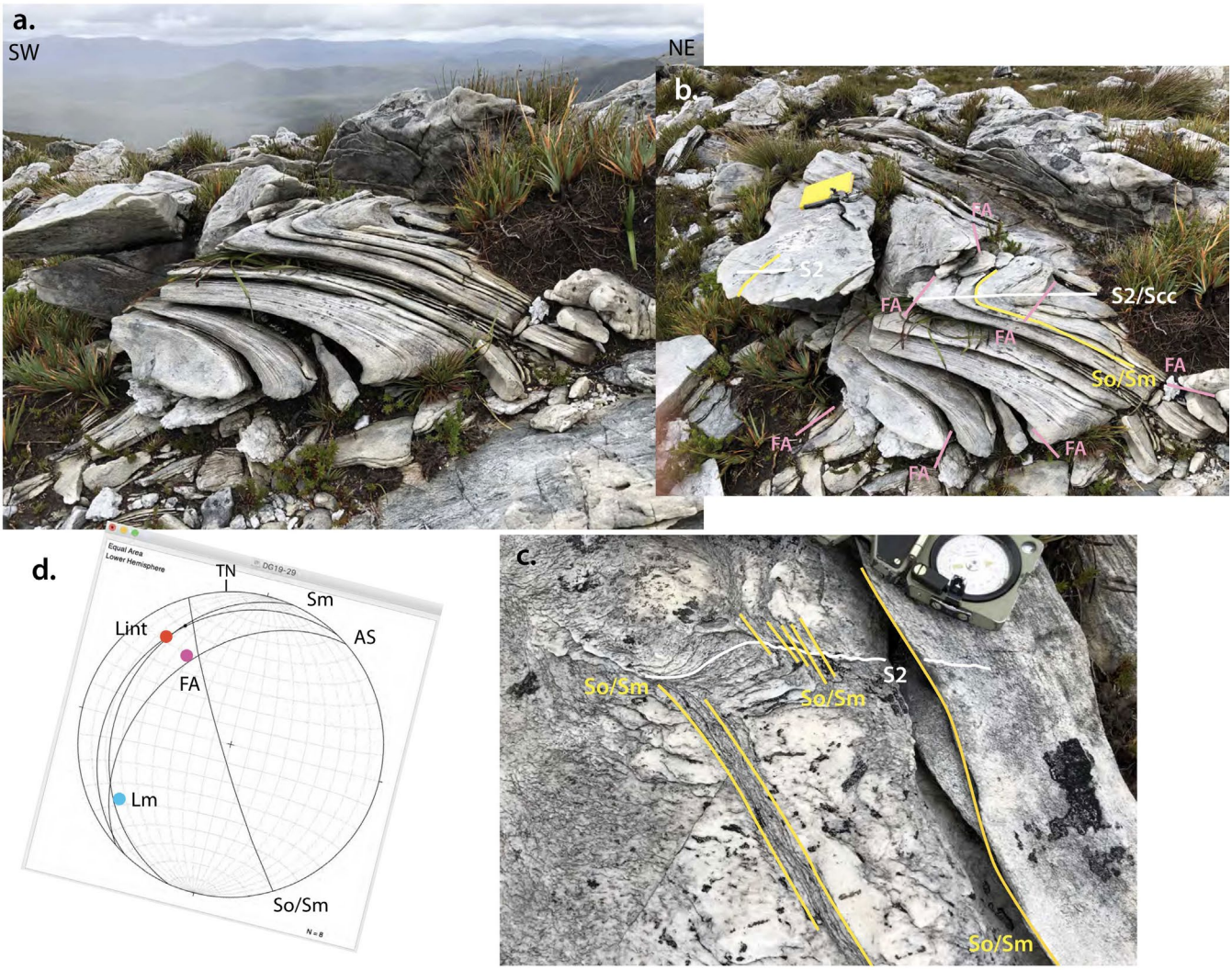

Figure 33. Reclined folds in intensely foliated, platy quartzite on ridgeline at DG19-29. a) Profile view of fold train bounded and truncated by high strain zones. b) Fold axis variation (FA: pink line traces) through fold train. Upper bounding platy mylonitic quartzite is shown through sedge grasses on middle right. Crenulation cleavage (S2/Scc) is axial surface fabric to folds. c). Oblique view of foliation-banding So/Sm in quartzite in one of the fold hinges with the crenulation cleavage S2 (white line traces) showing refraction across So/Sm.

3.6.3 Inner Shell or Sheath-core

The core of the De Witt-Propsting mega-fold is poorly exposed through the grassy hills of the Castle Hill-Upper Castle Hill ridgeline and the ridgeline flanking the De Witt River on the southwest (Figures 34 and 35). The outcrops are patchy and generally consist of weathered quartzite fragments and the occasional outcrops and part strike belts of quartzite that do provide windows into the larger structure. The trends of these ridgelines and apparent closures within them suggest a complex fold interference truncated by the sub-vertical Giblin River Valley Fault (Figure 35). The mega-fold core consists of a series of refolded macro-isoclines that can be seen in the air photo base maps (Figures 35 and 36a) and photos of the flanks of the ridges (Figures 37, 38 and 39).

Associated with the isoclinal macro-folds visible in the flanks of the ridgelines is a complexity of mesoscopic refolding and overprinting fabrics that detail the complicated history of the De Witt-Propsting Inner Shell. Mesoscale overprinting relationships show zones of crenulation cleavages with relicts of three isoclinal folding events (Figures 40 and 41). Hinge zones of the isoclinal folds preserve multiple sets of overprinting crenulation cleavages Scc1 and Scc2 (Figures 40c and 41c) with a third set Scc3 subparallel with the dominant foliation Sm (orange traces Scc2). This axial surface Scc3 transitions into fold limb zones dominated by intense foliation Sm that is subparallel with the original compositional layering So/Sm.

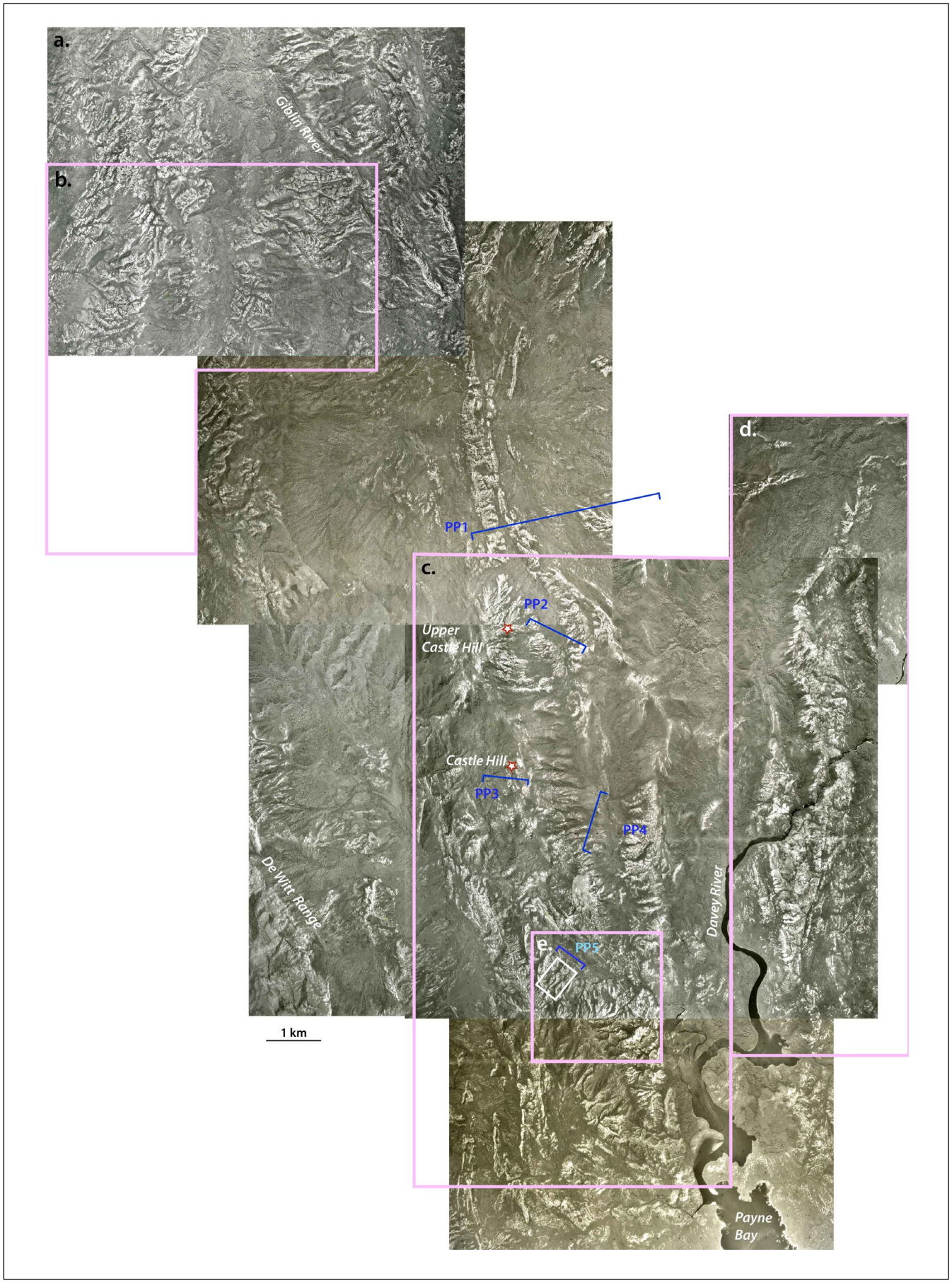

Figure 34. Internal architecture of the De Witt-Propsting mega-sheath fold shown in an air photo base stitch-image. Pink rectangles show the positions of air photo enlargements in other figures. b) Outer to Middle Shell folded zone (Figure 29a). c) Inner Shell along the Castle Hill-Upper Castle Hill ridgeline (Figure 35). d) Davey River nose air photo base (Figure 50). e) De Witt River air photo base (Figure 36a). The blue line segments with barbs are the positions and photo direction of the photo profiles. PP1: Photo profile across the Giblin River Valley to Upper Castle Hill (Figure 39). PP2: Photo profile of Upper Castle Hill ridgeline (Figure 38). PP3: Photo Profile of Castle Hill looking north to Upper Castle Hill (Figure 43). PP4: Photo profile of ridgeline below Castle Hill (Figure 37). PP5: Photo profile of ridgeline above the De Witt River (Figures 36a and b).

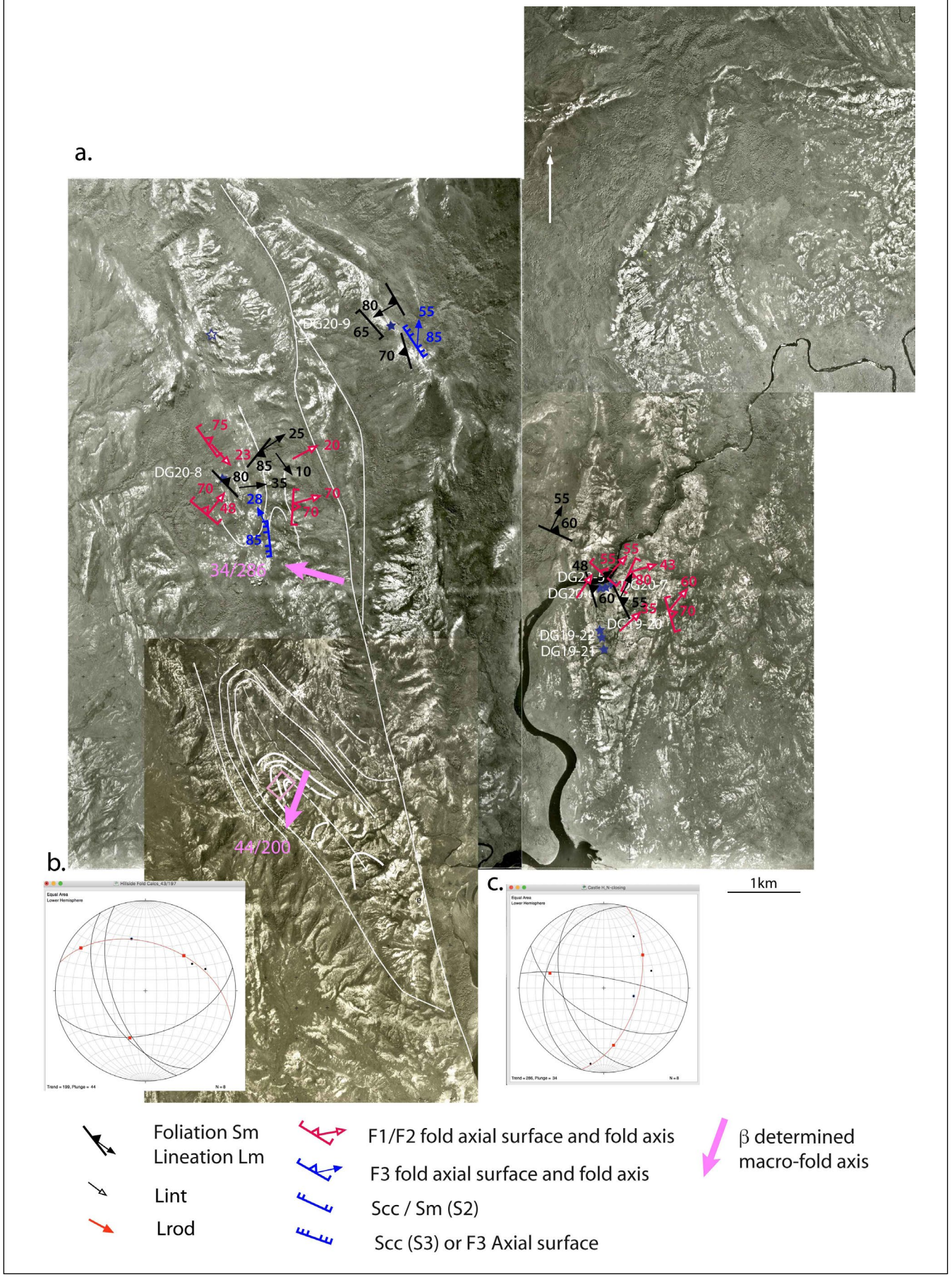

Figure 35. Structural data shown on air photo-stitch base of the Inner Shell of the De Witt-Propsting mega-sheath fold and the Davey River fold system as the nose of the mega-sheath fold. Formlines in So/Sm are shown by fine white line traces. The continuous white line trace: Giblin Valley-Payne Bay Fault trace. b) Stereonet with β axis determination (44°/200°) of the reclined macro-fold exposed in the hillside south of the Giblin River (Figure 36c). c) β axis determination (34°/286°) of the inclined plunging macro-fold in the Castle Hill ridge line (Figure 37).

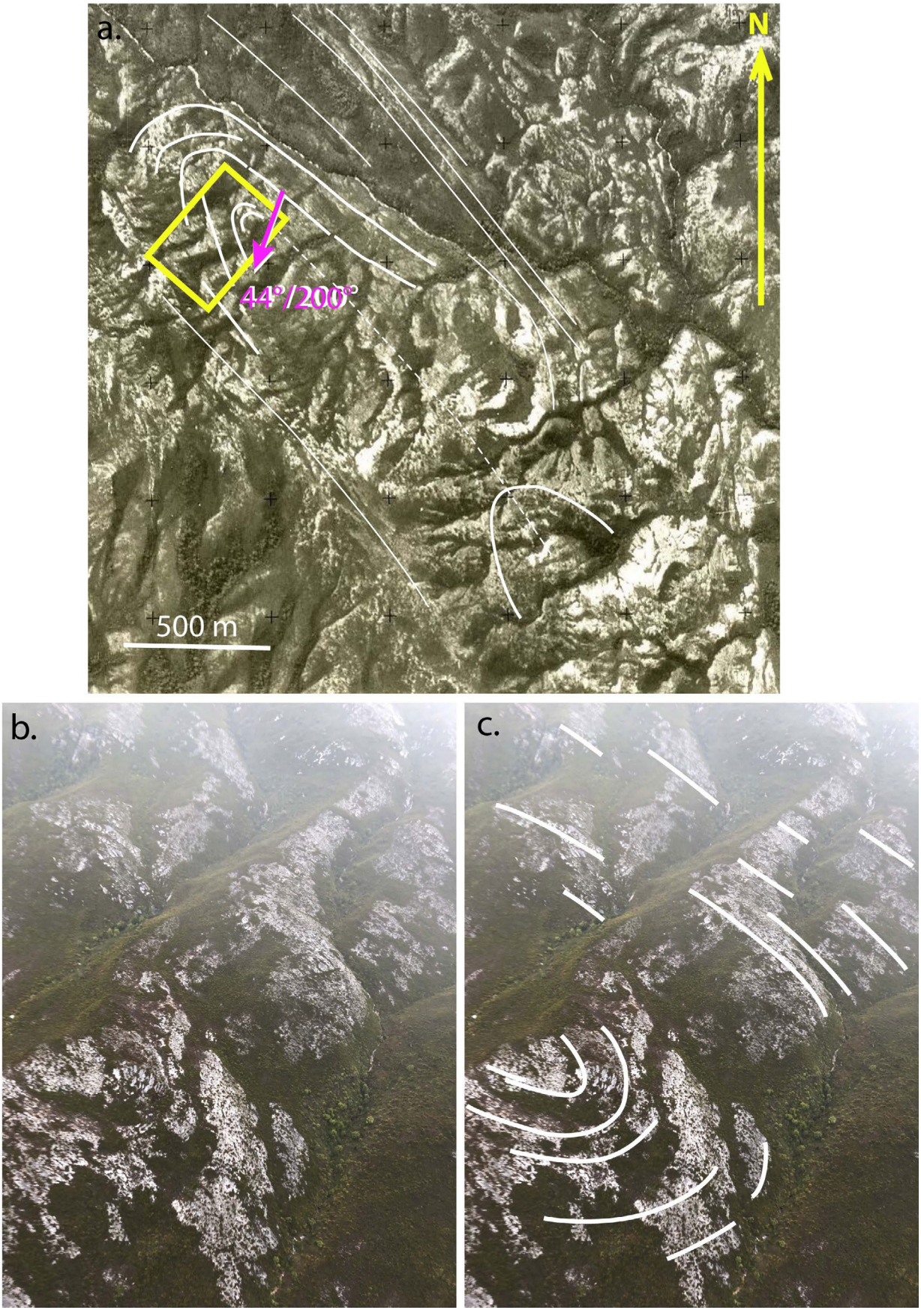

Figure 36. Southeast part of the core of the De Witt-Propsting mega-fold in weathered quartzite ridgeline south of the De Witt River. Photo profile PP5 shown on Figure 34. a) Formline traces on ridgeline showing north-closing recumbent macro-fold hinge. Using strike traces and apparent dips from the ridge-oblique photos the estimated macro-fold axis (β axis shown by the pink arrow) is 44°/200° giving the macro-fold an inclined, plunging to almost reclined geometry. b) Aerial view of the fold hinge in the side of the ridgeline with interpreted So/Sm formline traces (white lines) defining the hinge shown in (c). Note the helicopter flight path was northwards along the De Witt River with this photo looking to the southwest onto the ridgeline. The photo appears close to a profile view indicating that the macro-fold hinge is plunging to the south or southwest.

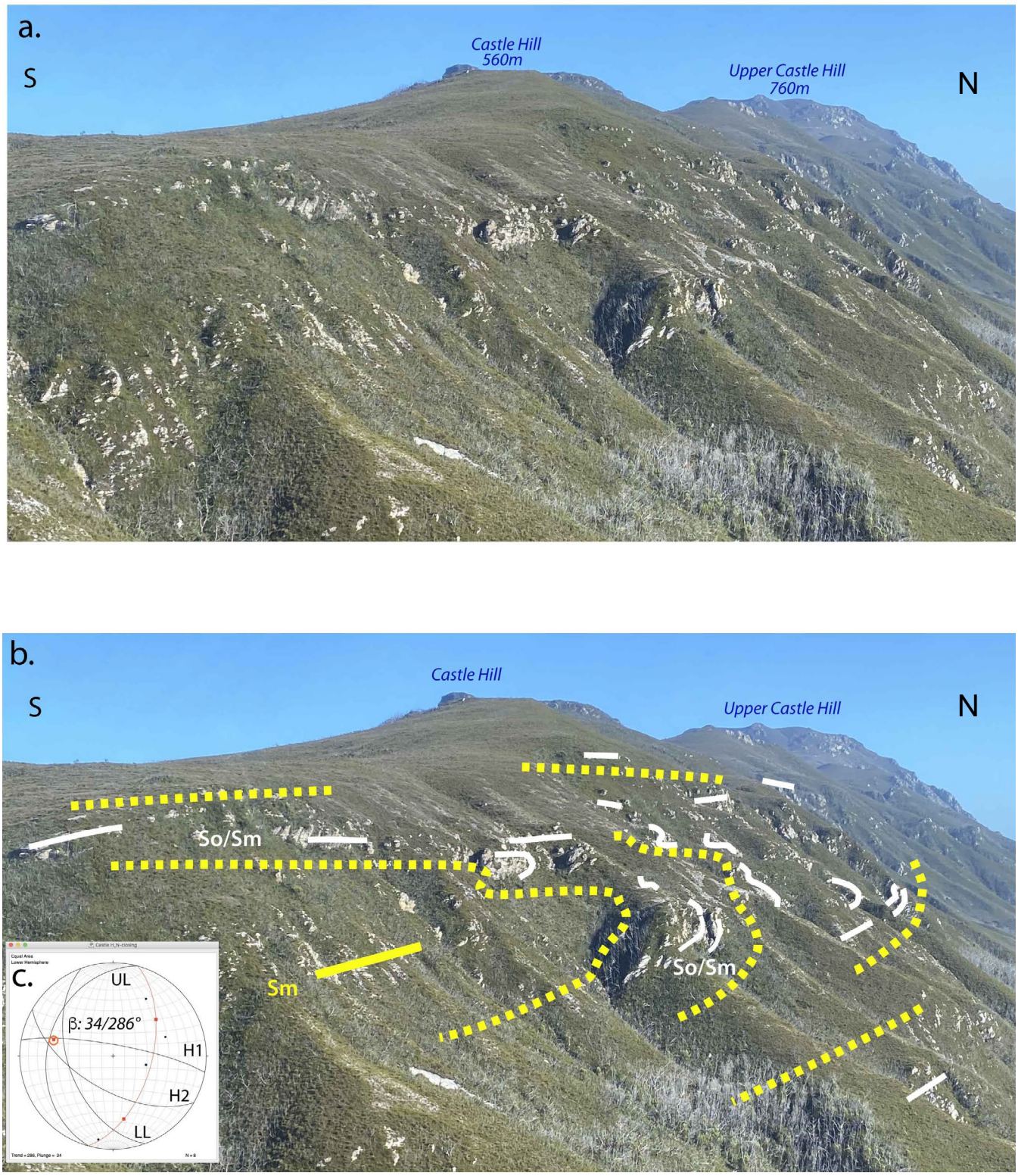

Figure 37. Oblique helicopter-aerial photograph of the eastern flank of the Castle Hill-Upper Castle Hill ridgeline. Photo profile PP4 shown on Figure 34. a) Castle Hill-Upper Castle Hill ridgeline photograph with b) showing an apparent, north-closing, recumbent isoclinal-macrofold. Yellow dashed lines are the interpreted formlines defining the macro-fold hinge based on extrapolation of the interpreted outcrop traces (white lines). c) Stereonet showing β axis of 34°/286° based on estimated dips of the upper limb (UL), lower limb (LL) and hinge segments (H1 and H2). Air photo outcrop traces were used to give strikes whereas dips were estimated from apparent dips in the oblique hillside photo (a).

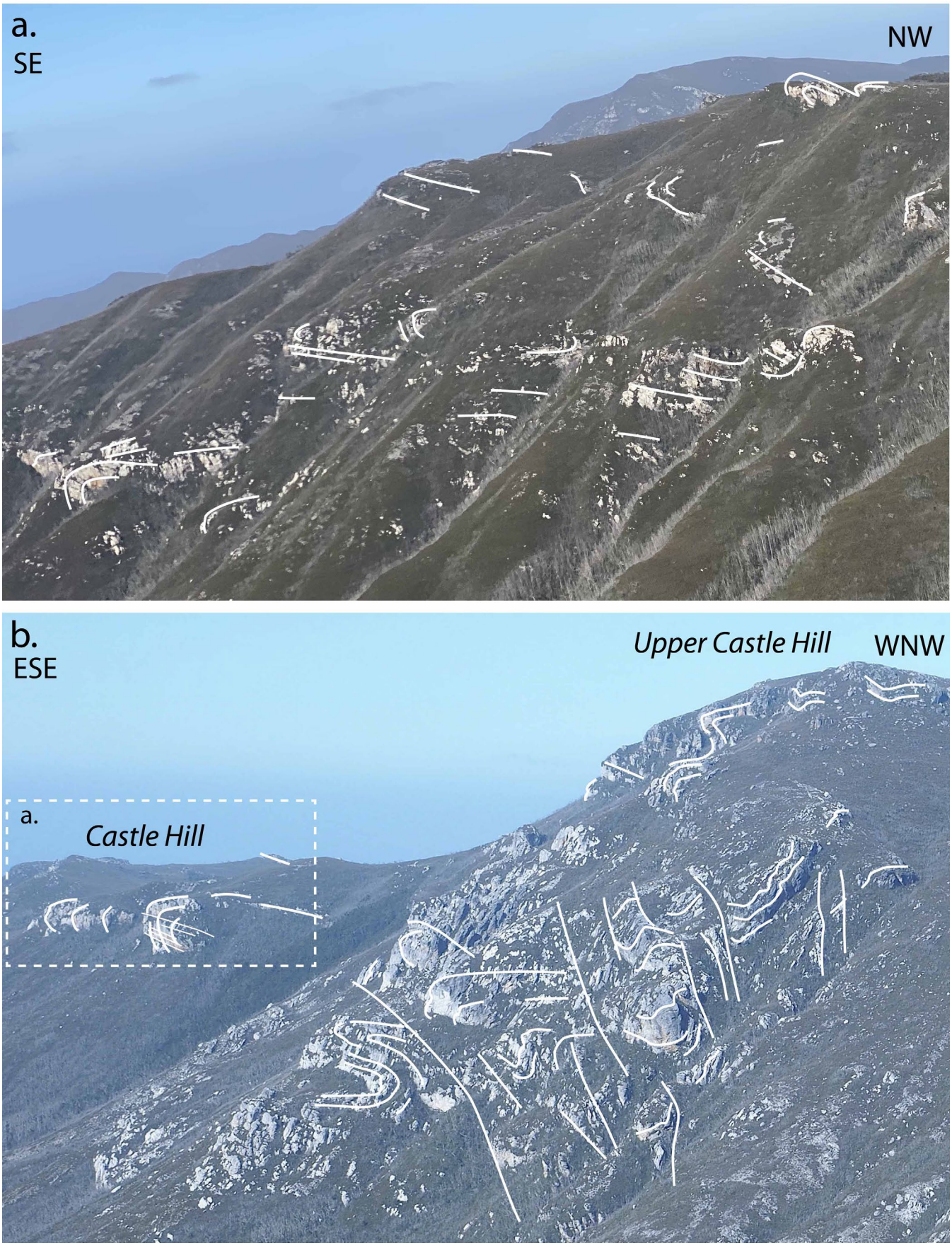

Figure 38. Castle Hill-Upper Castle Hill ridgeline photographs looking to the south with formline traces in compositional banding So/Sm depicting macro-fold hinges within the Inner Shell or core of the mega-sheath fold. Photo profile PP2 with location shown in Figure 34.

a) Enlarged view of hillside between Castle Hill and Upper Castle Hill showing the continuation of the north-closing fold hinge in Figure 37. The photo location is shown by the dashed box in (b). b) Oblique view of ridgeline below Upper Castle Hill showing a series of fold-closures cut by steep, west-dipping reverse faults.

Isoclinal folds with axial surface crenulation cleavage Scc2 and Scc3 show curvilinear fold hinges and classic sheath-folding with small scale sheath lobes or tongues extending subparallel to the stretching lineation Lm (Figure 42). Structural data presented in stereonet form (lower stereonet inset, Figure 43) suggests an early isoclinal fold set with a gentle east-dipping axial surface is refolded by another isoclinal fold set with steep plunges and steeply east-dipping axial surfaces (Scc2). These relationships change through the Castle Hill outcrop (Figure 34) as the early isoclinal folds are refolded by open, upright, gently-north-plunging chevron folds with axial surface Scc (Figures 40a, 41a and 43). This upright set of open folds dominates the structure of the Castle Hill-Upper Castle Hill ridge crest (Figure 43 and 44).

The relationships discussed for the Castle Hill outcrop are presented in a structural profile across Castle Hill (Figure 44a).

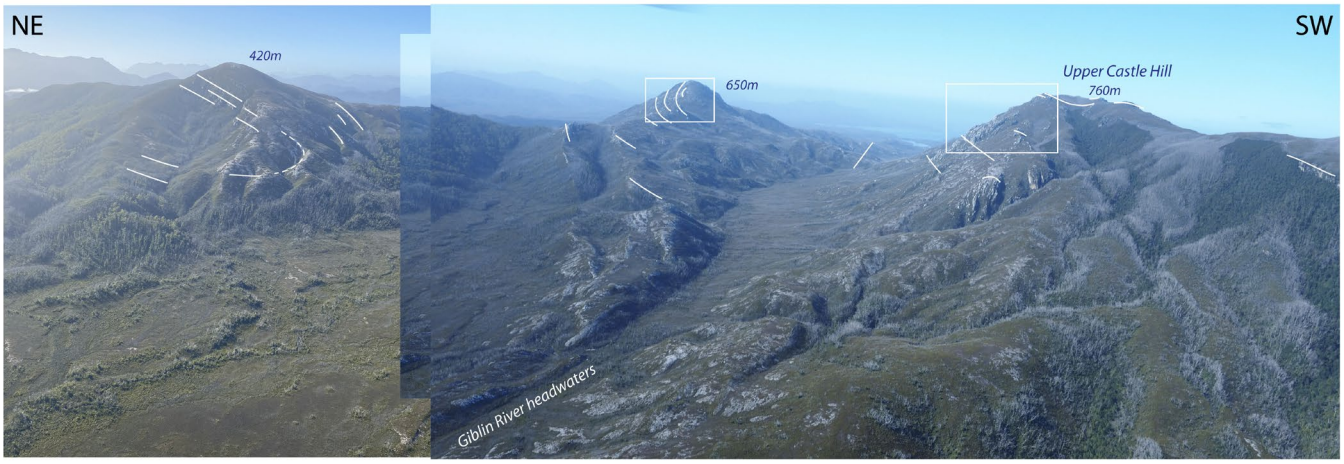

Figure 39. Ridgeline profile through Upper Castle Hill (on right) showing recumbent isoclinal macro-folds. Photo profile PP1 with location shown in Figure 34. The aerial view is to the southeast towards Davey River Gorge. The profile consists of a west-closing macro-fold on right with an east-closing macro-fold in the centre. White rectangles are parts of the fold train highlighted in Figures 38 (rectangle on right) and 45 (centre rectangle).

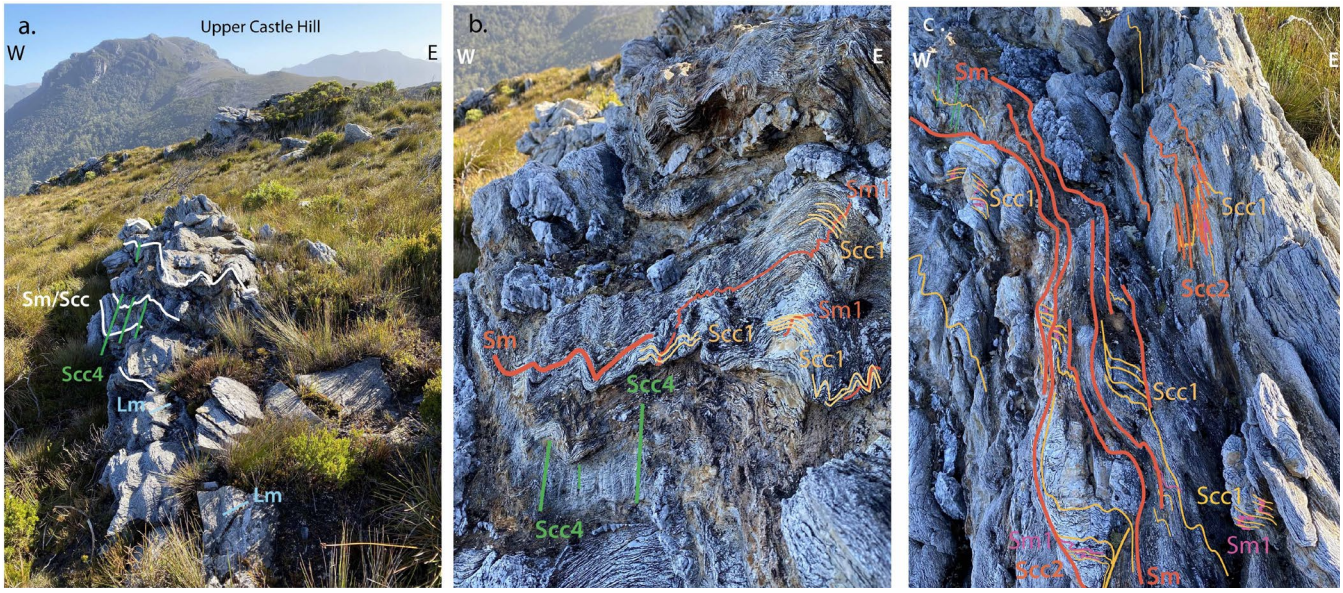

Figure 40. Castle Hill multiple fabrics typical of transposition cycling with development of crenulation cleavages Scc1 (thin orange lines) and Scc2 (light pink lines) at low angles to the composite dominant foliation Sm (heavy pink lines) all refolded by upright chevron folding with a weaker crenulation cleavage Scc4 as axial surface foliation (green lines) (compare with Figure 43). Sm1 (thin pink lines) the initial foliation is preserved in the Scc1 and Scc2 microlithons. a) Chevron folded Sm/Scc (white line traces) with Upper Castle Hill in background ridgeline. b) Relationships between the multiple fabrics. c) Limb zone of second-order late chevron fold showing discordance and refolding of Scc1 by Scc2 with Scc2 essentially sub-parallel to the dominant foliation Sm. This layering constitutes the So/Sm (white lines) sub-parallel with Sm (yellow dotted lines) in the general view of the Castle Hill outcrops shown in Figure 43.

Figure 41. a) Rollover in Sm from moderate east-dip (photo centre) to gentle west-dip (photo right) as part of larger hinge zone in the Castle Hill outcrop (see Figure 43). The enlargements b) and c) show the composite nature of the dominant foliation Sm in the Castle Hill outcrops. The dominant Sm is sub-parallel with the axial surfaces of the isoclinal folding event that folds both Sm1 (pink line traces) and Scc2 (white line traces) and relates to Scc3 (orange traces), suggesting the isoclinal folds represent a third phase of isoclinal folding. Hence the Scc3 (thin orange lines) is sub-parallel with Sm (thick orange lines) particularly shown in (c).

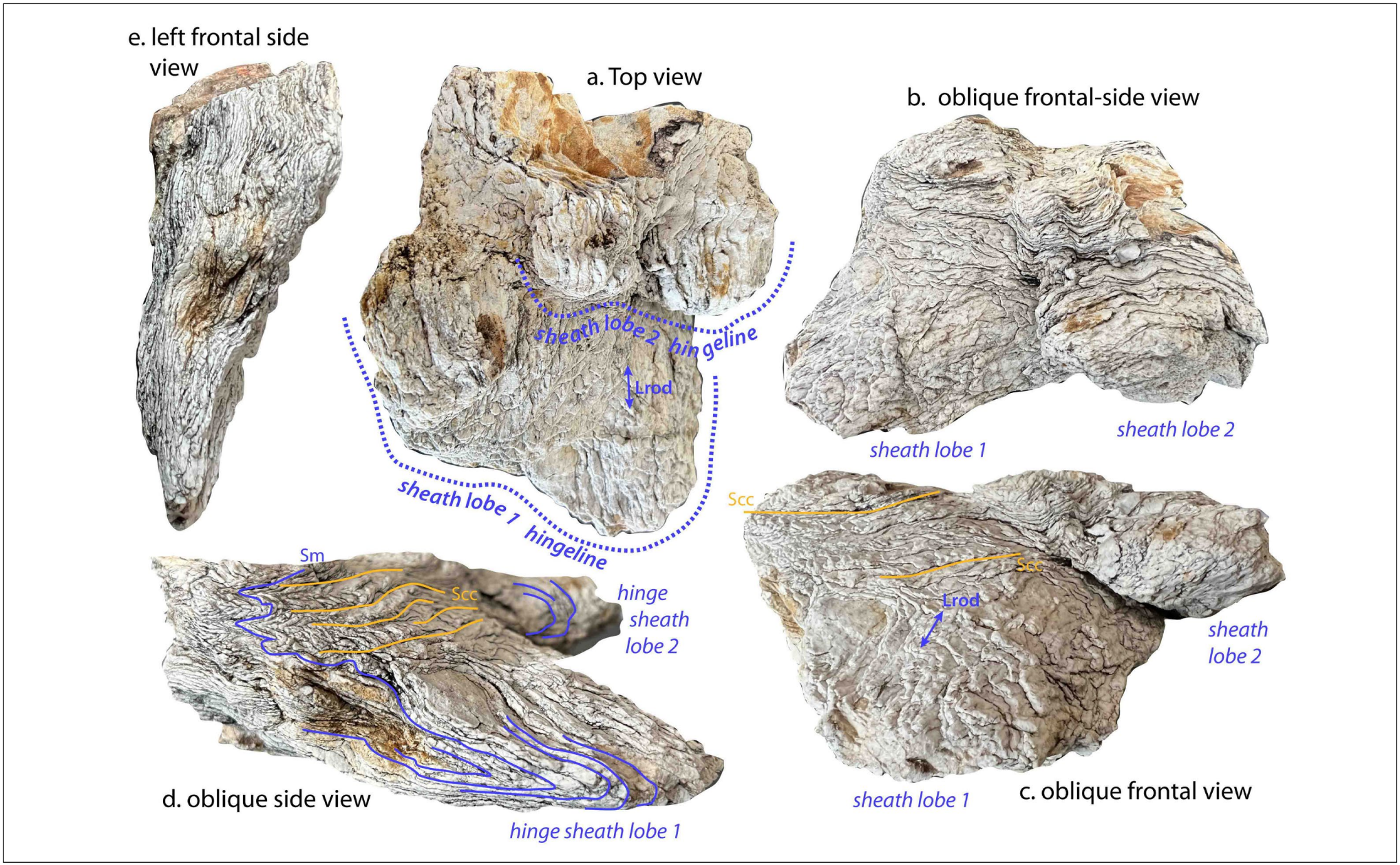

Figure 42. Mesoscopic sheath-fold sample in transposed quartzite layering showing two sheath-lobes both with axial surface crenulation cleavage Scc2. a) Top view showing the sheath lobes labelled 1 and 2 with hingelines depicted as blue-dashed heavy lines. b) and c) are oblique frontal-side and frontal view respectively. d) Oblique-side view of lobe 1. e) Left-frontal side view (profile) of sheath fold 1.

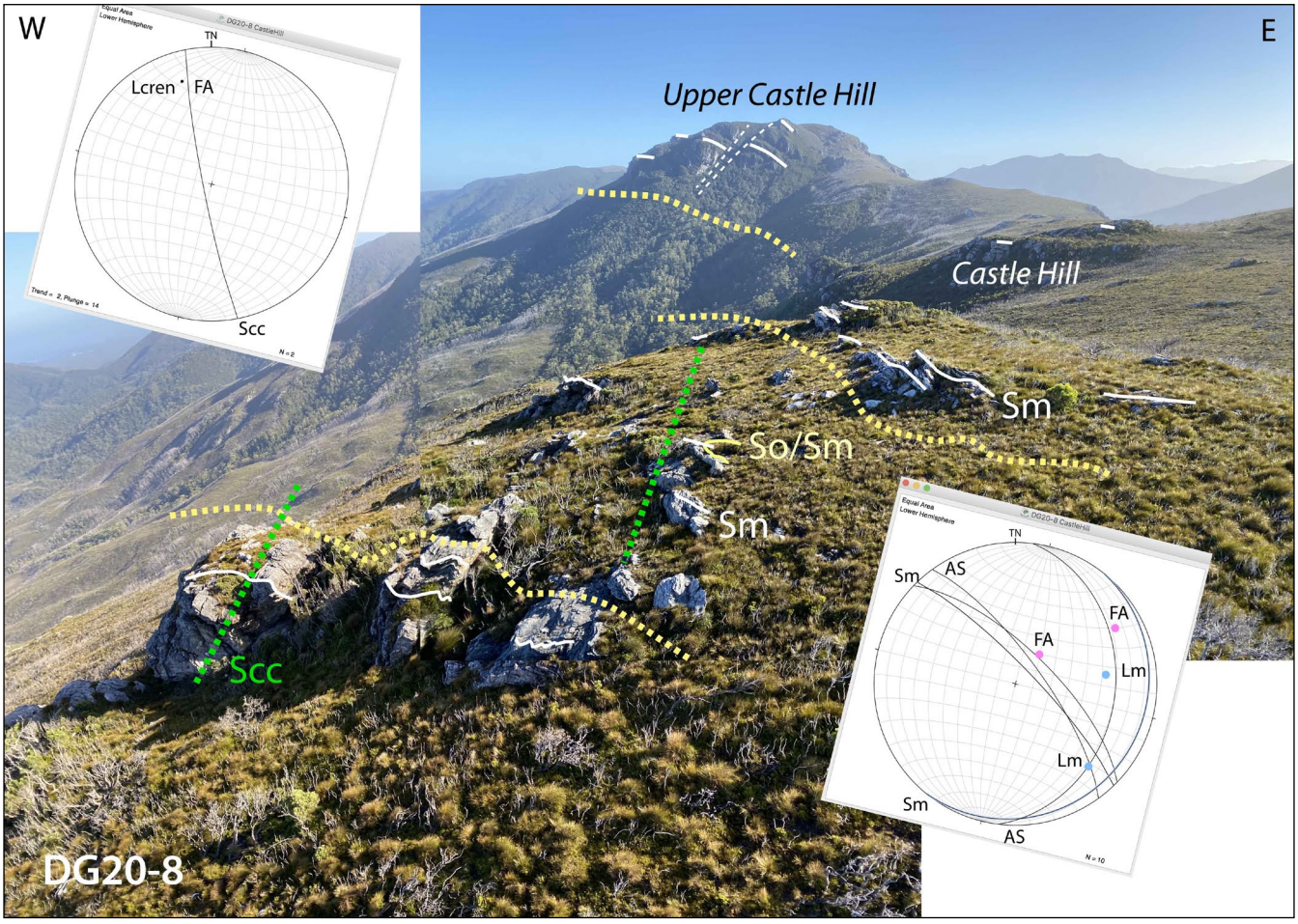

Figure 43. Aerial helicopter view of the west flank of Castle Hill looking north to Upper Castle Hill. The dominant foliation Sm traces are shown by white lines, with the generalised structure shown by the dashed heavy yellow lines. The attitudes of the overprinting Scc and axial surface of the accompanying chevron folding, is shown by the green dashed lines. The upper left stereonet shows the attitude of the Scc as a steeply west-dipping great circle trace and a gently north-plunging fold axis (FA) and Lcren trend. The lower right stereonet shows the Castle Hill structural data at station DG20-8, with Sm and meso-fold axial surface (AS) great circles and the fold axis and mineral lineation Lm data. Photo profile PP3 with location shown in Figure 34.

Figure 44. Sketch profiles based on oblique helicopter photographs and outcrop sketches and photographs. a) Castle Hill sketch profile A-A' with inset sketches showing outcrop structural relationships at DG20-8. Profile length is approximately 800 metres. Compare with Figure 38. b) Sketch Profile B-B' across the Giblin River headwater valley to Upper Castle Hill approximately 3 kilometres in length. Inset structural sketches show the local structural relationships at DG20-9. Compare with Figure 39.

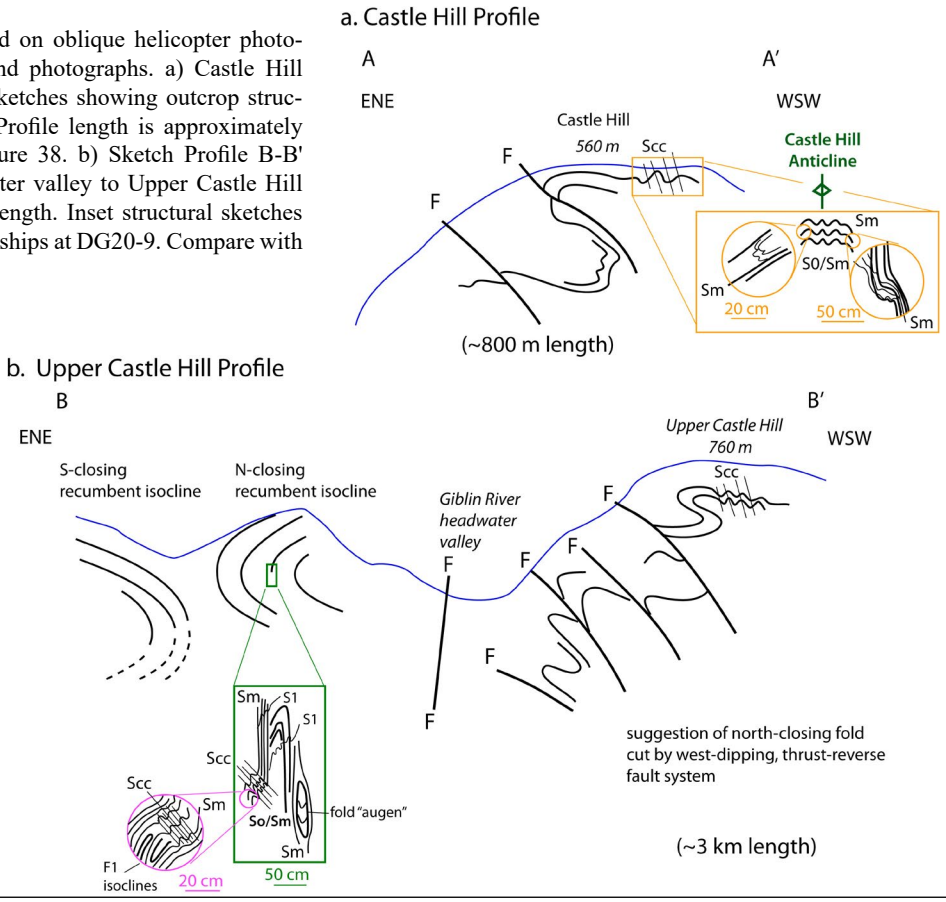

So/Sm is subvertical as part of this recumbent hinge (Figure 45) but shows tight to isoclinal folds within the So/Sm. The tightness of the mesofolds (Figures 46b, 47 and 48) and fabric relationships require this evolution to be part of the early recumbent macro-fold deformation. They are not related to the open, upright anticline within Sm shown in the frontal part of the ridge (Figure 45a). The overprinting foliations show similar relationships to those at the Castle Hill locality (station DG20-8) where an early foliation (Sm1) is crenulated by a wide spaced crenulation cleavage (Sm2/Scc2) and a localised crenulation cleavage (Sm3/Scc3). Within this intense foliation Sm are zones of mesoscopic isoclinal folds (Figures 46, 47 and 48b) that in places become isolated and enveloped by the Sm as fold pods (Figure 48a). The hinge zones of these folds show folding of the Sm2/Scc2 foliation (Figures 46c and 47c) designating the folding as third phase F3.

The intensity of deformation is shown in higher strain zones (Figure 49) that are sub-parallel to the So/Sm and essentially define the dominant Sm.

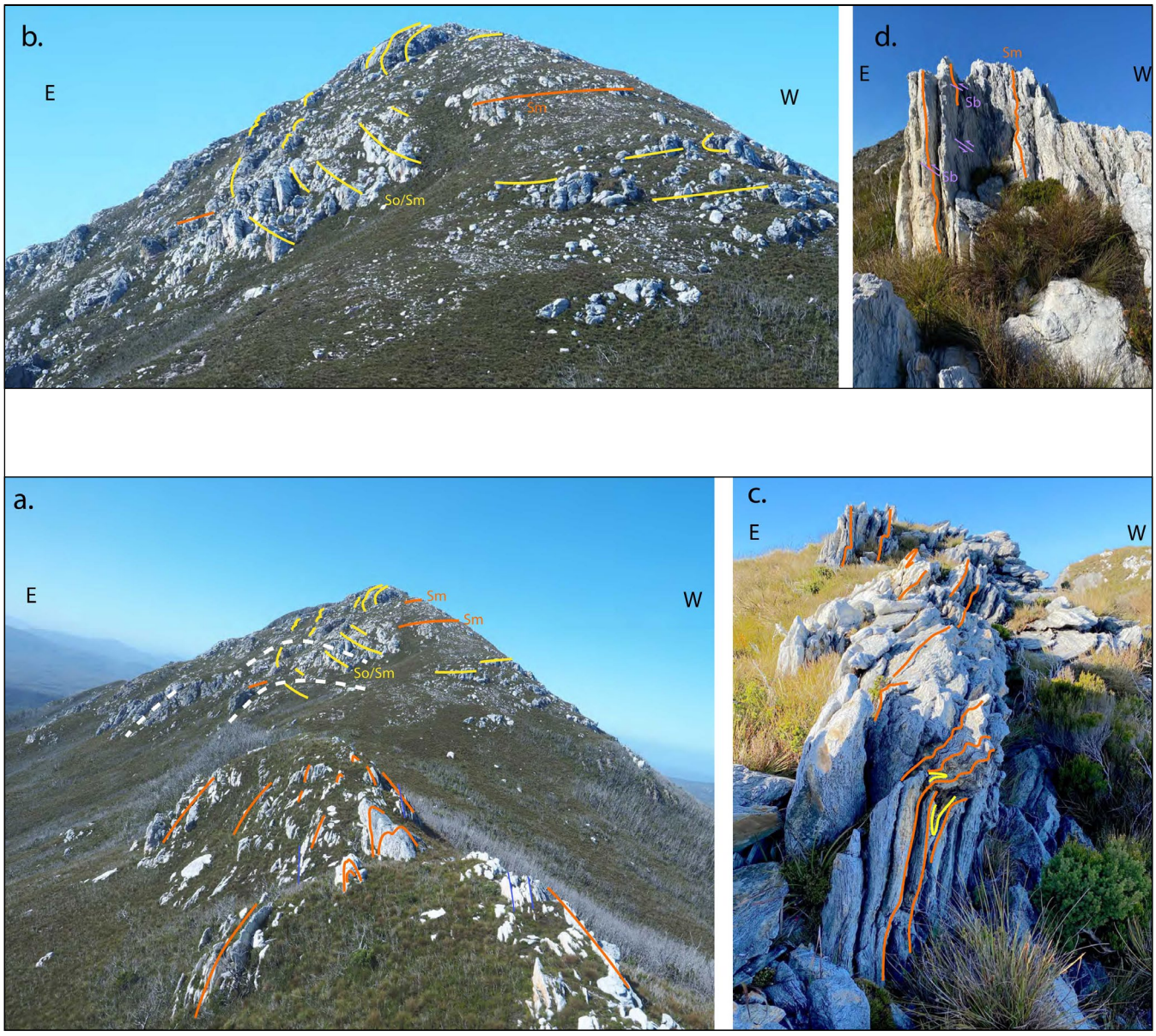

Figure 45. East-closing recumbent macro-fold in the hillside east of the headwaters of the Giblin River. a) Distant view of fold closure within So/Sm formlines (yellow line traces) with upright anticline in foliation Sm (pink line traces) in the front part of the ridge. Station DG20-9 is located in the hinge of the upright anticline. b) Closer view of the recumbent macro-fold hinge. Yellow line traces: foliation So/Sm. Pink lines: foliation Sm axial surface to recumbent macro-fold. c) and d) are outcrop photographs within the hinge zone of the north-closing isoclinal macro-fold. The axial surface foliation Sm is clearly folded and bounds relict meso-scale isoclines in So/Sm in (c). West-over-east shear bands can be seen in (d).

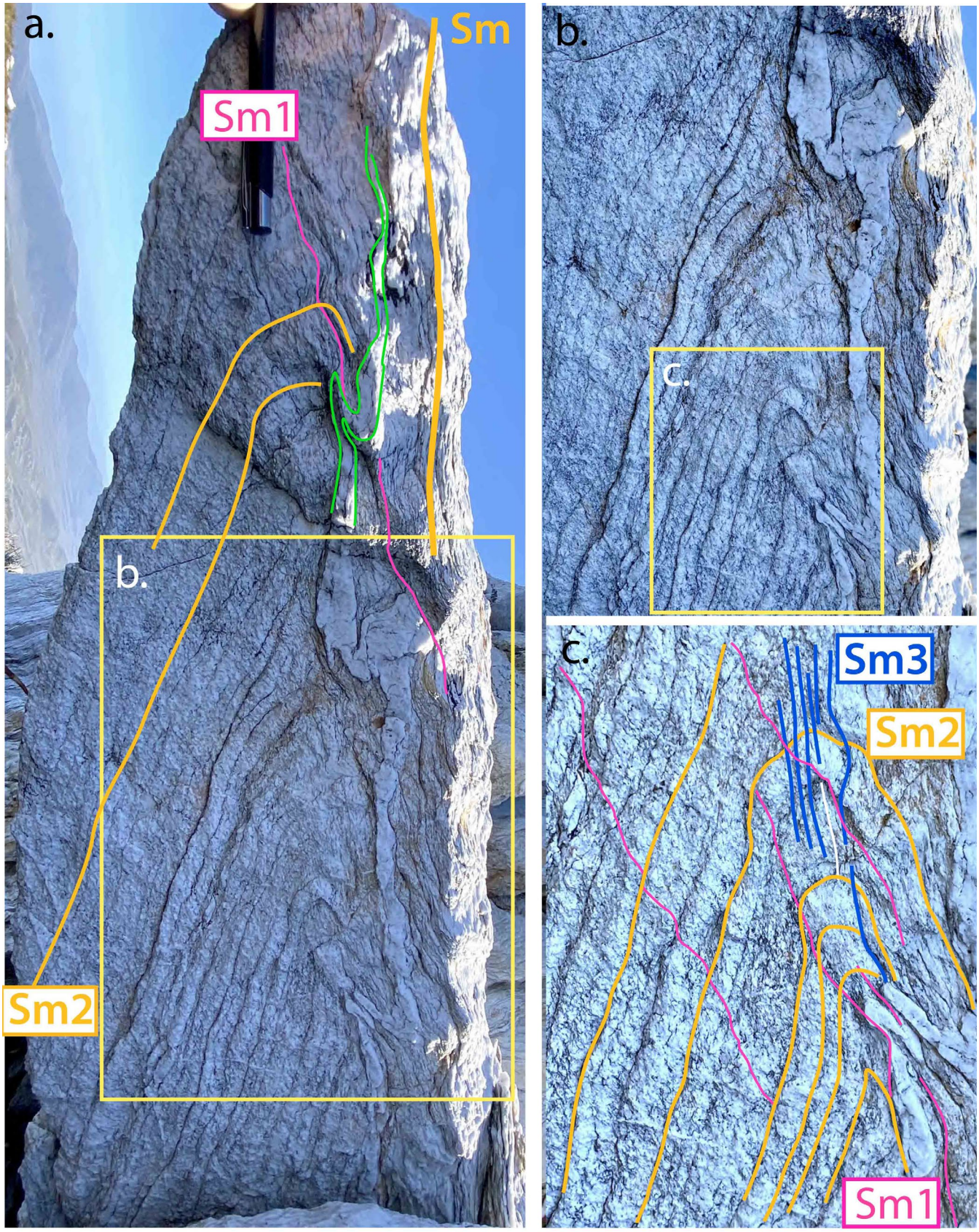

Figure 46. Upright tight to isoclinal-fold in the hinge zone of the east-closing recumbent macro-fold shown in Figure 45a. Station DG20-9.

Sm1 (pink line traces) is the axial surface foliation to the recumbent macro-fold. Sm2 (orange line traces) is a spaced crenulation cleavage (Scc2). Sm3 (blue line traces) is close spaced crenulation cleavage (Scc3) within the hinge of a tight fold within the Sm2. Note the eastern limb of this fold (right side of pillar) becomes attenuated and "strung out" such that Sm1, Sm2 and Sm3 become sub-parallel and define a dominant higher-strain foliation Sm.

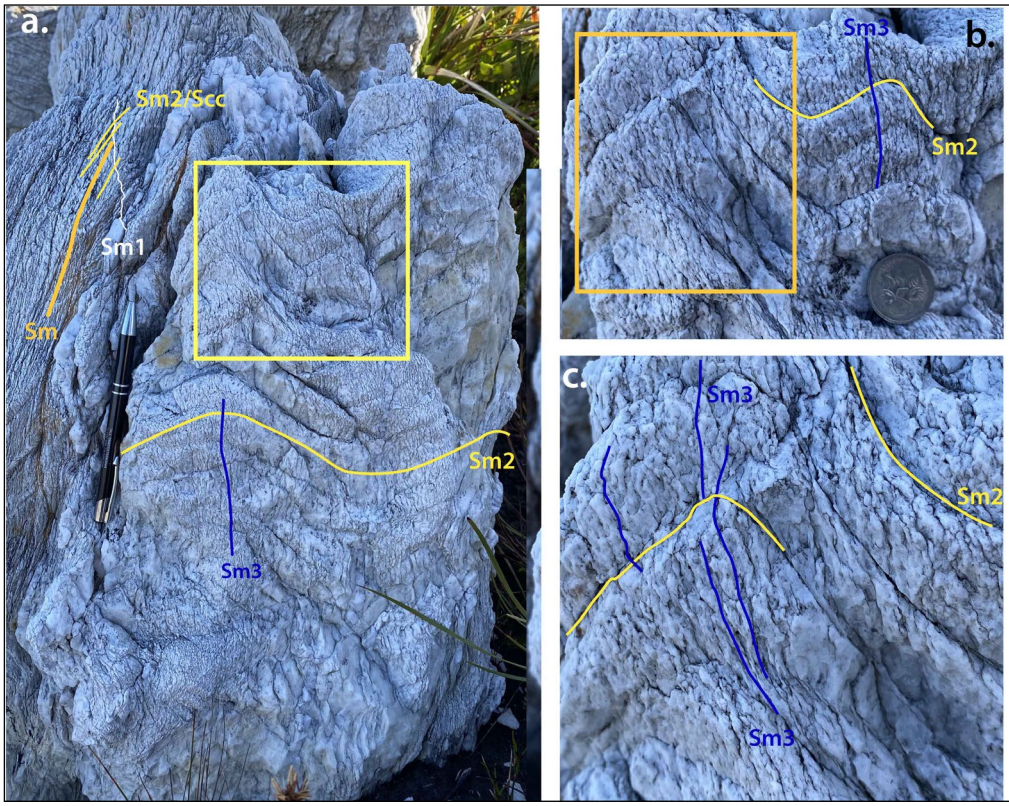

Figure 47. Upright, asymmetric fold developed within a spaced crenulation cleavage fabric Sm2 as in Figure 46c. Note the limb zones are an intense compound Sm foliation as seen in photo left in (a). b) Enlarged view of area in (a) showing the folded spaced crenulation cleavage and cross-cutting fabrics Sm1 and Sm3. Sm3 is a closer spaced crenulation cleavage fabric axial surface to the fold pair. Station DG20-9.

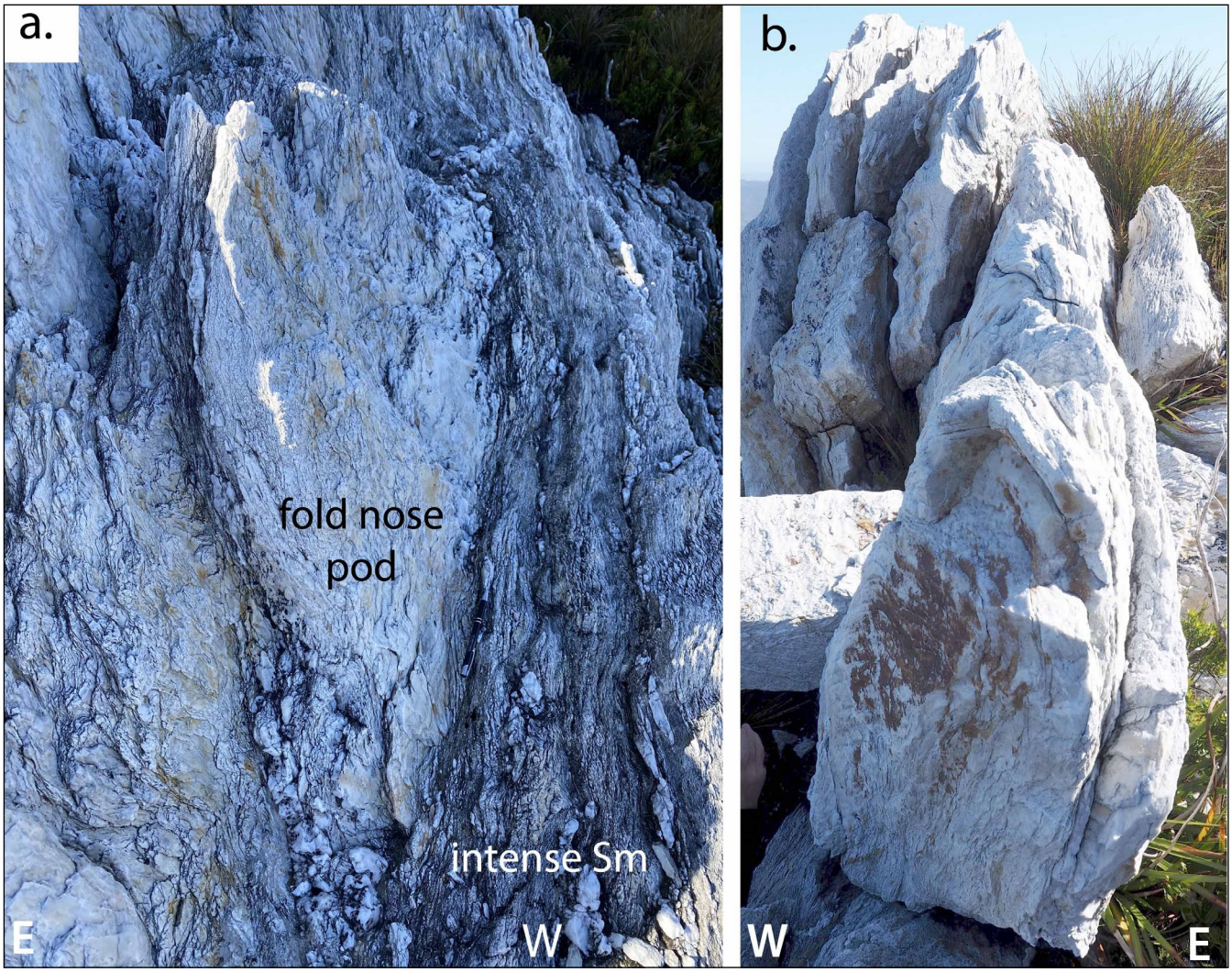

Figure 48. Varying fold geometry of the upright isoclinal folds within the macro-fold hinge (i.e. where So/Sm is sub-vertical). a) Attenuated synformal fold hinge preserved as an augen bounded by platy quartzite mylonite. b) Another profile through the antiformal isocline shown in Figure 46 showing a curving hingeline. Station DG20-9.

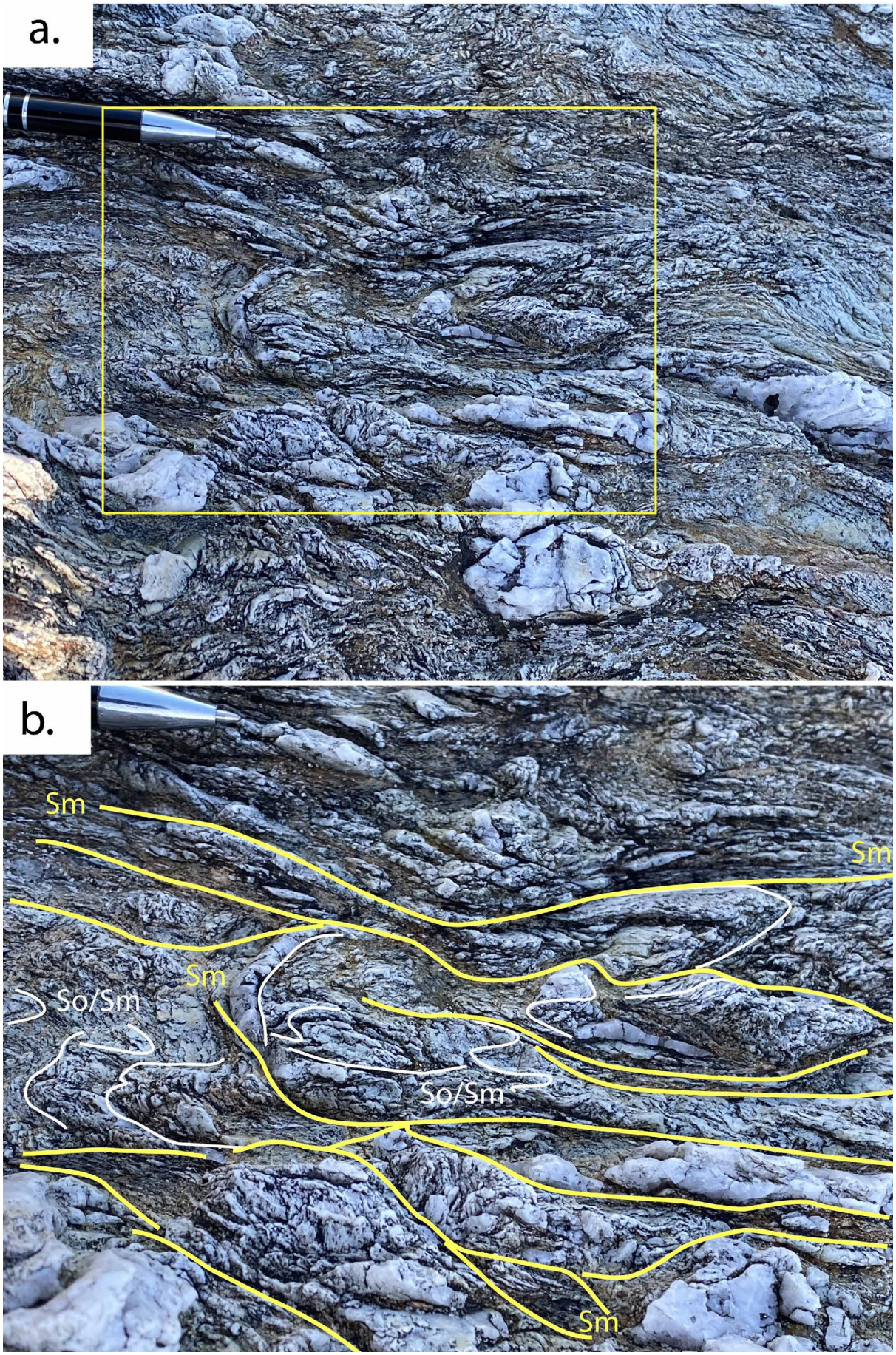

Figure 49. Plan view of sub-vertical, intense foliation Sm in a metre-scale, high-strain zone bounding the isoclinal folded zone in Figures 46 and 48. Sm (yellow line traces) is a contorted ductile-brittle fabric showing ghost isoclinal folds within So/Sm (white line traces). These have attenuated limbs that are drawn into centimetre-scale shear zones. Remnant quartz vein fold-augen and boudinaged quartz vein pods and lenses are enveloped by the intense Sm. b) is an enlarged portion of (a) shown by the yellow rectangle. Pen for scale (upper left). Station DG20-9.

4.0 DAVEY RIVER FOLD SYSTEM: EASTERN TERMINATION OR NOSE OF THE DE WITT-PROPSTING MEGA-SHEATH FOLD

The elongated S-shaped, sinuous quartzite ridge that extends from just north of Brooks Reach through Davey Gorge/Hells Gates to Davey Creek just north of the Davey-Crossing River junction (Figure 50) is overall moderately east-dipping and shows a closed-loop form with pinched, lateral fold-nose terminations (Figures 50 and 51). The form and terminations are analogous to sheath-like closures (cf. Henderson, 1981, Figure 1; Alsop and Holdsworth, 1999, Figure 2), as well as bifurcations controlled by steeply plunging F2 folds (Figure 51). These macro-folds are enveloped and overprinted by strong foliation that is transitional into or overprinted by the bounding high-strain zones.

4.1 Background

Mapping by Maclean and Bowen (1971) highlighted the Davey River area macro-structure as a series of tight to isoclinal F2 folds with sub-vertical, north-south trending axial surface and inclined-plunging geometry (Figures 51 and 52). These folded an S1 transposition foliation, occasionally containing minor F1 isoclinal folds, that is generally sub-parallel to regional lithological boundaries (Figures 51 and 52). The F2 folds have an axial surface crenulation cleavage.

Maclean and Bowen (1971, p.101) described varying fold axis orientation changes of up to 90° and fold plunge variation by as much as 60° within adjacent mesoscopic folds in individual outcrops (see Maclean and Bowen, 1971, Figure 6). They noted that these varying fold axes sat within the axial surface (i.e. defined a great circle distribution that was the generalised macro-fold axial surface).

4.2 Current Work

The structural interpretation presented here is based on 1) the mapping by MacLean and Bowen (1971), 2) limited structural data collected by BHP geologists (Hall, 1965), 3) structural observations and data collected by the authors on two helicopter visits to ridgeline south of Davey Gorge (Figure 53) combined with interpretation of 4) Google satellite imagery, 5) Tasmanian Department of Lands aerial photographs and 6) helicopter aerial photographs of the ridgeline south of Davey Gorge.

4.3 Geometry and Form of the Davey River Fold System

The Davey River fold system has a complex form and outcrop pattern defined by two sets of isoclinal macro-folds that are coaxially folded about a northeast plunging axis. The first set of isoclinal macrofolds are bounded and enclosed by high-strain, platy quartzite zones that are folded by the second set of isoclinal macro-folds. It is interpreted as the nose of the east-closing De Witt-Propsting mega-sheath fold and has a total length (unfolded) of 12.5 km (sheath 'y' dimension) and map width of 1.7 km giving a fold-thickness of 0.7 km (sheath 'z' dimension) (Figure 51).

The hook or 90° bend in the outcrop belt at the northern end (Figures 50 and 51) results from Devonian re-folding by north-south-trending, open folds (Davey Crossing Syncline). The F1 mesoscopic folds in the quartz-sericite schist hinge of the Davey River Syncline have east-west-trending, south-dipping axial surface with southwest-plunge (Figure 51).

The Davey River-Crossing River region mapped by McLean and Bowen (1971) consists of complex fold interference between the early F2 isoclines within the quartzite and the younger north-south trending Devonian folding (Figure 52). The platy quartzite has second- and third-order F2 folds that are folded by the younger north-south and northeast-trending Devonian fold sets (Figure 52).

4.4 Mineral Lineation and Fold Axis Relationships

Mesoscopic F2 fold axis data from McLean and Bowen (1971) and lineation Lm from BHP mapping are shown in Figures 51 and 52. Data collected by the authors on the ridgeline south of Davey Gorge is shown in Figure 53 and presented in stereonet form in Figures 51c, 54 and 55.

Structural data from the northern part of the ridgeline (Figure 53b) show that the early F1 mesoscopic isoclinal folds have northeast plunges within northwest-striking, northeast-dipping axial surfaces (Figures 54a, b, c and d). The axial surfaces have 50°-20° obliquity to the enveloping intense foliation Sm (Figures 54b, c and d). The fold axis data (pink dots) are either sub-parallel to (Figure 54c) or more generally lie north of the lineation Lm data (blue dots) (Figures 54b and d). The second-generation F2 folds have steeply-dipping, northeast-trending axial surfaces (AS2 in Figure 54a).

Structural data further south on the ridgeline (Figure 53c) are from or near the hinge zone of the major F2 synformal fold. Both F1 and F2 fold axes are more north-northeast plunging (Figure 54e, f and g) but again plunge north of the mineral stretching lineation Lm (Figure 54f). The dominant early-fold axial surfaces are moderately to steeply northeast-dipping with a north-northwest strike. Structural data further south on the ridgeline (Figure 53c) are from or near the hinge

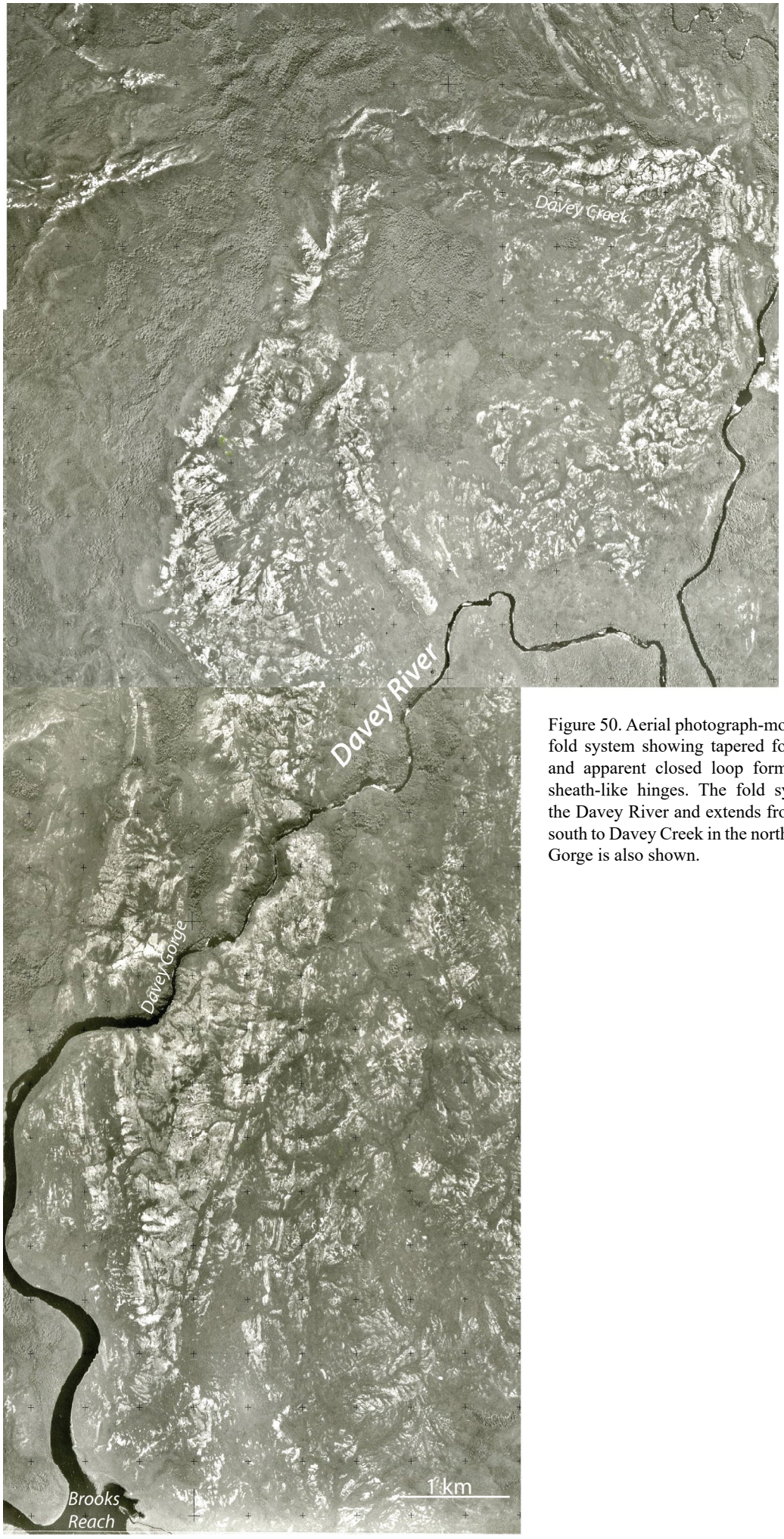

Figure 50. Aerial photograph-mosaic of the Davey River fold system showing tapered fold-closure terminations and apparent closed loop form suggestive of curved sheath-like hinges. The fold system is transected by the Davey River and extends from Brooks Reach in the south to Davey Creek in the north. The position of Davey Gorge is also shown.

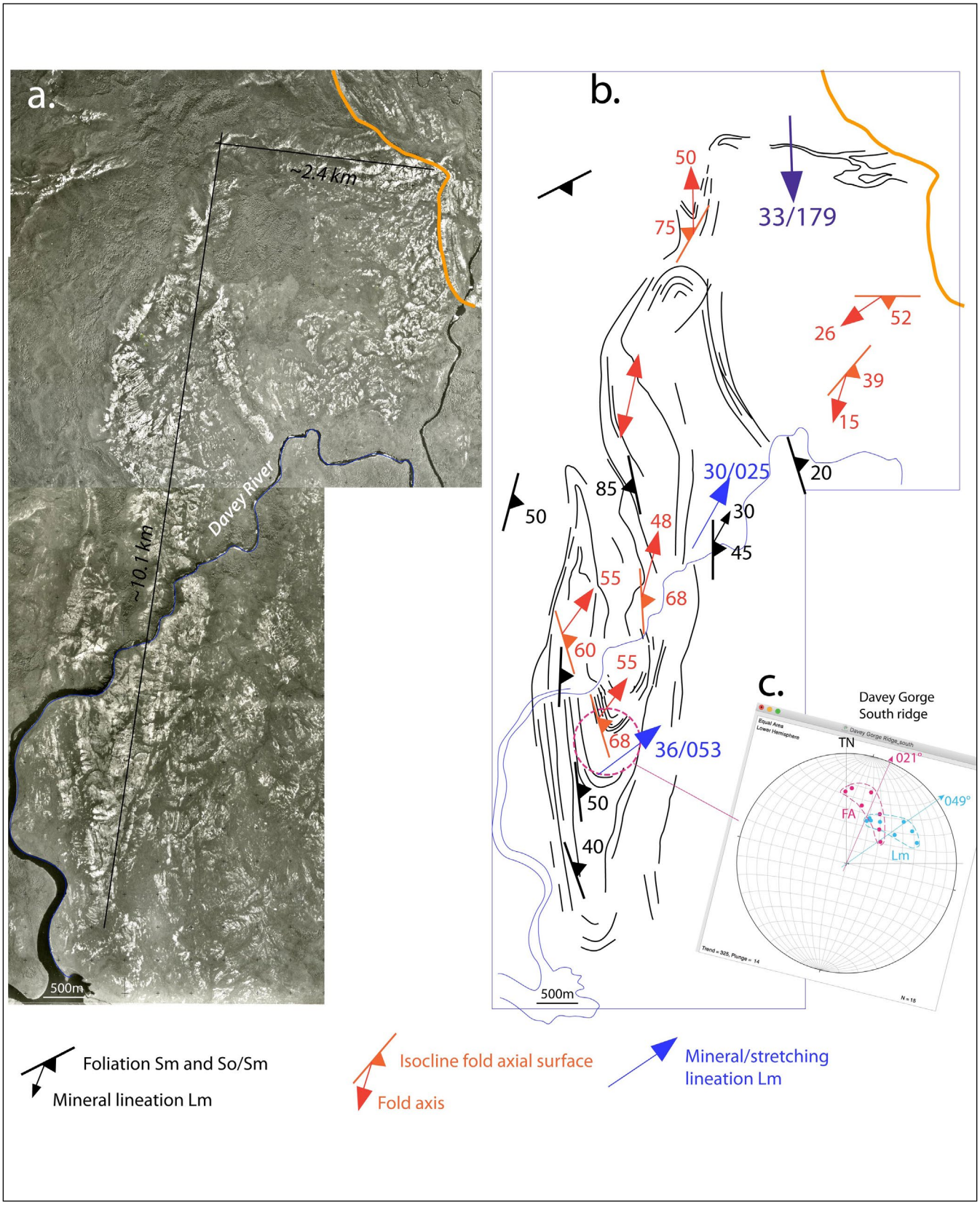

Figure 51. Davey River fold system structural relationships a) Google Earth image of quartzite with apparent closed form showing unfolded length of ~12.5km. b) Form-line map from satellite image with selected structural data, and c) Stereonet showing plotted meso-isocline fold axis FA and lineation Lm data collected by the authors on the ridgeline south of Davey Gorge. Vector mean azimuths are shown for the fold axis and lineation data (cf. Figure 55). Orange line is Palaeozoic cover.

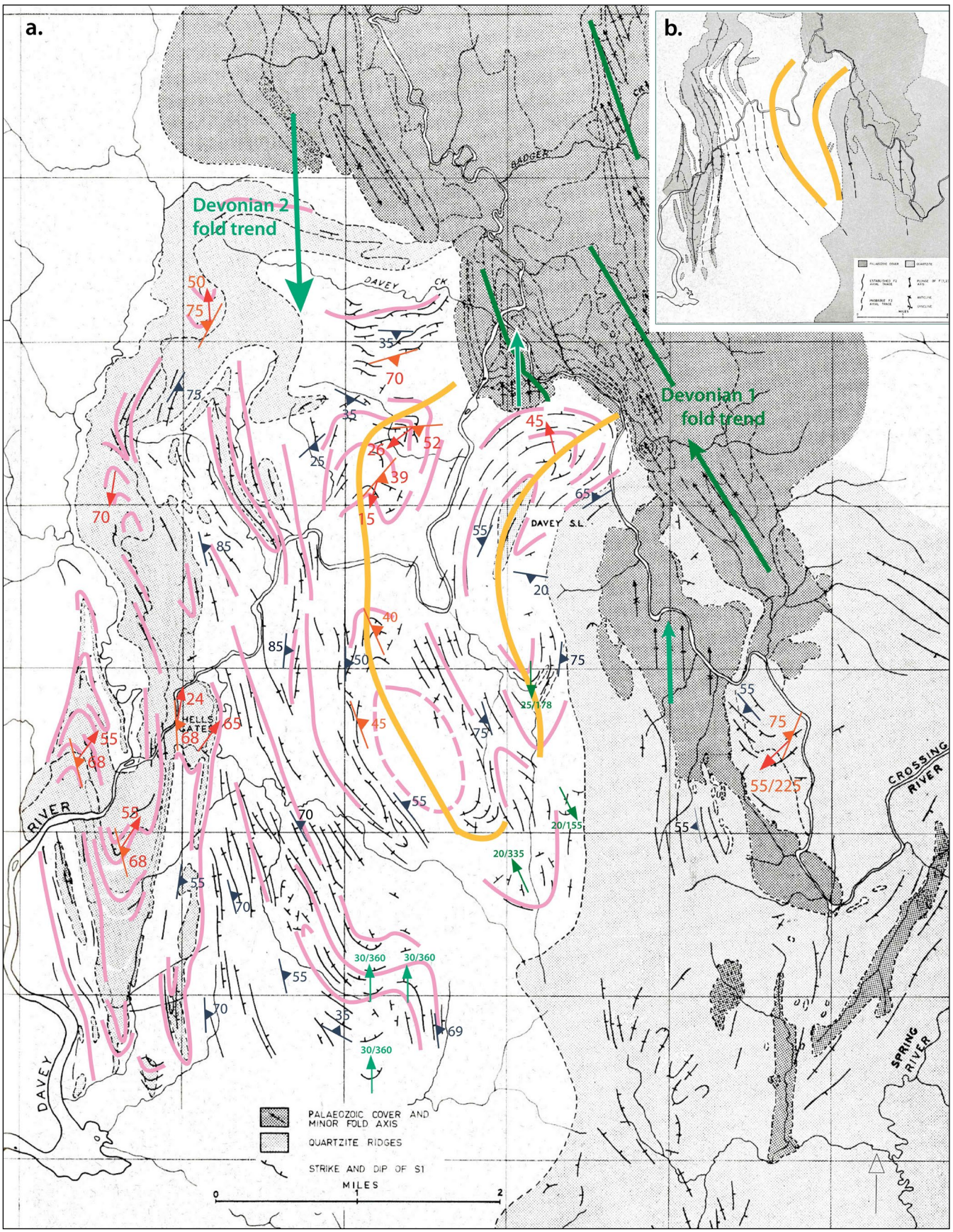

Figure 52. Maclean and Bowen's (1971) form-line structure map of the Davey River-Crossing River area. a) Formline map with formlines in transposed layering (So/Sm) and S1. The form of the banded quartzite unit is highlighted by the light grey stipple area. Darker grey stipple represents the distribution of the unconformably overlying Palaeozoic succession. White areas are platy or schistose quartzite. Early F2 fold axial surface attitudes and fold plunges are shown by red dip/strike symbols and arrows respectively. Compositional banding Sm is shown by the black strike/dip symbol. Younger Devonian fold sets are shown by the green arrows. Darker green represents the northwest-trending Devonian 1 fold set trend, whereas the lighter green arrows depict the north-trending Late Cambrian - Devonian 2 fold set trend. b) Inset top right shows general geometry of F2 fold axial surface traces.

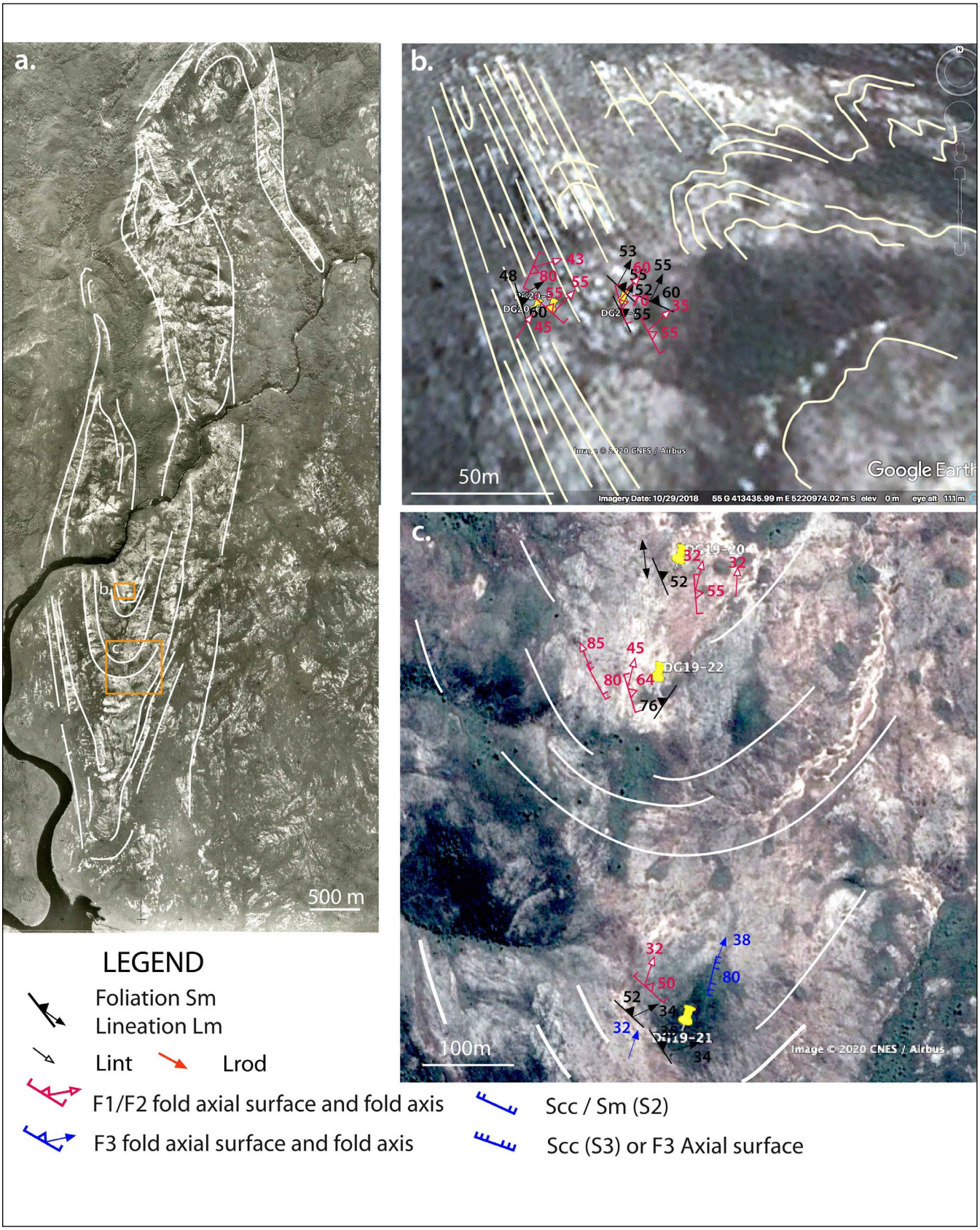

Figure 53. Davey Gorge complex fold system showing fold-nose hooks and apparent closed loop form. The orange rectangles are the regions highlighted in (b) and (c) for structural data collected by the authors in day-helicopter flights into the southwest in 2019 and 2020. a) Tasmanian Department of Lands air photo base with formlines in both So/Sm and Sm shown by white line traces. b) Google satellite image of early F1 macro-fold hinge (image top right) transition into a bounding high-strain zone (image left) just south of Davey Gorge. c) Google satellite image of the main synformal F2 closure south of Davey Gorge.

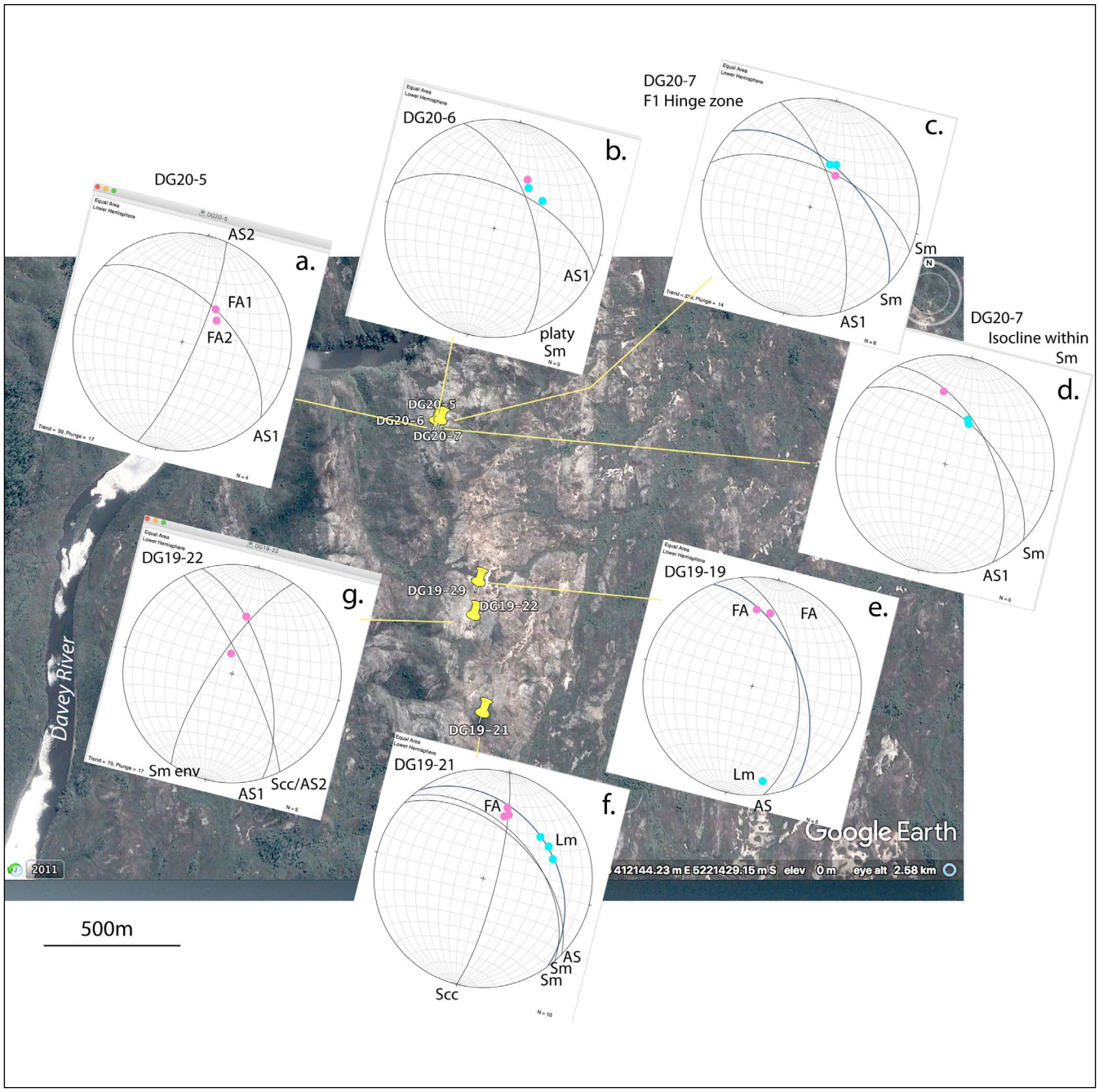

Figure 54. Stereographic projection representation of fold axis (FA), fold axial surface (AS), foliation Sm and lineation Lm attitudes at the outcrops visited by the authors in 2019 and 2020 on the ridge south of Davey Gorge. Pink dots are fold axes. Blue dots are lineations.

zone of the major F2 synformal fold. Both F1 and F2 fold axes are more north-northeast plunging (Figure 54e, f and g) but again plunge north of the mineral stretching lineation Lm (Figure 54f). The dominant early-fold axial surfaces are moderately to steeply northeast-dipping with a north-northwest strike.

The FA^Lm obliquity for the outcrops (Figures 54 and 55a, b) on the ridgeline south of Davey Gorge give a clockwise fold-hingeline vergence on the southern end of the proposed Davey River sheath nose, supporting an east-closing De Witt-Propsting mega-sheath fold (cf. Figure 16).

Both the early fold axial surfaces (Figure 55c) and the foliation Sm (Figure 55d) are folded, with a calculated p axis of 51°/030° for the major F2 folding determined from folding the early F1 axial surfaces. Most of the Sm structural data collected was bounding or defining the limbs of the early F1 isoclines, such that the defined π axis of 54°/059° is a generalised fold axis for the early F1 isoclinal folding phase. Although F1 and F2 folding is broadly coaxial these data show a ~20°, angular discordance between them (Figure 55c, d).

4.5 Elements of the Davey River Fold System

The structure of the ridgeline south of Davey Gorge was used to validate the structural interpretation for the Davey River sheath nose (Figure 50). This work suggests the presence of major F1 hinge zones that are folded by the major F2 closures identified by MacLean and Bow-

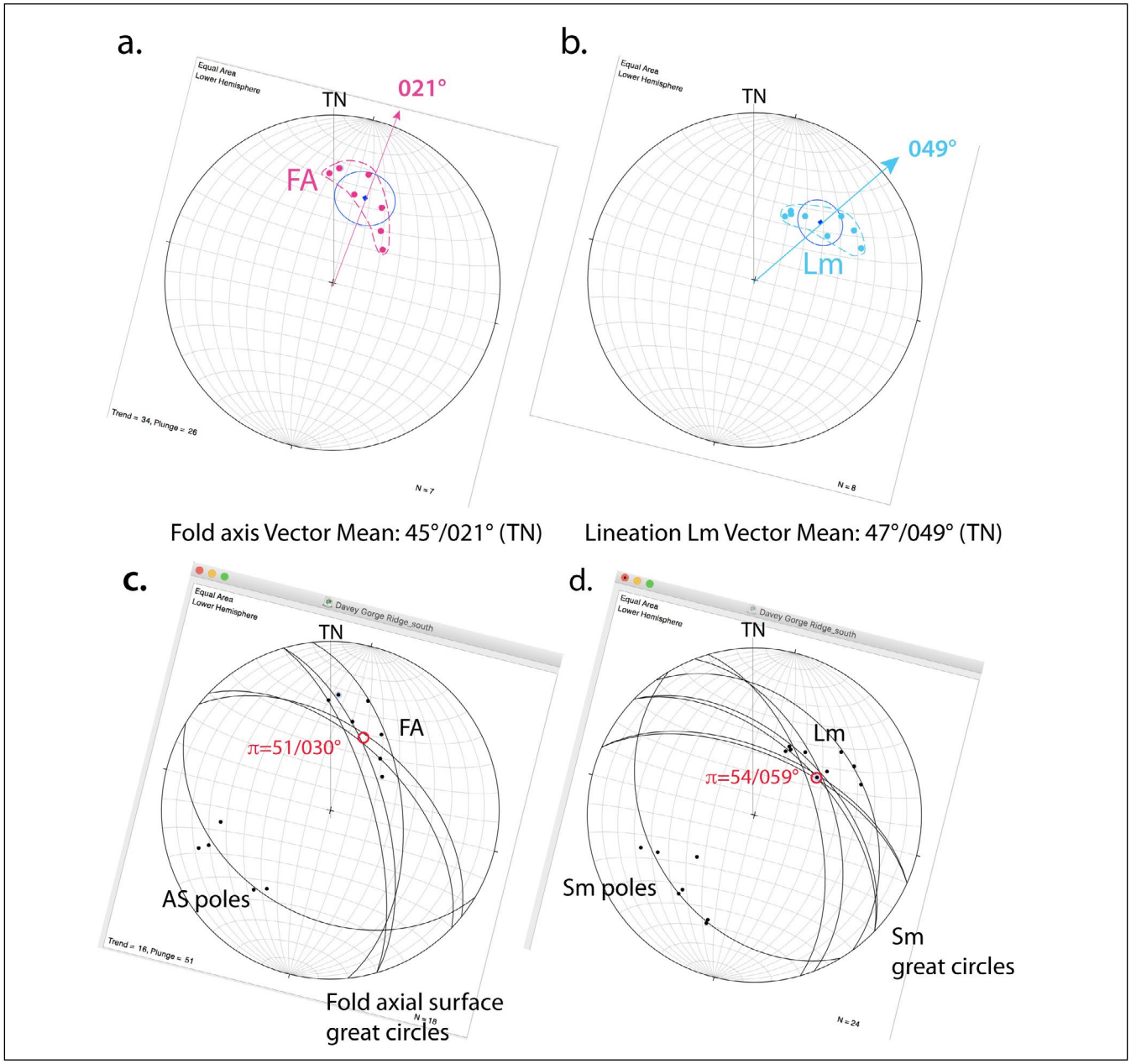

Figure 55. Summary stereonets of structural data collected by the authors on the ridge south of Davey Gorge (compare with Figure 54). a) Fold axis plot with vector mean orientation of 021°. b) Lineation Lm plot with vector mean orientation of 049°. c) Fold axis (FA) and axial surface great circle/pole plot. The axial surfaces are folded with a π axis of 51°/030°. d) Foliation Sm and lineation Lm plot. Sm is plotted as great circles with poles. The Sm data are folded about a π axis of 54°/059°.

en (1971). They recognised small-scale, mesoscopic F1 isoclinal folds within the dominant foliation Sm were coaxially refolded by larger F2 macro-folds. The F2 macrofolds were shown with north-south-trending axial surfaces (Figure 52b) with inferred inclined plunging geometry (Figure 51).

This geometry holds, but interpretation of Tasmanian Department of Lands air photos (Figures 50 and 51a), Google satellite imagery (Figures 53b, c and 57), helicopter oblique aerial photographs (Figures 58, 59 and 60) of the ridgeline south of Davey Gorge combined with limited field outcrop investigation by the authors (Figures 53b, c and 56) suggest at least two larger F1 macro-folds occur within the F2 dominant Davey fold system.

4.5.1 Early F1 Macro-Fold Hinge

The northern part of the ridgeline (Figures 53b and 56) show recumbent folded zones within and bounded by the platy quartzite/mylonite that are part of a north-closing macro F1 fold (Figure 57). This F1 hinge zone was identified in the oblique helicopter views of the Davey Gorge ridgeline (Figures 58, 59 and 60).

A composite photo-profile of part of this F1 macro-hinge (Figure 61) shows transition from the macro-hinge in Sm containing early, recumbent isoclines in So/Sm (Figures 61b and c). Younger F1 vergence folds in So/Sm (Figure 61e, f and g) occur on the lower limb transition into a structurally lower, bounding high-strain zone.

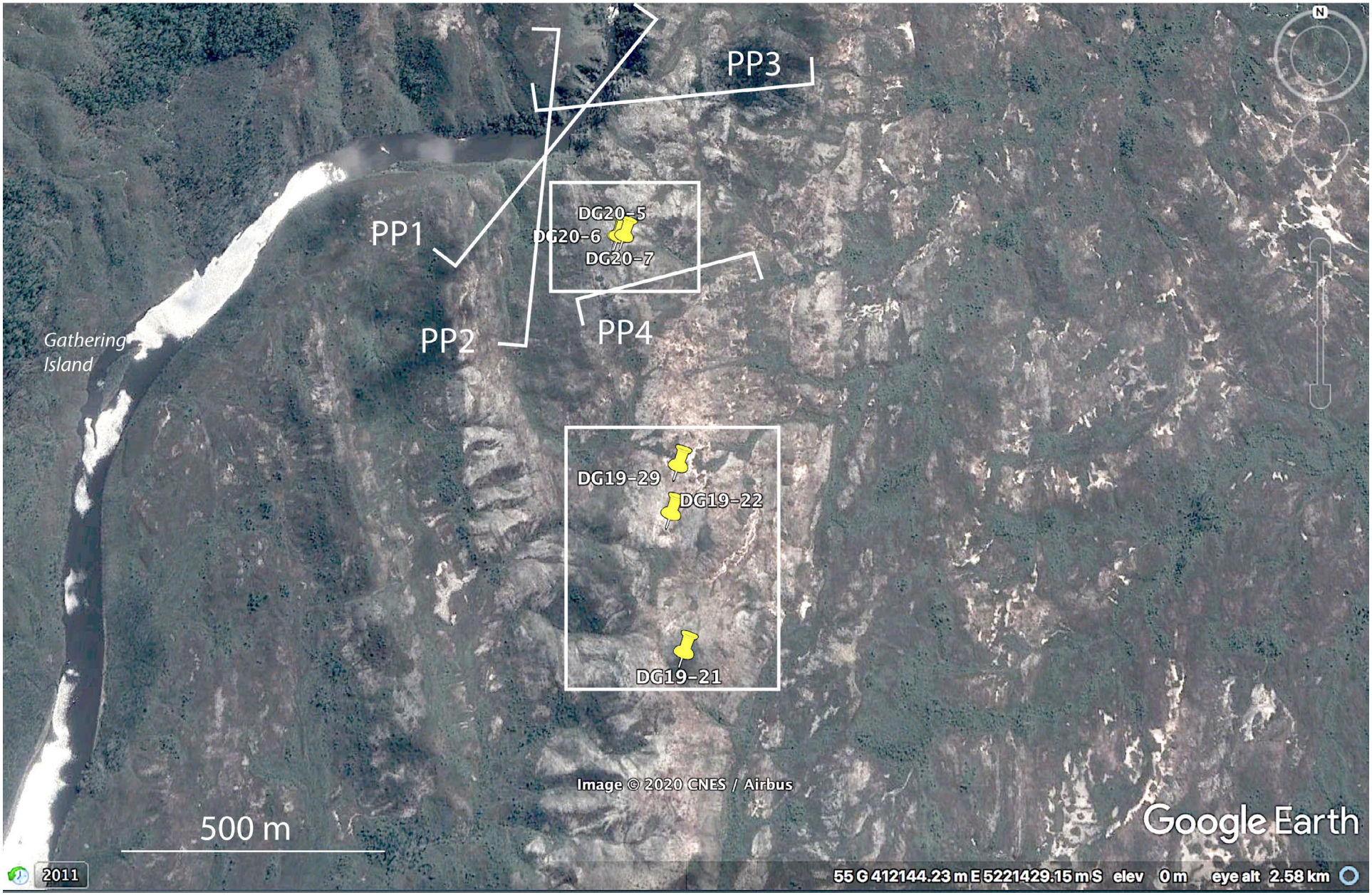

Figure 56. Google satellite image with DG station locations for field data collected in helicopter visits 2019 and 2020. The location of photo profiles (PP) is shown for Figures 59 (PP1), Figure 58 (PP2), Figure 60 (PP3) and Figure 61 (PP4). The map areas shown in Figure 53b and c are shown by the white rectangles.

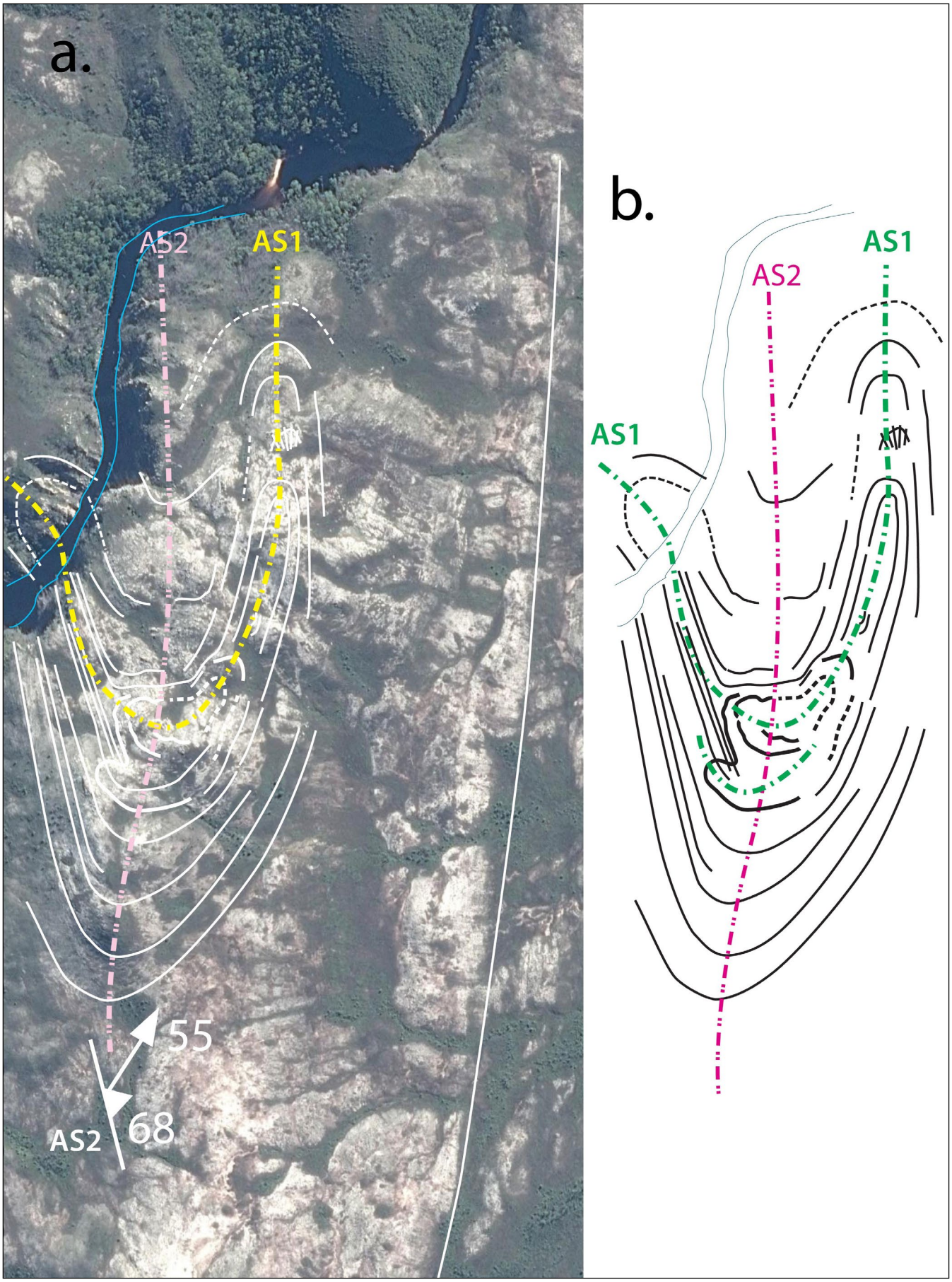

Figure 57. Detailed structural So/Sm and Sm formline interpretation of the northern part of the ridgeline south of Davey Gorge. Google satellite image as base. b) F1 and F2 fold interference pattern with axial surface traces shown as AS1 (green dashed trace) and as AS2 (pink dashed trace). Outcrop traces suggest the early isocline (AS1) has doubly plunging sheath-like form refolded with a banana-like outcrop pattern by the north-south-trending macro-isocline set.

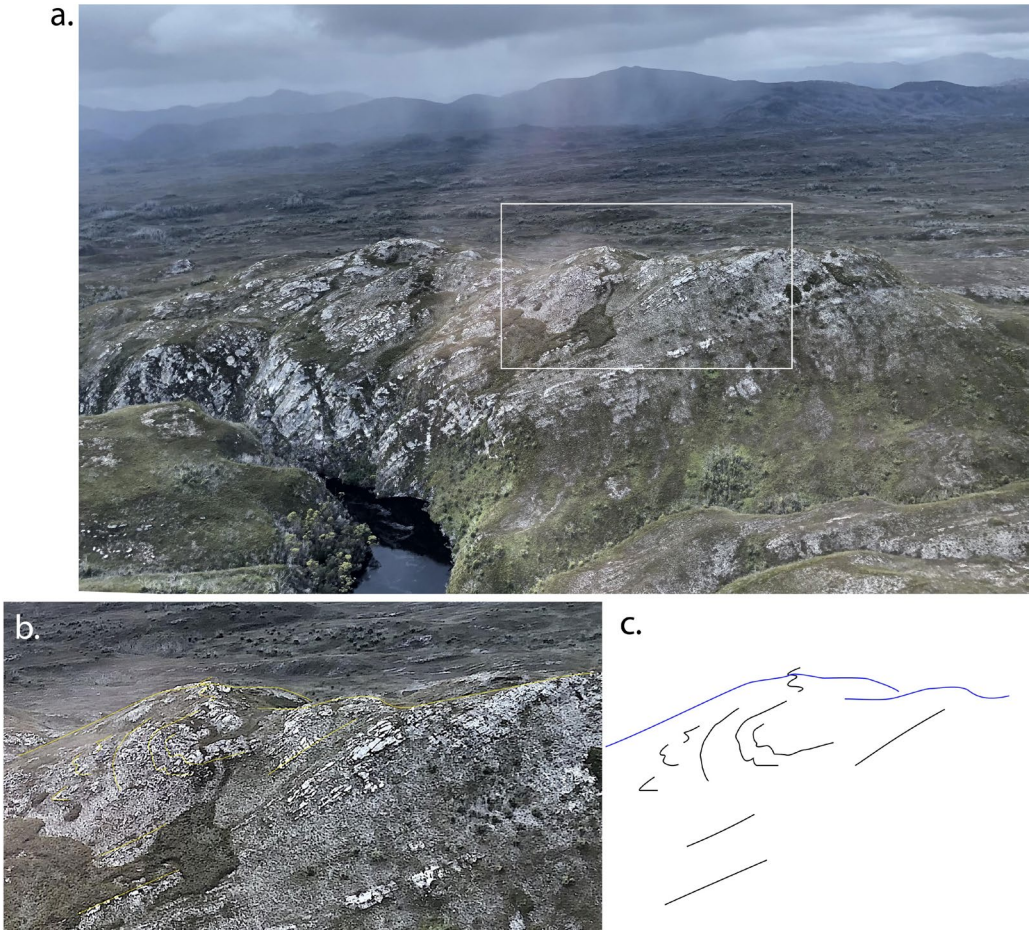

Figure 58 (left). Helicopter aerial photo looking east at the quartzite ridgeline above the entrance to Davey Gorge. The photo location is given by PP2 in Figure 56. b) Photo enlargement of the area depicted by the white rectangle in (a). c) Formline interpretation of the ridgeline in (b) showing the hinge area of the inferred north-closing macro-isocline (see Section 4.7 for structural explanation). The macro-fold plunge is northeast into the hillside.

Figure 59 (right). Oblique view (looking southeast) of quartzite ridge at the start of Davey Gorge. The photo location is given by PP1 in Figure 56. The quartzite in the gorge appears homoclinally, northeast-dipping with the fold structures plunging moderately to steeply northeast in the plane of the photograph. b) Formline interpretation of (a) with white traces depicting compositional layering So/Sm, Yellow dashed traces are axial surface traces of interpreted north-closing (ridge centre) and south-closing (ridge right) macro-isoclines.

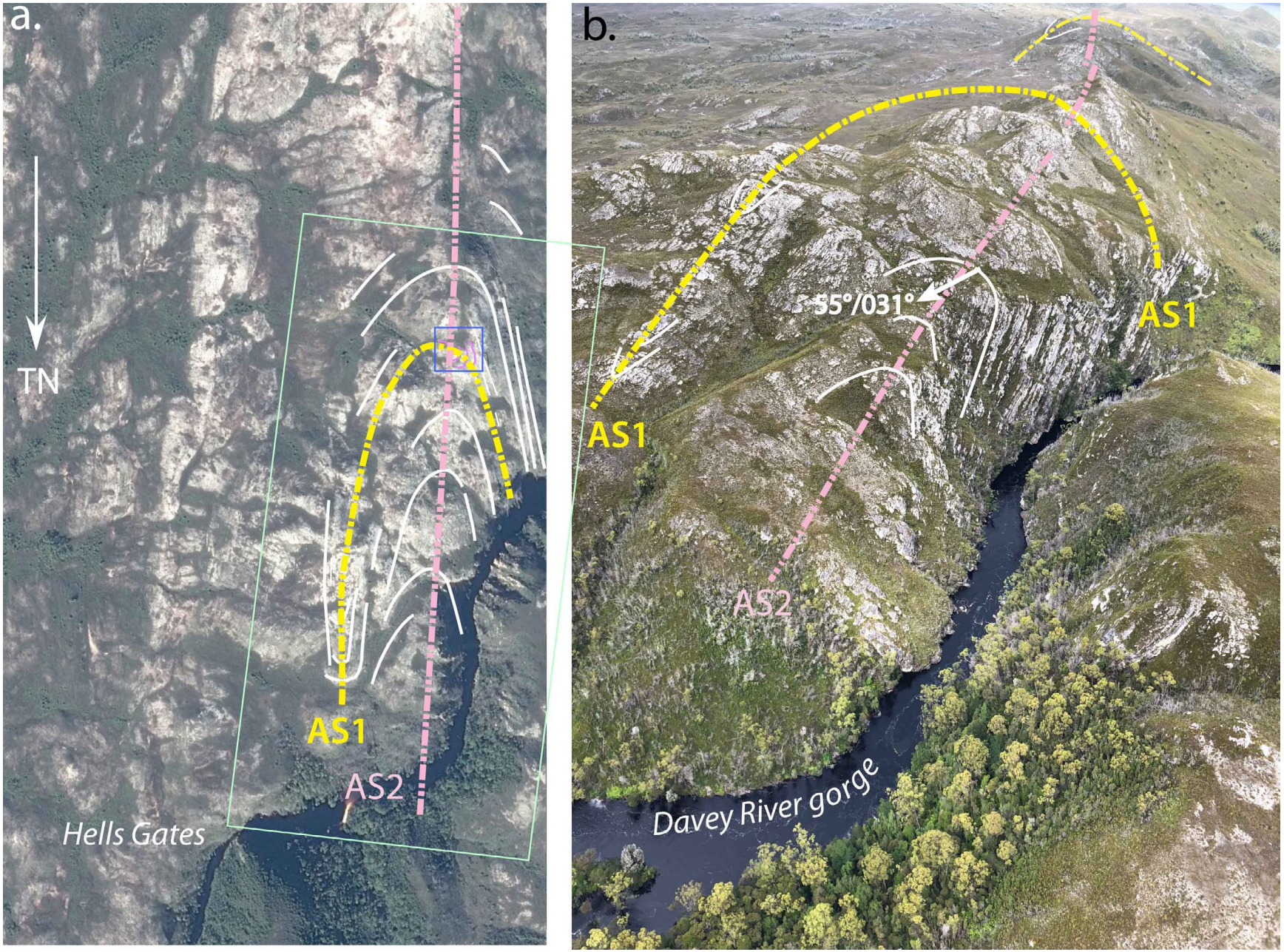

Figure 60. Structural interpretation of ridgeline south of Davey Gorge. a) Google image oriented to match the photo in (b). b) Photo of ridgeline south of Davey Gorge from helicopter. View is looking to the south. The photo location is given by PP3 in Figure 56. Fold plunge is 55°/031°. Formline interpretation shows compositional banding So/Sm and Sm (white line traces) and axial surface traces of inferred two sets of isoclinal macro-folds. AS1 trace: yellow dashed line. AS2 trace: pink dashed line.

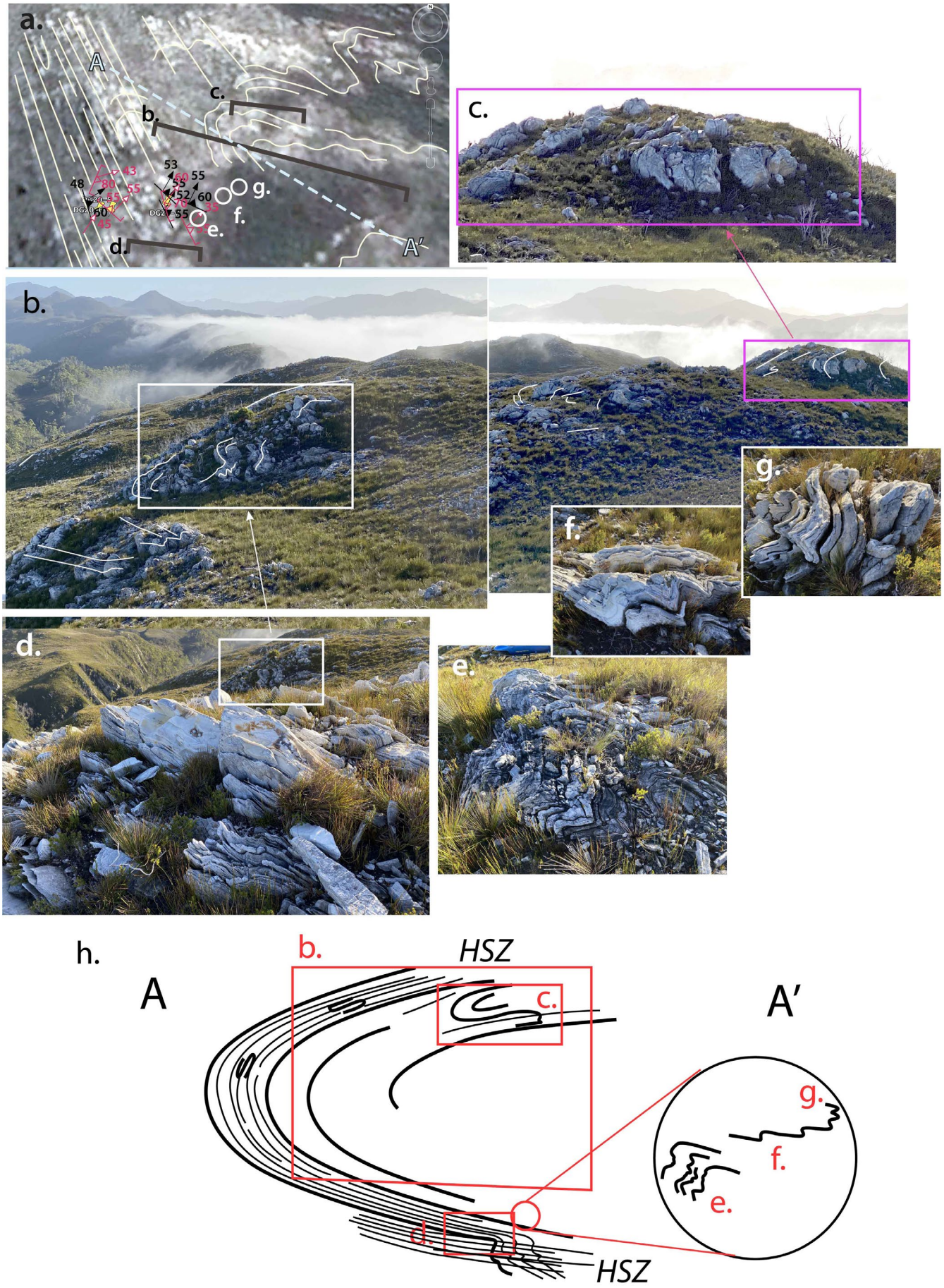

Figure 61. Composite Photo profile of north-closing, earliest-phase (F1) isoclinal macro-fold on ridge above Davey Gorge. The photo-stitch profile location is given by PP4 in Figure 56. a) Formline interpretation structure map on Google image base. Positions of photos and the photo profile in (b) are shown. b) Photo-stitch profile of hillside providing an oblique view of the early macro-fold hinge, with a third-order recumbent fold in hillside (upper right). c) Enlargement of recumbent fold shown in (b). d) Platy quartzite typical of the high-strain zone bounding the hinge zone on the recumbent fold lower limb. e), f) and g) are photos of mesoscopic folds transitional from the hinge into the lower limb. h) Sketch profile A-A' show the approximate form of the early fold closure with red outlines indicating the positions of the photos and photo-profile above.

Figure 62. Banded to platy quartzite high-strain zone (HSZ) below the north-closing F1 macro-isocline on the ridgeline south of Davey Gorge. The gorge is hidden (photo mid-left) and filled with fog (photo upper-right). The F1 fold hinge crops out on the ridgeline behind and right of the helicopter. Station DG20-5.

Figure 63. Platy quartz mylonite below the north-closing isoclinal macro-fold hinge. Ridgeline south of Davey Gorge. Station DG20-5.

The high-strain zones consist of banded compositional layering So/Sm (Figure 62) transitional into intense Sm with platy mylonitic character (Figure 63). Relicts of fold-augen as pods are enveloped by this intense foliation (Figure 64). The fold-augen generally consisting of Z-shaped asymmetric fold pairs cut by axial surface foliation that is sub-parallel to the bounding foliation of the high-strain zone (Figure 64). The folds within the augen commonly have curved hingelines with sheath-like character. In places the intense Sm foliation is also folded as part of an evolving fold-fabric evolution (Figure 65).

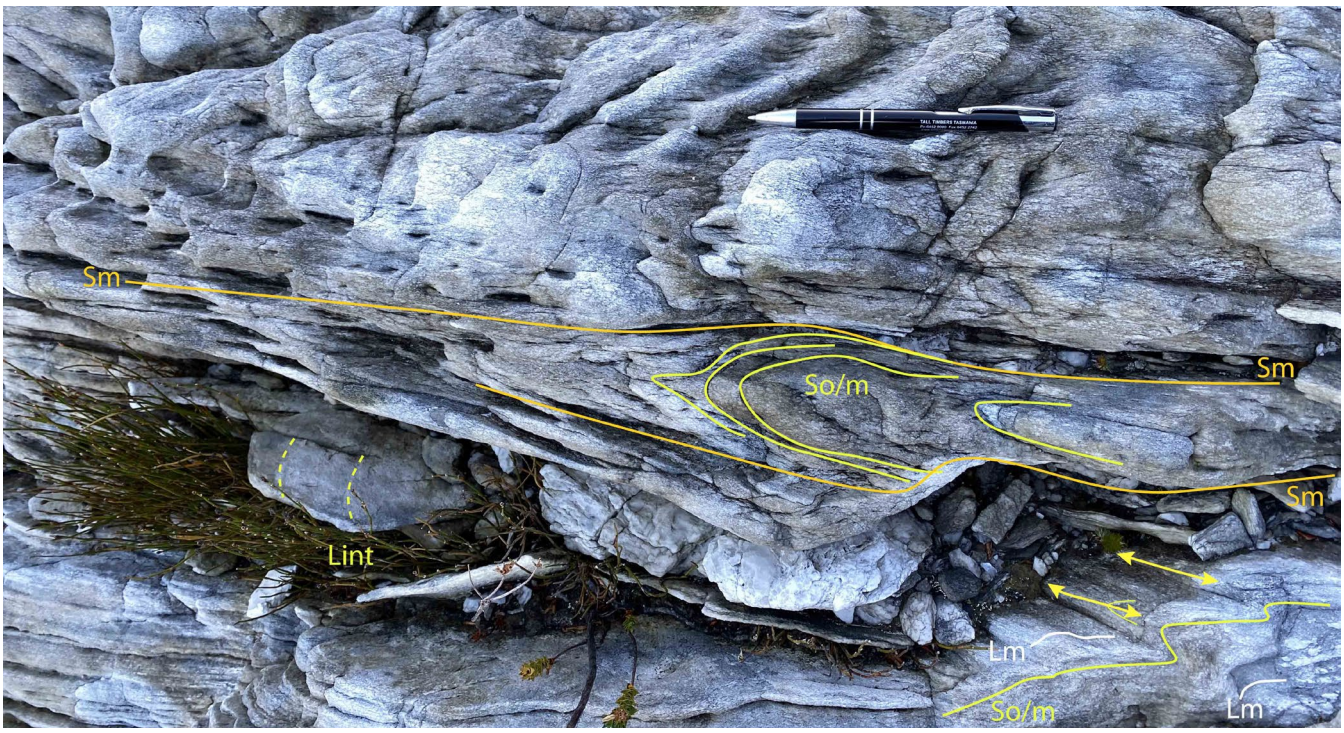

Figure 64. Asymmetric Z-vergence folds within fold-augen bounded by intense Sm of the high-strain zone. The folds have chevron-like form within relict compositional banding So/Sm and are cut by a spaced axial surface foliation that is coplanar with the bounding Sm. Fold hingelines vary in orientation at different levels through the fold-pair suggesting curvilinear form. The mineral lineation Lm is visible on the ledge in Sm (photo bottom right) with fold hingelines on ledge above (bottom photo-right) at ~70°-80° to Lm. A curvilinear intersection lineation Lint is visible on ledge (bottom photo-left). Station DG20-6.

Figure 65. Asymmetric S-vergence fold within quartzite "mylonitic" layering. Station DG20-6.

4.5.2 F2 Macro-fold Hinge Zone

The southern map area (Figure 53a) contains the hinge of the major, reclined, S-closing F2 macro-fold (Figure 53c). This F2 macro-fold coaxially refolds mesoscopic F1 isoclines within So/Sm in the hinge zone (Figures 66 and 67). Many of the F1 isoclinal folds show curvilinear hingelines (Figures 68) indicating sheath-like fold geometry.

In places, isoclinally folded quartzite is transitional into platy, mylonitic quartzite with rootless fold hinges enveloped or enclosed by the platy, schistose to mylonitic Sm (Figure 69). In some instances these zones are sub-parallel to the F2 macro-fold axial surface, and as such cut the macro-fold hinge. In places, isoclinally folded quartzite is transitional into platy, my-

Figure 66. Early F1 isoclinal fold (blue dashed axial surface trace) coaxially refolded by approximately upright to inclined plunging F2 folds (pink dashed axial surface traces) within the hinge zone of the F2 macro-fold shown in Figure 60. Station DG19-21. AST: fold axial surface traces.

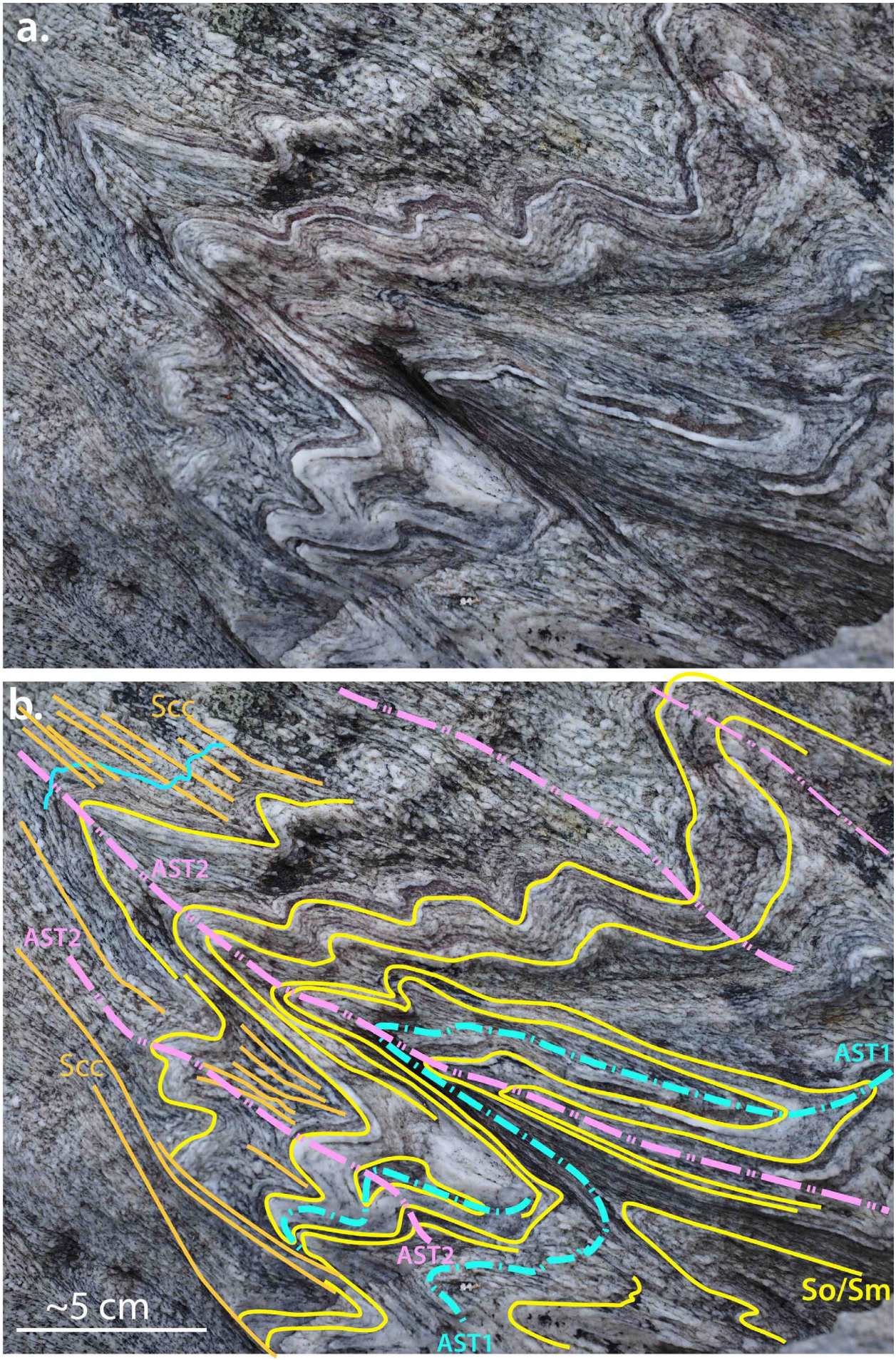

Figure 67. Partly closed, sheath-like isoclinal F1 folds (blue dashed axial surface traces) refolded by inclined plunging F2 folds (pink dashed axial surface traces)in the hinge of the F2 macro-fold shown in Figure 60. Station DG19-21. AST: fold axial surface traces.

Figure 68 (above). Curvilinear intersection traces Lint on the foliation surface Sm reflecting early stages of F1 sheath folding at the mesoscopic scale. Note the hingelines defined by the intersection traces of So/Sm with Sm initiate at high angles to the mineral stretching lineation Lm with the limbs rotating towards Lm. Station DG19-22.

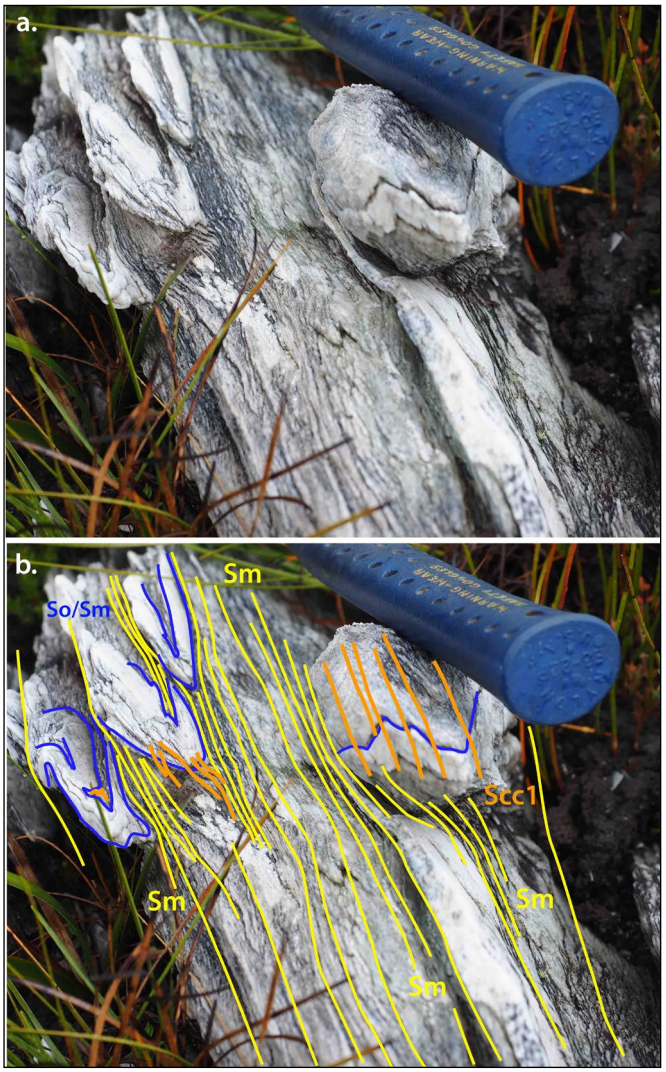

Figure 69 (left). Rootless isoclinal fold pairs in quartzite layers disrupted by intense foliation Sm. a) and b) are non-annotated and annotated photographs respectively. Compositional layering So/Sm: blue line traces. Spaced cleavage Scc1: orange line traces. Foliation Sm: yellow line traces. Note the earlier-formed spaced cleavage (orange traces) preserved within the relict fold hinges in So/Sm is sub-parallel to the intense, more-evolved dominant foliation Sm (yellow traces). This is a process of cannibalism where the intense foliation engulfs and subsumes the earlier fabrics (see Section 6.4). Station DG19-22.

lonitic quartzite with rootless fold hinges enveloped or enclosed by the platy, schistose to mylonitic Sm (Figure 69). In some instances these zones are sub-parallel to the F2 macro-fold axial surface, and as such cut the macro-fold hinge.

Opaque skeletal meshes within quartzite on the ridgeline south of Davey Gorge (Figure 70) provided an estimate of the XY strain as ~3.2:1 with the ellipse long axes sub-parallel to the mineral lineation Lm. This demonstrates that Lm is parallel to the stretching direction Lstretch. Limited measurements of these skeletal meshes in the fold profile plane (Figure 70a) equate to an XZ strain of ~6.2:1, such that X:Y:Z=3.2:1:0.52.

4.6 Significance and Implications

Incorporating outcrop fabric and refolding relationships with the Davey Gorge oblique ridgeline photographs give a revised macro-geometry of the Davey River Fold system (Figure 71). At the regional scale the Davey River sheath-nose has elongated, pod-like, tectonic fish geometry with bulbous terminations enveloped by schistose platy quartzite. Internal structure includes a series of shells that envelope early F1 macro-folds refolded by younger F2 isoclinal macro-folds. The F2 isoclinal folds are dominant and control the sigmoidal shape (Figure 71).

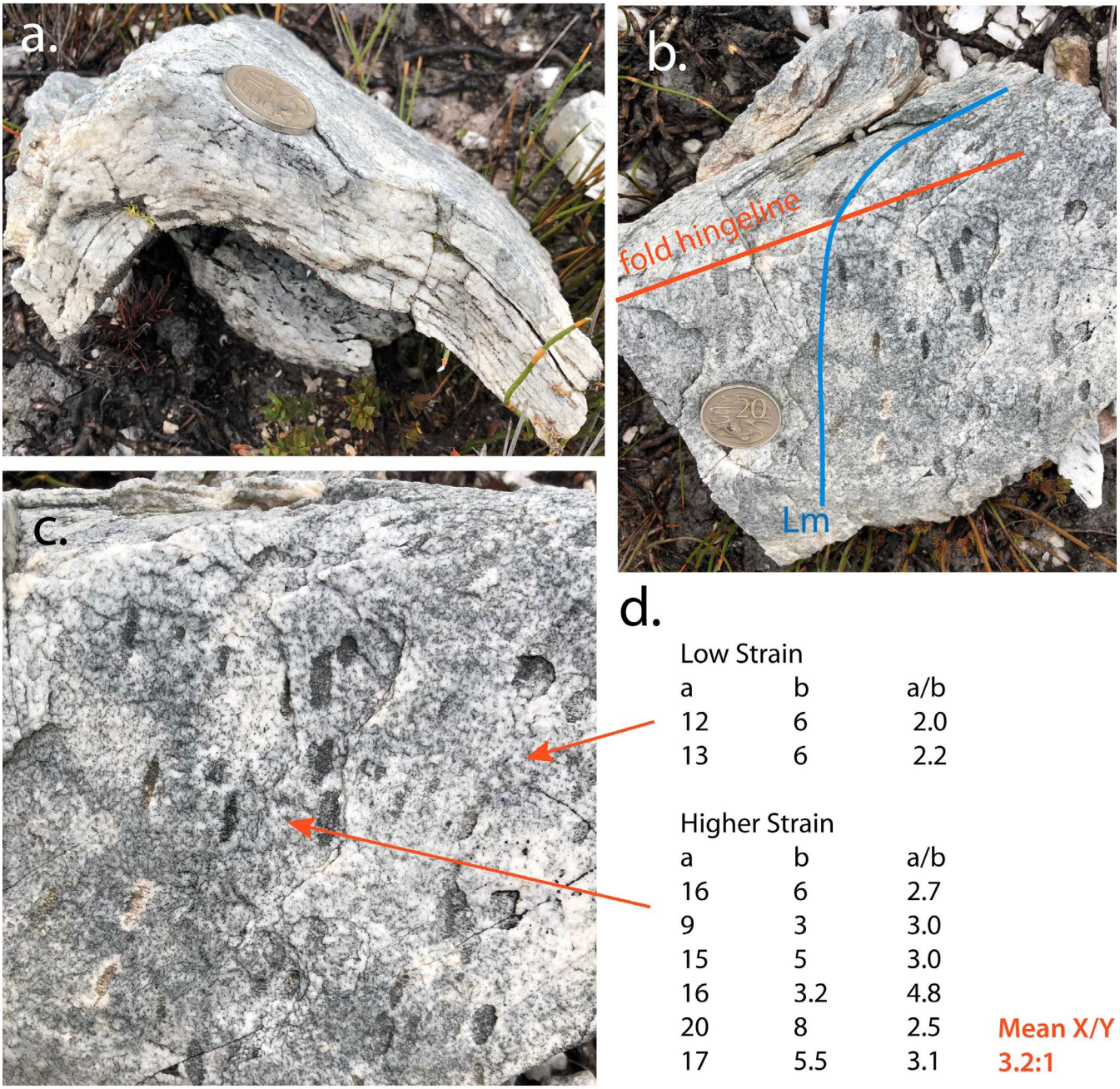

Figure 70. Folded foliation Sm with mineral lineation and ovoid skeletal opaque webs as strain markers. a) Fold profile view of open mesoscopic F2 fold. b) Top view of fold showing fold hinge (red line trace) and folded lineation Lm (blue line trace). c) Enlarged view of Sm with elliptical opaque skeletons flattened in Sm . d) Dimension and aspect ratios of skeletal opaque webs shown in (c) with the assumption these were originally spherical, like framboidal pyrites. Between Stations DG19-20 and Station DG19-21.

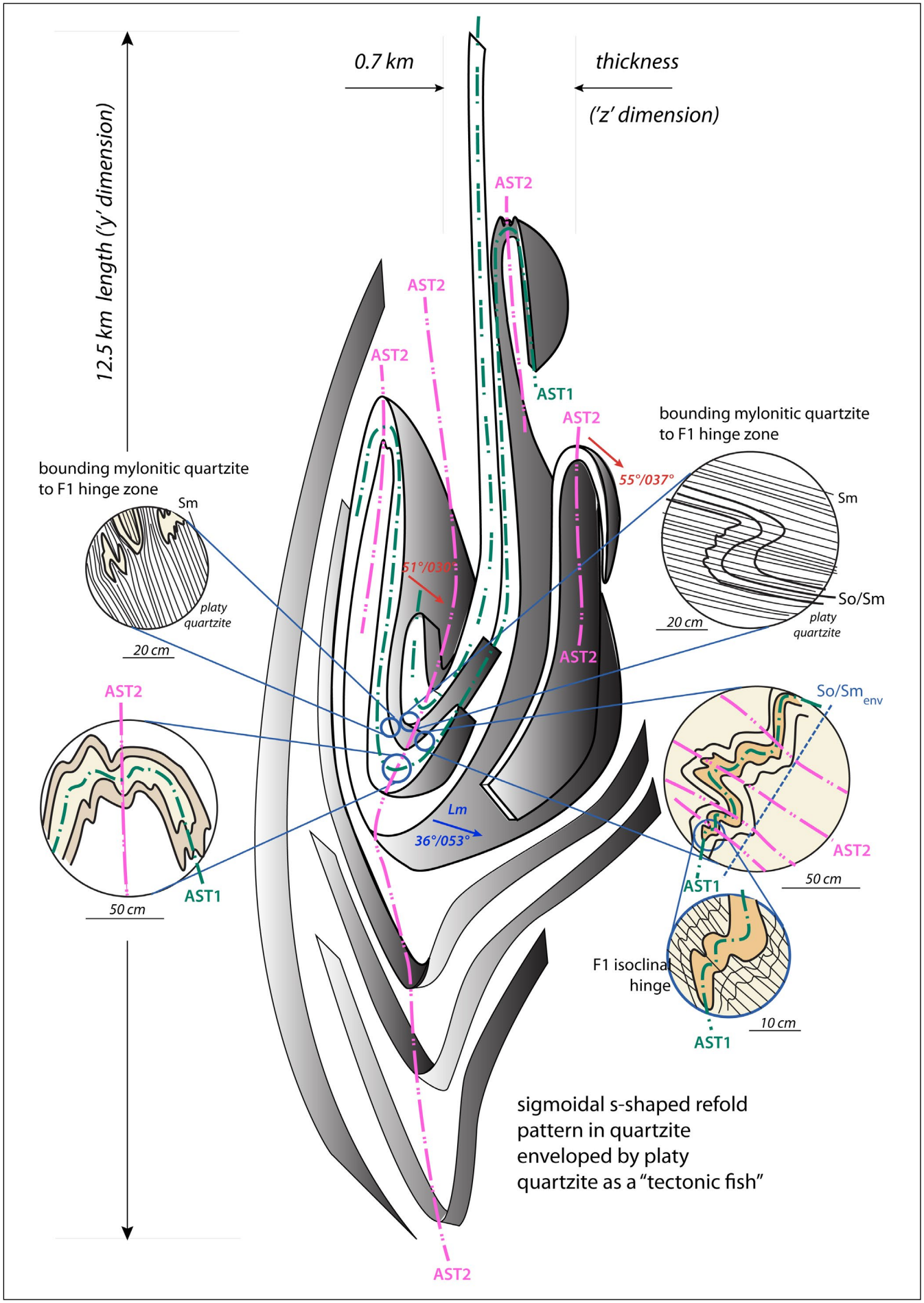

Figure 71. Schematic 3D diagram illustrating the internal structure of the "tectonic fish" that defines the nose of the De Witt-Propsting mega-sheath fold. Inset circled diagrams are schematic sketches of key fabric elements and relationships used to refine the geometry of the mega-sheath fold nose.

5.0 SOUTH WEST CAPE MEGA-SHEATH FOLD SYSTEM

The South West Cape mega-sheath fold system does not have distinct topographic form like the De Witt-Propsting mega-fold (see Figure 2) and is "hidden" within the ranges of the southwest including the South West Cape, Melaleuca, and Pascoe Ranges (Figure 72a). The litho-tectonic map of the South West Cape fold system (Figure 72b) suggests a regional-scale Type 2 fold interference (Ramsay, 1967), where early F1 macro-isoclinal folds are refolded by upright, north-south-trending isoclinal folds (Figure 72b).

The South West Cape mega-sheath fold system is considered en echelon with, and complementary to, the De Witt-Propsting mega-sheath fold as part of a regional-scale, oppositely-closing sheath-fold pair (Figure 4). Internally it shows elements more closely related to the refolding within the inner shell and nose of the De Witt Propsting mega-sheath fold (see Section 6.3).The possible sheath-like form is investigated with respect to fold-limb vergence concepts, fold axis FA to lineation Lm obliquity and the general lineation Lm relationships (after Alsop and Holdsworth 1999, 2004 and 2006).

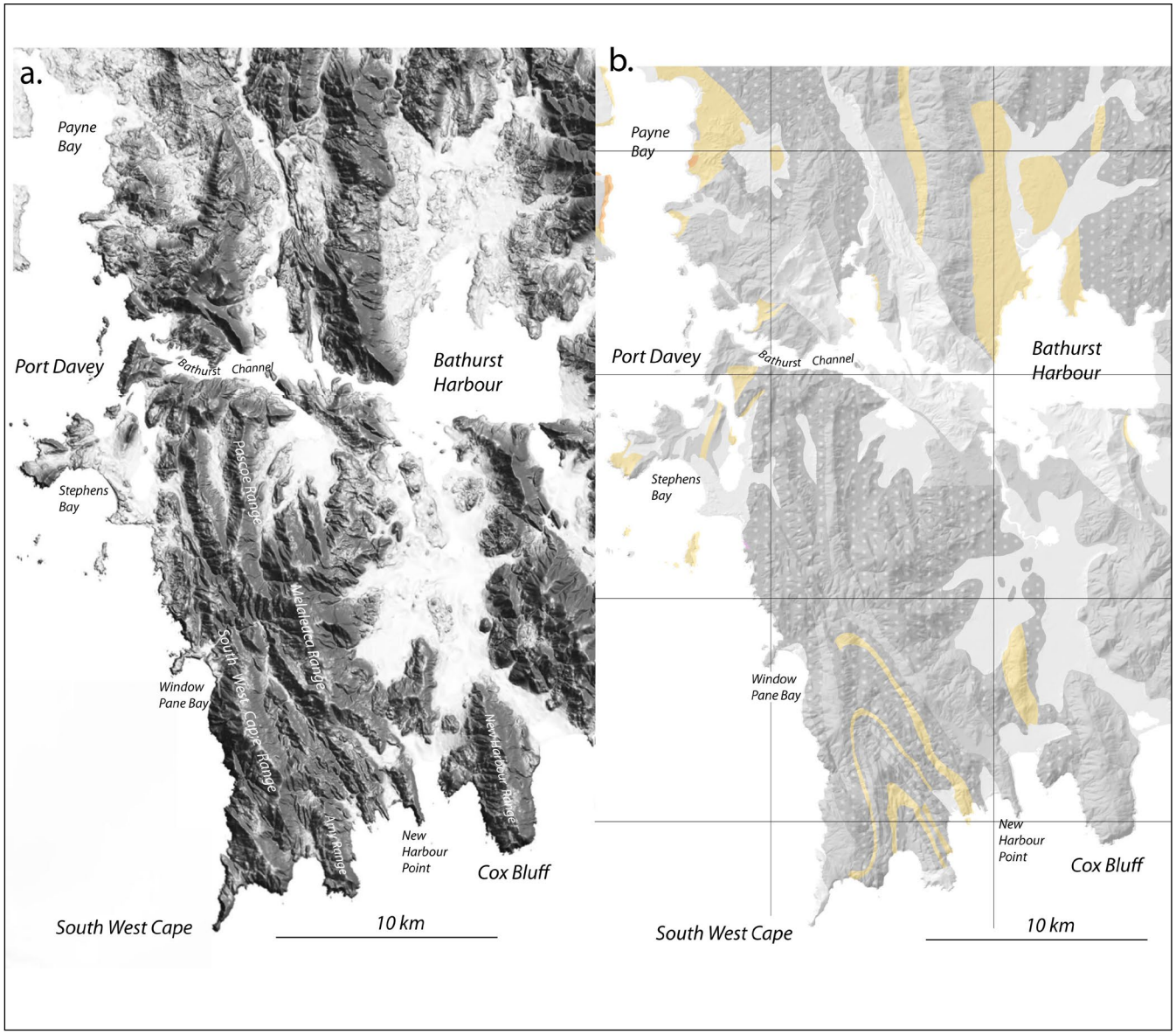

Figure 72. Digital Elevation Model (DEM) of the South West Cape area. a) Tasmanian ListMap greyscale DEM showing the southwest topography with ranges and coastline, extending north to Payne Bay and east to Cox Bluff and Bathurst Harbour. b) Litho-tectonic map units draped on the DEM showing a regional-scale, macro-fold centred on Amy Range and Wilson Bight. The litho-tectonic map base is from the Mineral Resources Tasmania 1:250000 digital atlas. The map units are: 1) pale orange: low-grade pelite, 2) grey: low-grade quartzite, 3) dark grey with white stipple: low-grade platy and/or schistose quartzite, and 4) light grey: younger cover and Cambiran turbidites and conglomerate.

5.1 Background

The Port Davey-Cox Bight area has undergone preliminary field investigations by Stefanski (1957a, b) and by BHP Exploration geologists in 1965 (Hall, 1965), with geological survey mapping of the Davey Sheet by Williams (1978, 1982) in the northwest part.

Stefanski (1957a, p.96) showed 1) the sequence consisted of quartzites, platy quartzites and pelite, 2) the units were isoclinally folded, with 3) an early lineation present as "ribbing in quartzites, parallelism of hornblende laths in hornblende-zoisite schists and of muscovite flakes in mica quartzites", and 4) the lineation had quite constant orientation throughout the area and was commonly parallel to the hinges of mesoscopic isoclinal folds.

As part of BHP Exploration Lease mapping Hall (1965) further established the litho-stratigraphy of the area as dominated by low-grade quartzite and quartz-sericite schist. The sequence is generally steeply west-dipping, with a southwest-plunging mineral lineation and where individual beds were complexly deformed. At the regional scale (Hall, 1965) defined three macro-isoclinal folds (Figure 73). From from west to east these are 1) the South West Cape antiform (south-closing macro-isoclinal fold), the Amy Range synform (north-closing macro-isocline) and 3) the Melaleuca Range antiform (south-closing isoclinal macro-fold). These folds are truncated and offset by a series of steeply-dipping, northwest trending, oblique-slip faults with right-lateral movement in plan. The major faults were named the Window Pane Fault, the Hannant Fault and the New Harbour Fault (Figures 73 sanfd 76).

In a geometrical interpretation (Figure 74) Hall (1965, Figure 3) argued for two phases of regional-scale isoclinal folding where the South West Cape and Melaleuca Range antiforms were part of the same macro-isocline refolded by the Amy Range synform. Plunge changes along the Melaleuca Range antiform suggested a sheath-like, domal culmination in the "core" of the fold (Figure 74b).

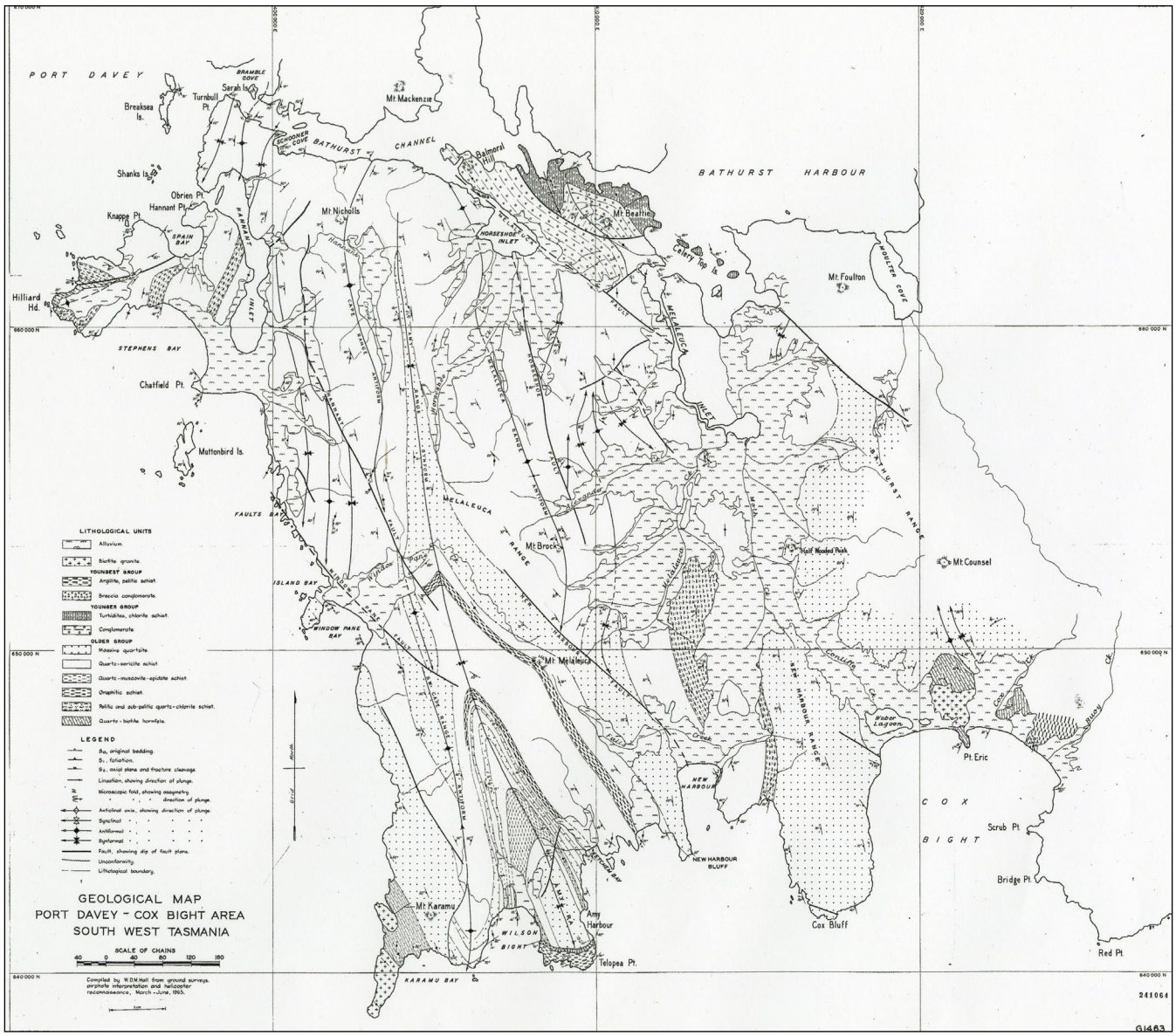

Figure 73. Geological Map of the Port Davey-Cox Bight area of southwest Tasmania compiled by W.D.M. Hall (1965) as part of the BHP Exploration Lease E.L. 13/65.

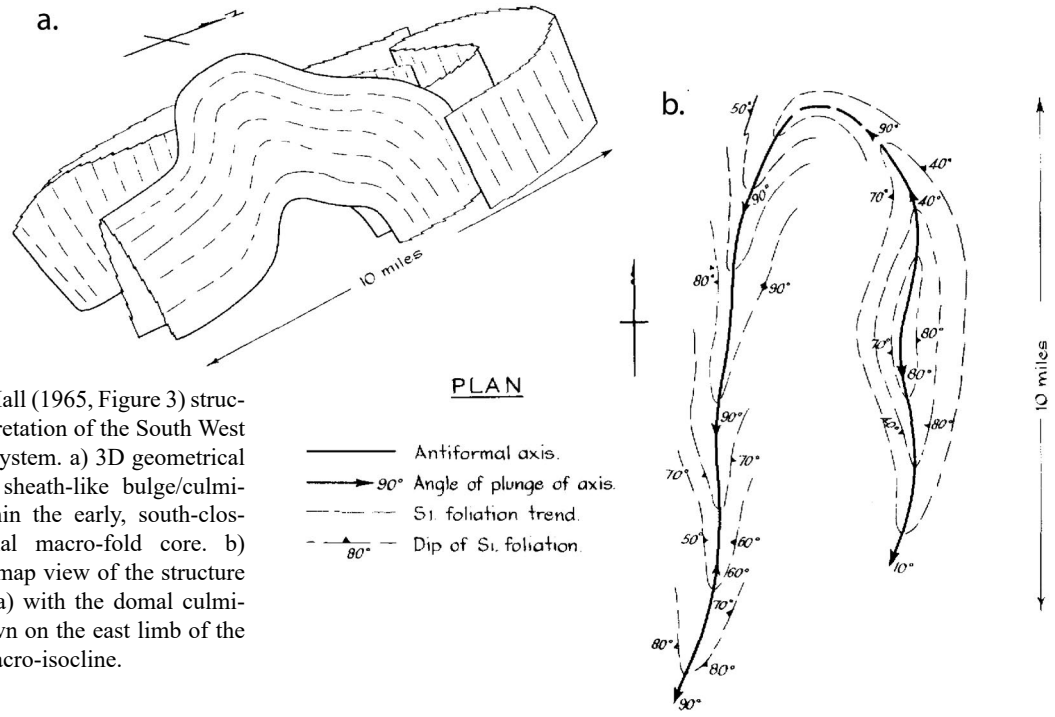

Figure74. Hall (1965, Figure 3) structural interpretation of the South West Cape fold system. a) 3D geometrical form with sheath-like bulge/culmination within the early, south-closing isoclinal macro-fold core. b) Schematic map view of the structure shown in (a) with the domal culmination shown on the east limb of the refolded macro-isocline.

5.2 Current Work

The structural interpretation presented by the authors is a compilation of all the existing structural data, primarily from the BHP Port Davey-Cox Bight Area Geological Map (Figure 73), as the Stefanski map (Stefanski, 1957b) had no structural attitude data. The BHP map (Hall, 1965) shows foliation So/Sm, S1 and S2 attitudes, lineation Lm and fold axis (FA) attitudes as well as fold vergence. Field checking of the area and the interpretation has not been undertaken by the authors.

All of the BHP geologist structural data has been recompiled as a series of maps (Figures 75 and 76) in an attempt to validate and/or establish the geometry the South West Cape fold-system.

5.3 Geometry of the South West Cape Mega-Sheath Fold System

As mentioned above, the litho-tectonic map of the South West Cape mega-sheath fold system (Figure 75) suggests a regional-scale Type 2 fold interference (Ramsay, 1967), where early F1 macro-isoclinal folds are refolded by upright, north-south-trending isoclinal folds. This is similar to the initial interpretation of Hall (1965) (Figure 74), although β and/or π analysis of fold segments indicates the macro-folds have inclined plunging to reclined geometry with west-plunge (see pink arrows, Figure 75). According to Hall (1965, p.12-13) the Melaleuca Antiform shows marked plunge variations from subvertical to steep south plunge (head of Alexander Creek) to ~10° south close to the New Harbour Fault (Figure 73), accompanied by an elongated closure within the S1 formlines (Figure 74b).

Differences with the previous interpretation are:

1. The inverted-Y-shaped quartzite outcrop pattern (Figure 75) necessitates another isoclinal macro-fold closure inside the previously defined Melaleuca Range-South West Cape Range antiform. The axial surface trace of this south-closing macro-isoclinal fold lies within the quartzite (Figure 76) and has been re-configured or redrawn to accommodate this (compare with Gray et al., 2022, Figures 71, 72d and 73d). The new fold axial surface trace (AST2) coincides with the South West Cape Range on the west and passes offshore at New Harbour Point (Figure 76). As a consequence this fold has been renamed the South West Cape Range-New Harbour Point fold.
2. The axial surface trace (AST) of the previously defined Melaleuca Range-South West Cape Range Antiform (Figure 73) lies within the outer platy quartzite, with the newly defined AST1 extending offshore at Window Pane Bay (Figure 76). This fold is renamed the Melaleuca Range-Window Pane Bay fold. North of the New Harbour Fault the AST1 has been reinterpreted to lie within the isolated pelite "pod" north of New Harbour.
3. Repetition of the pelite bands in the southern part of the Amy Range Synform (AST3, Figure 76) suggests the presence of second- and third-order isoclinal folds on the structurally lower limb of the South West Cape Range-New Harbour Point fold.

The South West Cape mega-sheath fold system has dimensions of 25 km length scale ('y' dimension) and a half-width of 8 km ('z' dimension). By closing out a possible oval or eye-shaped form to the inner most shell/core potentially half of the structure is offshore. The 3D form of the South West Cape mega-sheath fold system is shown in Figure 77a, with measured and calculated fold plunges highlighting the fold geometries within the interpreted external sheath form (Figure 77b).

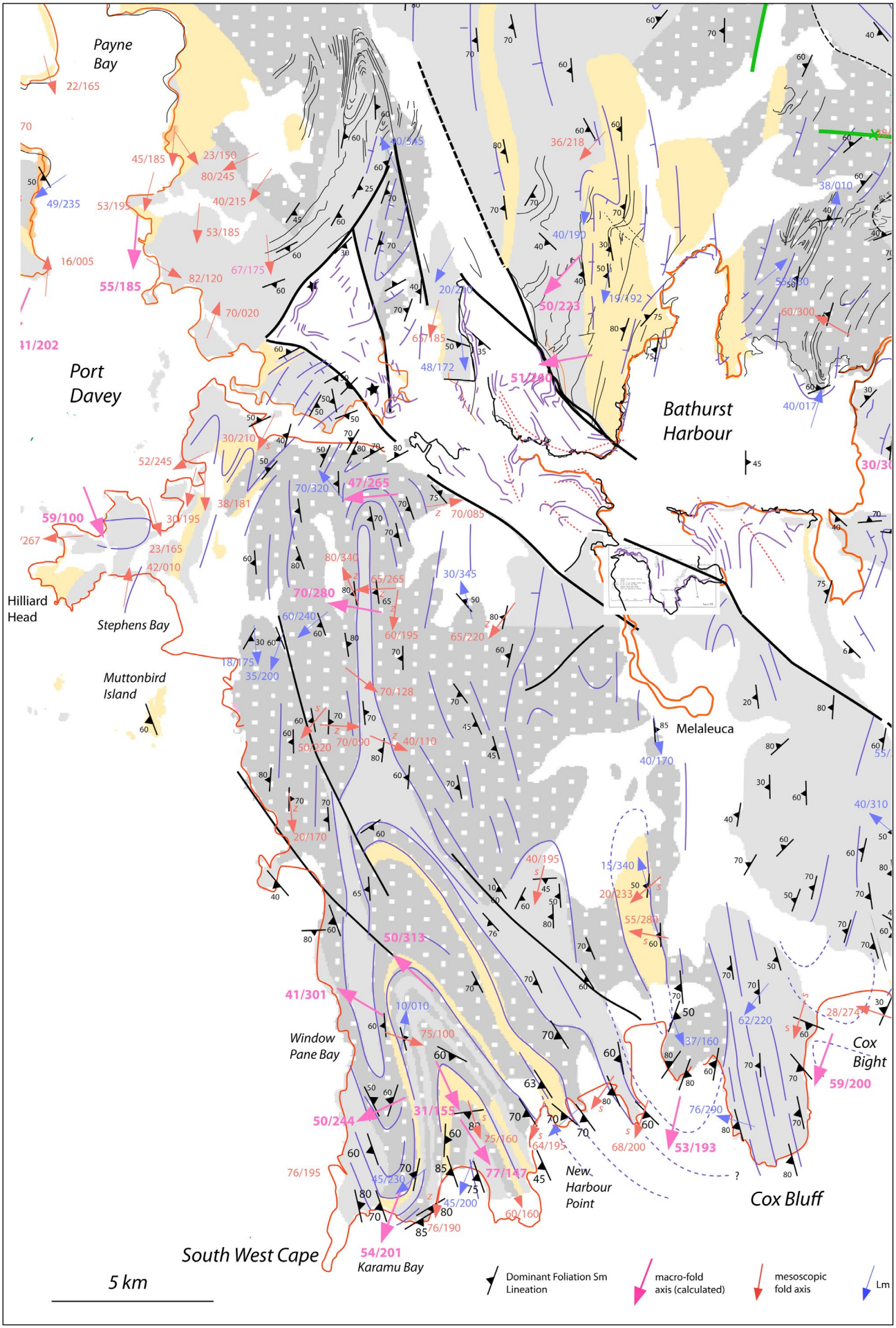

Figure 75. Geological map of the South West Cape area. The litho-tectonic map base is from the Mineral Resources Tasmania 1:250000 digital atlas. The map units are: 1) pale orange: low-grade pelite, 2) grey: low-grade quartzite, 3) dark grey with white stipple: low-grade platy and/or schistose quartzite.

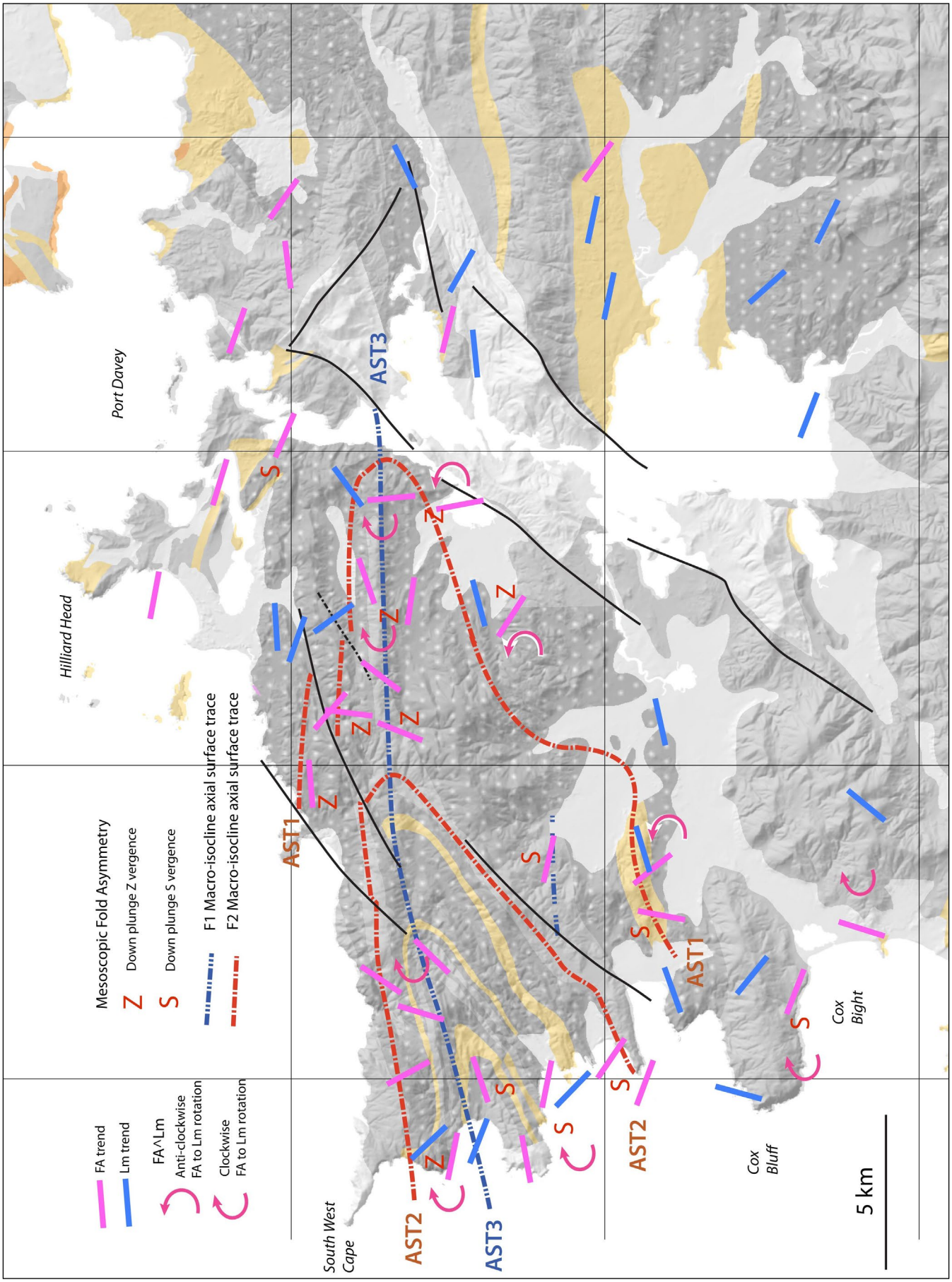

Figure 76. Detailed structure map of the South West Cape mega-sheath fold system with axial surface traces for the large regional scale early (F1) isoclinal folds (red dot-dashed lines) and F2 macro-isocline (blue dot-dashed lines), mesoscopic fold vergence (S versus Z down-plunge asymmetry) and mesoscopic fold-hingeline vergence (clockwise or anticlockwise rotation of FA towards lineation Lm).
AST1: axial surface trace for the Melaleuca Range-Window Pane Bay fold.
AST2: axial surface trace for the South West Cape Range-New Harbour fold
AST3: axial surface trace for the Amy Range synform.

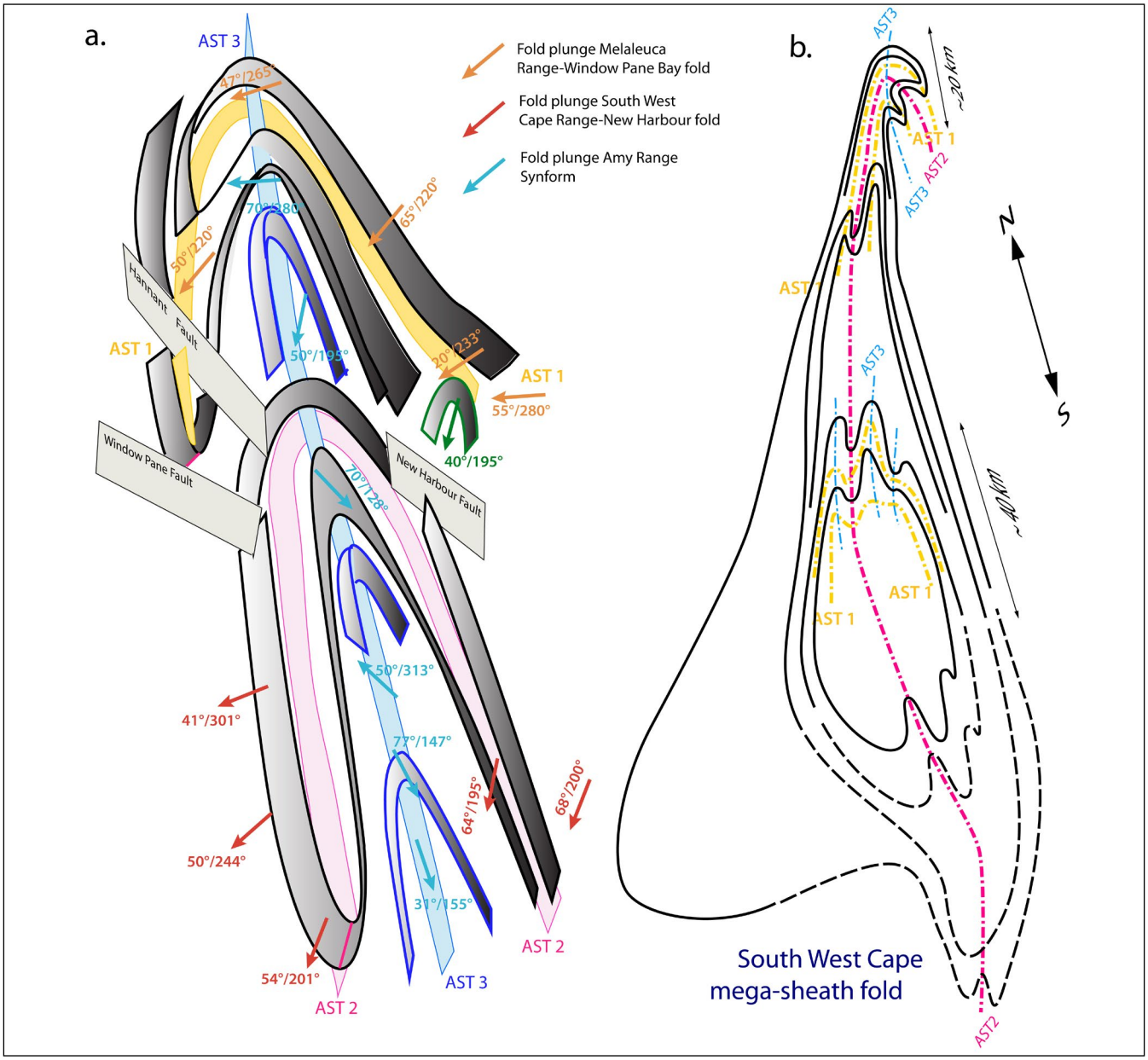

Figure 77. South West Cape mega-sheath fold reconstructions. a) Schematic 3D diagram looking north-northeast at the South West Cape mega-sheath fold system. The axial surface traces of the three macro-isoclinal folds are shown as AST1 (orange surface), AST2 (pink surface) and AST3 (blue surface). Fold plunges are shown for these macro-folds along with the geometry of individual fold segments. The earlier folds with AST1 and AST2 generally have west-plunge but can be to the southwest and northwest. The younger macro-isocline AST3 has more south-plunge.
AST1: axial surface trace for the Melaleuca Range-Window Pane Bay fold.
AST2: axial surface trace for the South West Cape Range-New Harbour fold
AST3: axial surface trace for the Amy Range synform.
b) Schematic 3D form of the outer shell of the South West Cape west-closing mega-sheath fold. AST1, AST2 and AST3 refer to the different generations of isoclinal folding

5.3.1 Analysis of Fold Pattern using Fold Vergence and Fold-Hinge Vergence

Analysis of the South West Cape mega-sheath fold system is through a series of maps including the early mesoscopic fold axis (FA) pattern (Figure 78), the mineral lineation Lm pattern (Figure 79), the mesoscopic fold-hingeline vergence pattern (Figure 80) and the early mesoscopic fold asymmetry (Figure 80).

In summary, the South West Cape structure map summary (Figure 76) shows apparent complexity in fold- and fold-hingeline vergence patterns with no simple fit of the Lm pattern, the meso-fold S and Z vergence pattern and the fold-hingeline vergence pattern to the geometric interpretation presented in the 3D schematic South West Cape meag-sheath fold model (Figure 77).

The detailed structure maps show:

1. The early isocline-hingelines (short pink lines in Figure 76 and heavy pink lines in Figure 78) are overall south-southwest trending, west-northwest trending and west-trending (Figure 78).
2. The lineation Lm pattern (Figure 79) appears complex with three main trends: southwest-trending, northwest-trending and north-trending. Simple modeling using 1) a sheet of paper containing Lm

and the fold axis directions and 2) folding the paper to fit an inclined, west-plunging macro-isoclinal fold geometry shows that the northwest-trend potentially sits on the upper limbs and the southwest-trend on the lower limbs. This pattern has been observed or inferred for macro-folds within the Central Tyennan domain (see Gray and Vicary 2021, Figure 22d). The north-trending Lm matches the north-trend of the Amy Range synform and either represents reworking or re-orientation of the Lm (see Gray et al., 2022, Figures 41c and 52) or recording of a younger Lcren by the earlier BHP geologists.

3. Clockwise mesoscopic fold-vergence dominantly occurs within the refolded inner portion of the South West Cape-New Harbour Range fold (Figure 80). Counterclockwise mesoscopic fold-vergence occurs on the eastern outer portion of the refolded Melaleuca Range-Window Pane Bay fold (Figure 80).
4. Mesoscopic Z-vergent folds occur predominantly on the inner western re-folded limb of the outermost Melaleuca Range-Window Pane Bay fold (Figure 80). Mesoscopic S-vergent folds predominantly occur on the inner eastern limb of the re-folded, innermost South West Cape Range-New Harbour Fold (Figure 80).

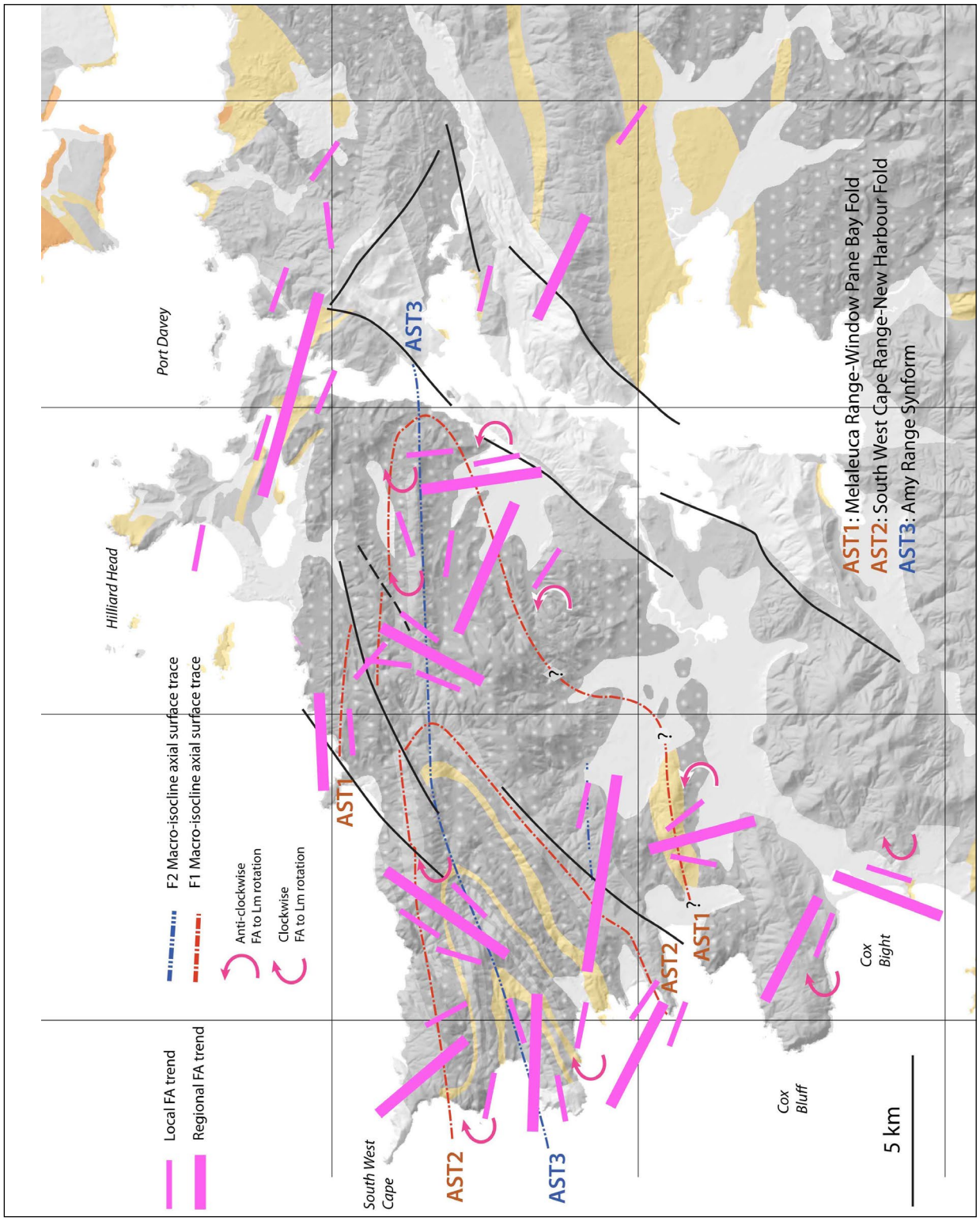

Figure 78. Simplified Fold hingeline (FA) map with axial surface traces for early (F1) macro-isoclines (red dot-dashed lines) and F2 macro-isoclines (blue dot-dashed lines). Mesoscopic fold axis trends are shown by short pink lines. Regional trends are shown by the thick pink lines.

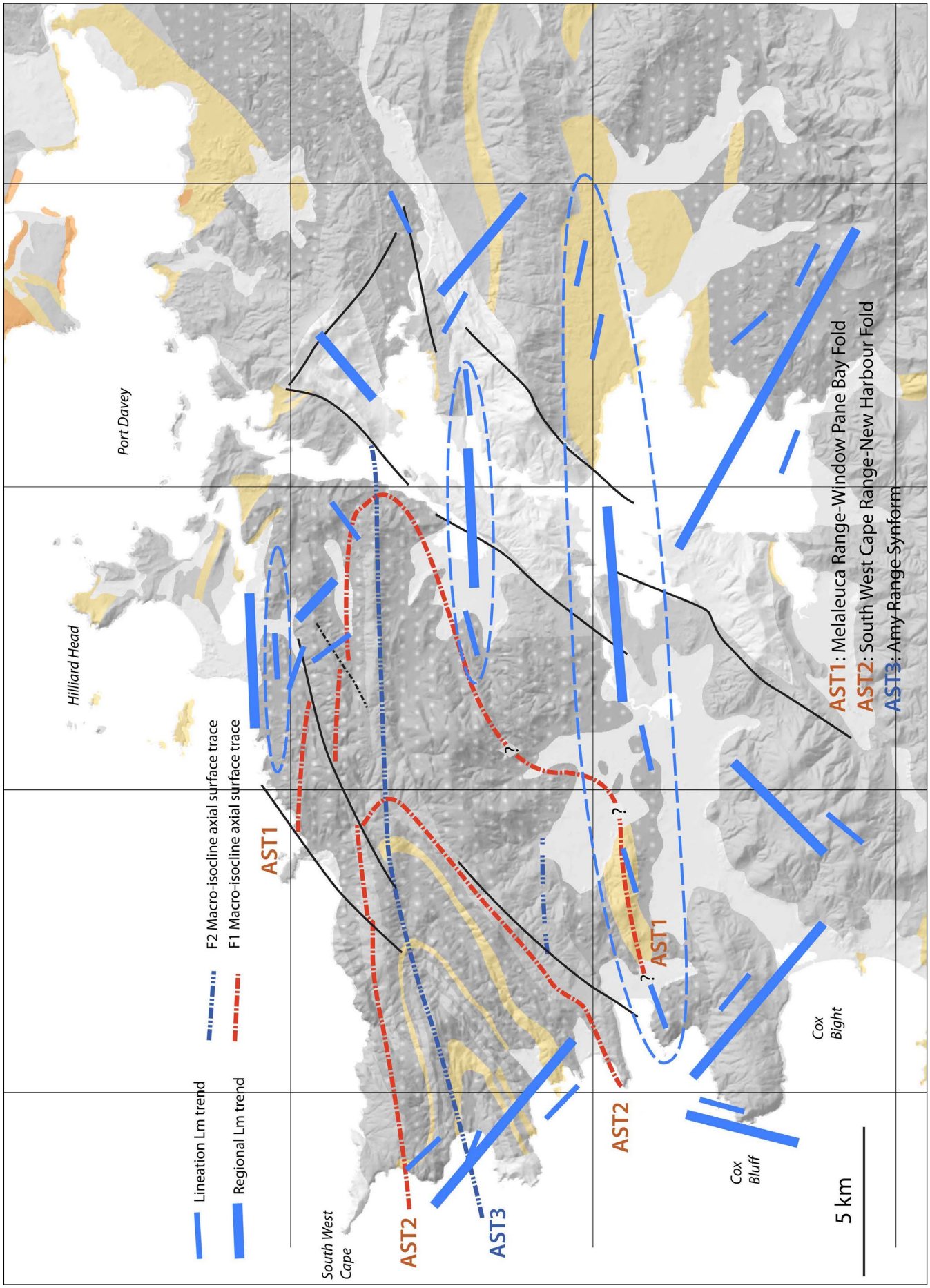

Figure 79. Simplified lineation Lm map with axial surface traces for early (F1) macro-isoclines (red dot-dashed lines) and F2 macro-isoclines (blue dot-dashed lines). Lineation Lm trends are shown by short blue lines. Regional trends are shown by the thick blue lines. The blue dashed lines define envelopes around north-south trending lineations Lm.

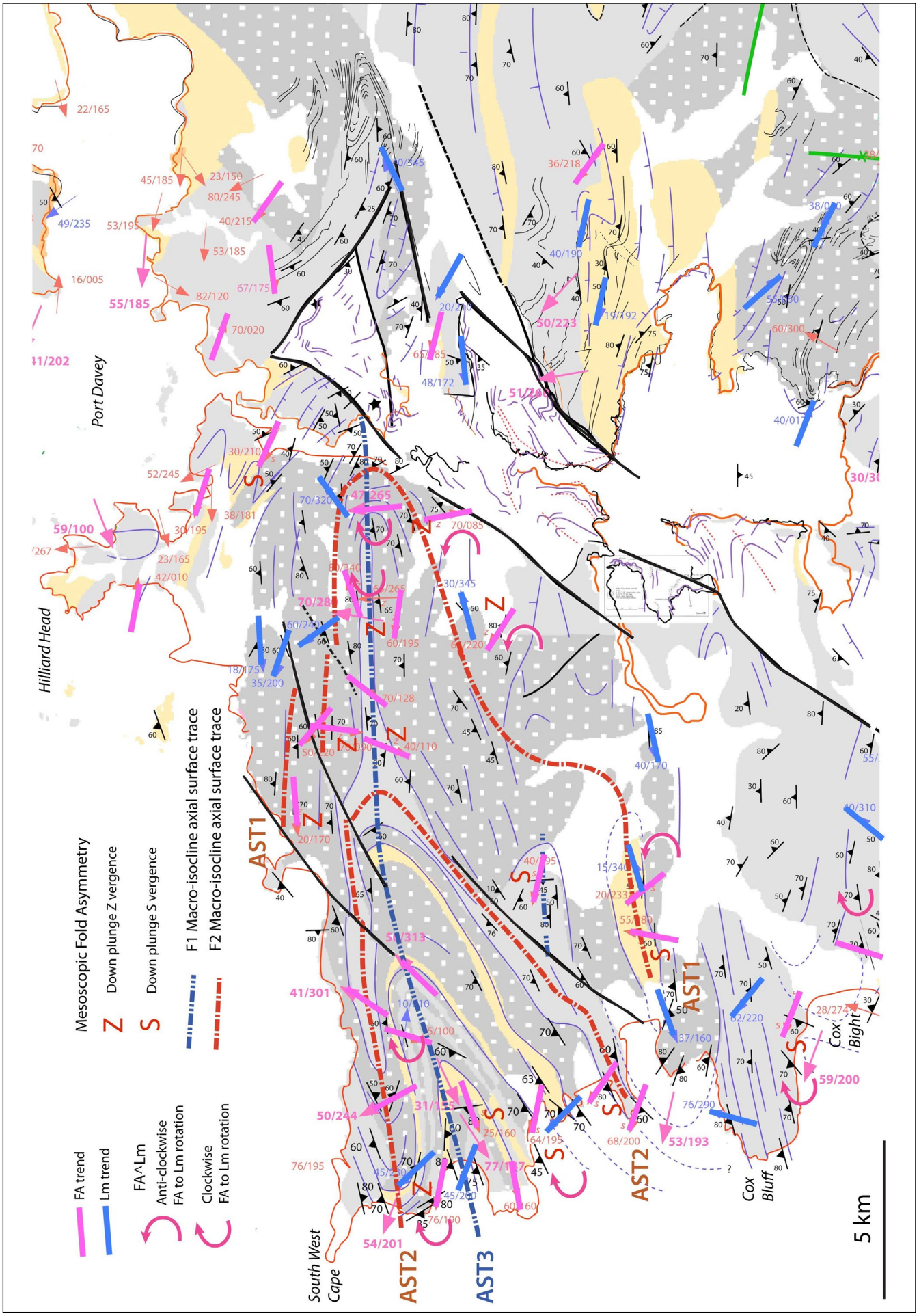

Figure 80. Simplified fold asymmetry and fold-hingeline vergence map with axial surface traces for early (F1) macro-isoclines (red dot-dashed lines) and F2 macro-isoclines (blue dot-dashed lines). Faults are shown by the thick black line traces. Fold axis trends are shown by the short pink lines. Fold asymmetry-vergence is given by the pink S and Z letters with domains highlighted by the pink dashed lines.

The lack of uniformly spread data on fold-hingeline vergence (Figure 80) as well as the fold asymmetry/vergence (Figure 80) makes the interpretation of the South West Cape mega-fold system difficult. The early F1 macro-isoclines are coaxially refolded about west-plunging fold axes (Figure 77). The determined macro-fold axes at different positions around the mega-fold system typically show a west-plunge. These include orange FA plunge arrows for the Melaleuca Range-Window Pane Bay fold, red FA plunge arrows for the South West Cape Range-New Harbour fold and blue arrows for the second generation Amy Range Synformal fold (Figure 77). This relationship suggests either 1) refolding about the 'X' dimension of the original sheath (see Section 5.3.3) or 2) that the second generation isoclinal fold also has sheath-like geometry where associated F2 mesoscopic fold axes have rotated towards the 'X' direction .

5.3.2 Refolding Models

Geometric refolding models (Figures 81, 82 and 83) were constructed to evaluate the geometrical implications for mesoscopic fold axis (FA), mineral lineation (Lm), mesoscopic fold-hingeline vergence and mesoscopic fold asymmetry/vergence relationships in relation to the South West Cape mega-sheath fold system.

Three scenarios include:

1. Refolding of first generation (F1) isoclinal sheath-fold (AST1) by a second generation (F2) isoclinal fold (AST2) about a fold axis parallel to the 'X' direction of the first phase sheath fold, contained within or parallel to the median line ML (Figure 81).

2. Refolding of first generation (F1) isoclinal sheath-fold (AST1) by a second generation (F2) isoclinal fold (AST2) about a fold axis parallel to the 'Y' direction of the first phase sheath fold (Figure 82).

3. Coaxial refolding of an asymmetric fold-pair with first and second generation fold axes at high angles to the shear direction (Figure 83).

In scenario 1 a first phase F1 sheath fold is folded back on itself about the medial line (equivalent to the 'X' dimension of the sheath). The inner part of the second generation F2 fold (AST2) contains Z vergence/symmetry folds with S vergence folds in the outer arc outboard of the first phase axial surface trace (AST1). There is a change in fold hingeline vergence across the second-generation axial surface (AST2).

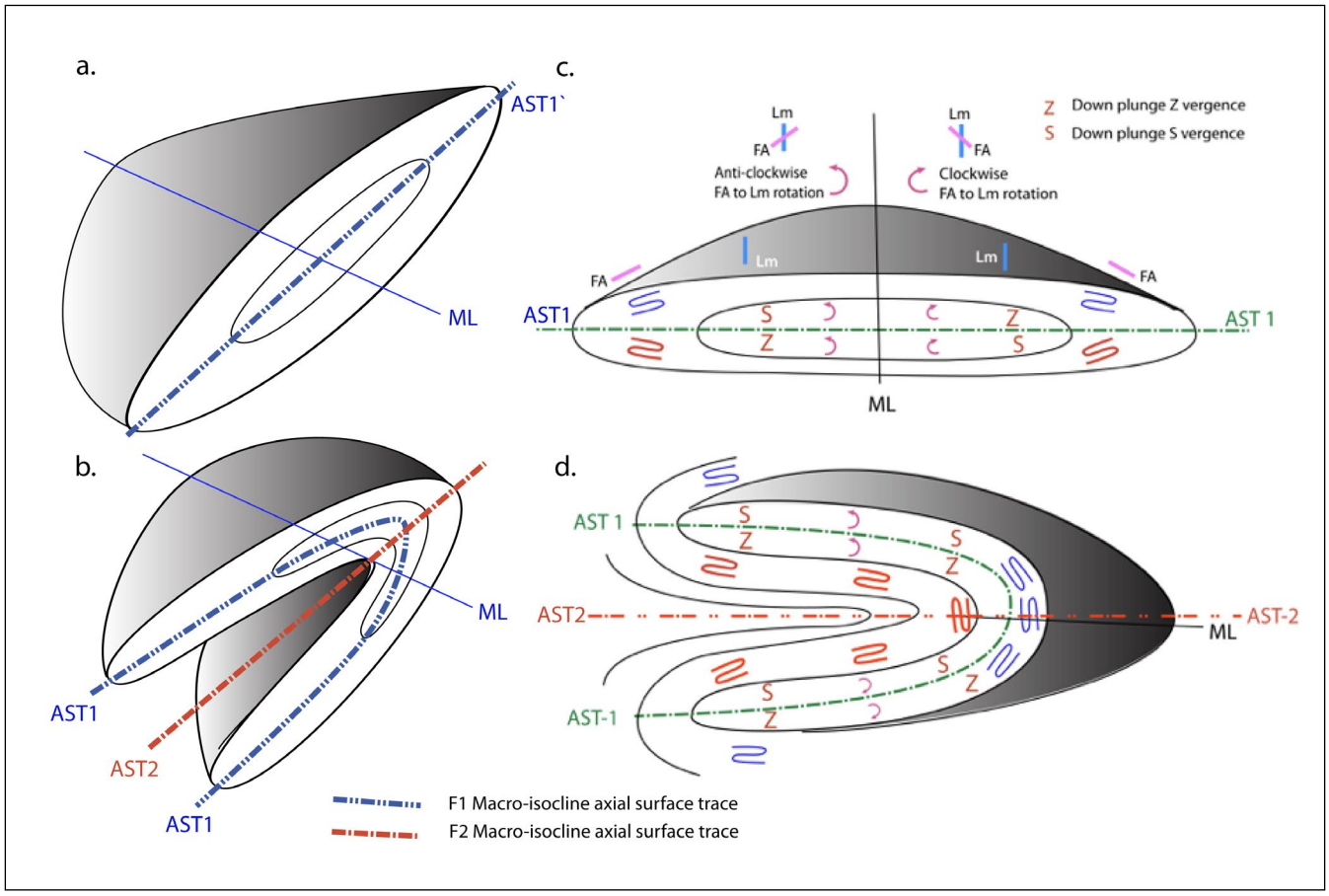

Figure 81. Schematic diagram illustrating refolding about the 'x' direction of a sheath-fold. a) Oblique view of initial sheath fold. b) Refolding by folded back on itself about the medial line (ML) in the 'X" direction of the original ellipse. c) Tilted profile view of the initial sheath form showing the down-plunge fold-vergence patterns and the fold-hingeline vergence (clockwise versus anticlockwise rotation of the FA towards Lm). d) Profile view of refolded geometry shown in (b) showing the expected down-plunge fold-vergence patterns and the fold-hingeline vergence.
ML: Medial line for the initial sheath fold. AST1: axial surface trace of the F1 sheath-fold. AST2: axial surface of the F2 fold.

In scenario 2 the first phase F1 sheath tube (Figure 82a) is folded back on itself about a fold axis F2 (Figure 82b) at high angles to the sheath nose ('X' direction). With ongoing shear strain the second-generation F2 fold develops a curvilinear hinge (Figure 82c). The mesoscopic fold vergence relationships have been projected onto the medial plane that bisects the original sheath-fold in the various evolutionary stages (right side of Figure 82).

In scenario 3 the first phase F1 sheath fold pair (Figure 83a) undergoes two different coaxial deformation sequences. In sequence 1 (Figure 83) the early stage of second phase F2 fold development is an upright open fold with hinge aligned at high angles to the shear direction. With ongoing shear strain the second-generation F2 fold rotates in the direction of shear (to the right) such that the angle between AS2 and the early axial surface AS1 decreases (Figure 83, 1b to 1c) and eventually becomes sub-parallel with a possible a curvilinear F2 hinge (Figure 83, 1c).

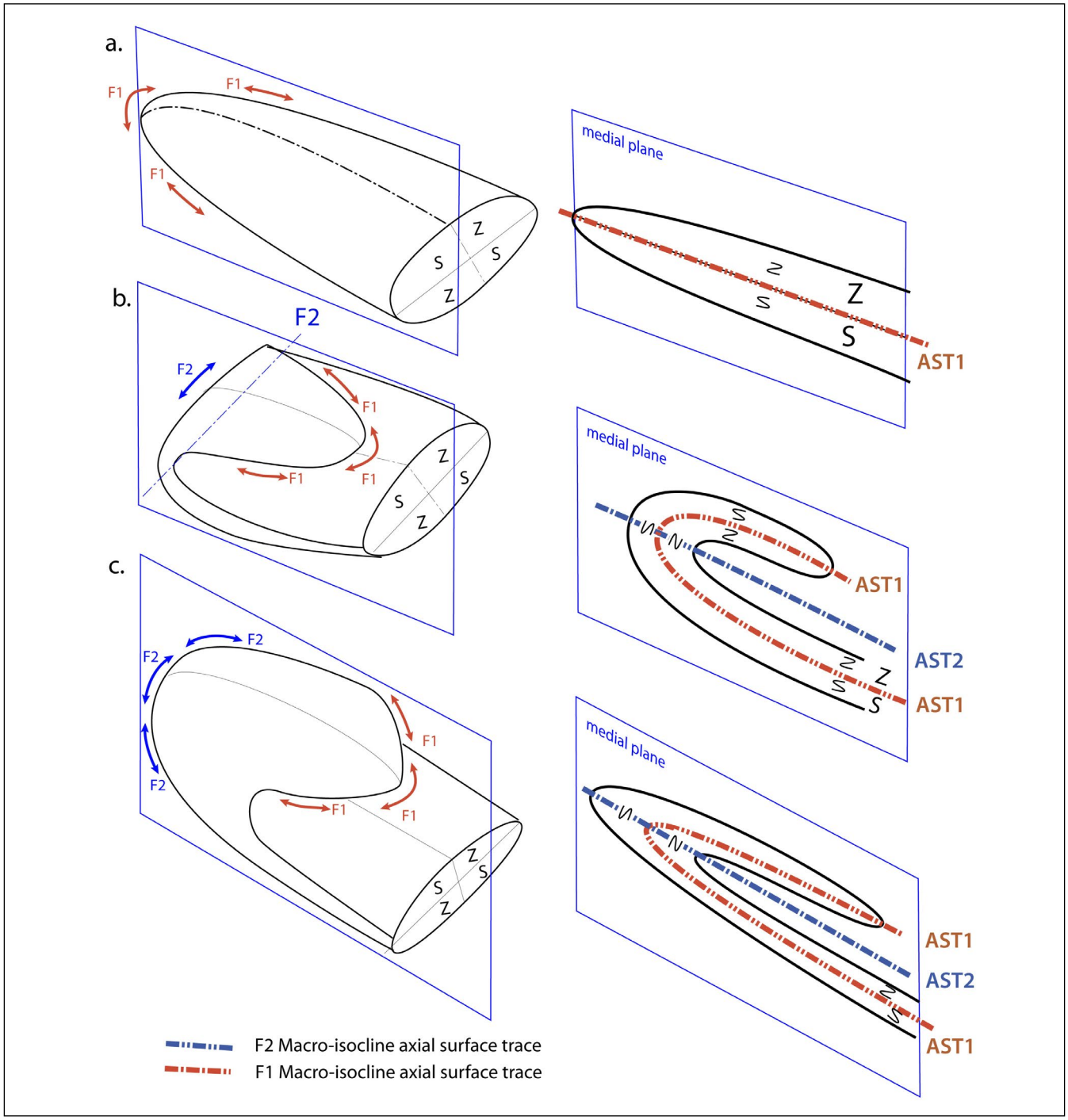

Figure 82. Progressive refolding of F1 sheath fold with sections through the refolding sheath-fold evolution stages (blue dot-dashed line) on the diagram-right. a) Initial sheath fold. b) Refolded sheath tongue about an F2 axis orthogonal to the shear direction (i.e. sheath 'x" direction). c) Elongation of the second-generation (F2) fold into an F2 sheath fold. AST1: axial surface trace of F1 sheath fold. AST2: axial surface trace of F2 fold. The medial plane is the symmetry plane through the sheath-fold that separates fold vergence and fold-hingeline vergence (see Section 2).

Z and S are the mesoscopic fold vergences projected onto the medial plane from the far-side part of the sheath fold. The red and blue arrows show the fold axis trends for F1 and F2 folds respectively.

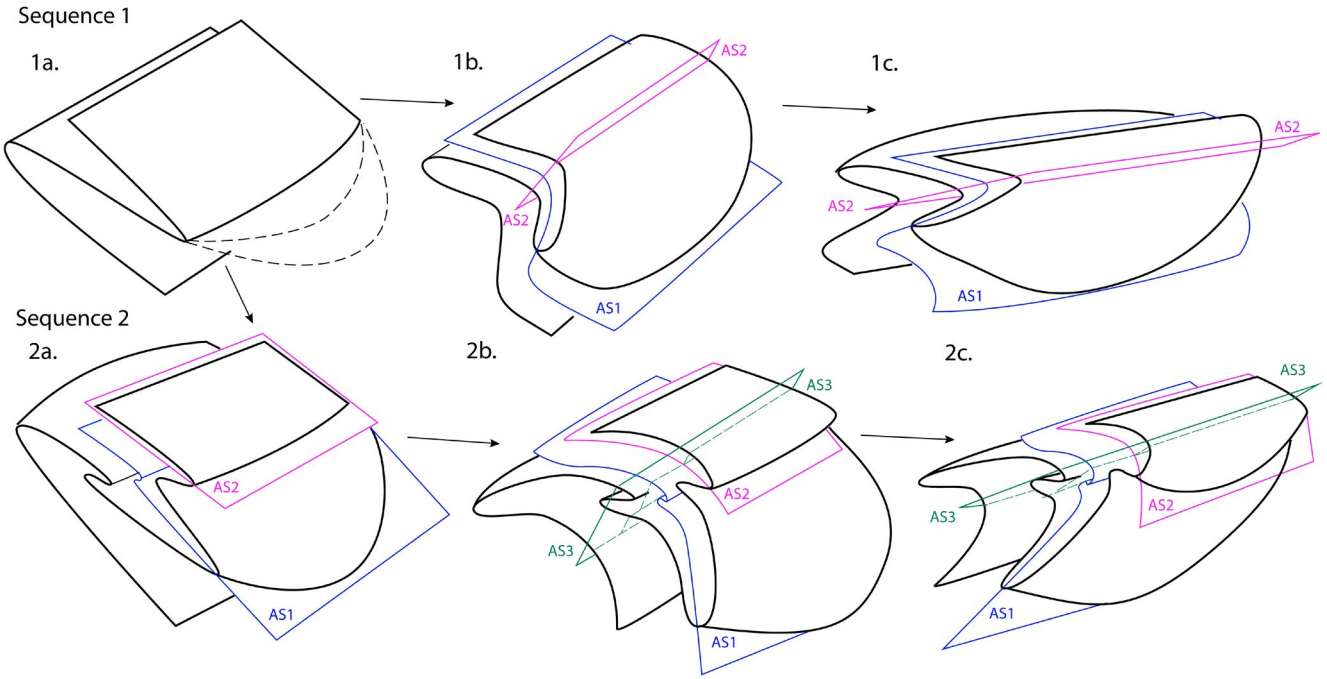

Figure 83. Other examples of refolding relationships in progressive dextral shear (shear to the right of the diagram) for initial F1 sheath folds shown in 1a. Two scenarios are presented. 1a represents the initial First generation F1 Isoclinal macro-fold pair that deforms by coaxial refolding in 1b or into second generation (F2) coaxial asymmetric isoclinal folds along the F1 fold pair limbs. With increased shear strain 1b and 2b show an initial stage of refolding as open upright folds that tighten and progressively change into inclined, tight to isoclinal folds shown by AS2 (pink plane) in 1c and AS3 (green plane) in 2c. Stages 1a to 1c give two sets of refolded isoclinal folds, whereas sequence 2a to 2c give three sets of isoclinal folds.

In Scenario 3 sequence 2 (Figure 83) second-order isoclinal asymmetric folds develop within the F1 macro-fold (Figure 83, 2a). With continued shear strain an upright open fold with hinge aligned at high angles to the shear direction develops (Figure 83, 2b) but is subsequently rotated and tightened (Figure 83, 2c). Such relationships have been seen at the outcrop scale (see Section 6.3).

5.3.3 Refolding- Devonian or Cambrian Refolding

Both the F1 and F2 fold sets that make up the South West Cape mega-sheath fold system (Figures 76 and 77) have tight to isoclinal form with limb dips>60° and mostly 70° to 80°. Most of the Devonian folds have open form and limb dips <45° (see Gray & Vicary, 2022a, Gray et al., 2022). This suggests that all the sets of isoclinal folds (AST1, AST2 and AST3) shown in Figure 77 have been generated during the early Cambrian deformation with subsequent fold-tightening of the second generation synformal fold (AST3) by the younger Devonian co-planar north-south folding.

These relationships and overall fold-nappe geometry are similar to that of folding in the Foxe Fold Belt of the Melville Province of the Canadian Shield where a first generation macro-sheath fold is refolded by a second generation isoclinal, upright synform (Henderson, 1981, Figure 3).

6.0 SIGNIFICANCE AND IMPLICATIONS OF THE MEGA-SHEATH FOLD SYSTEM

6.1 Location and Presence of the Mega-Sheath Fold System

The size and dominance of these mega-sheath folds in the Southern Tyennan are somewhat anomalous compared to the Tyennan nucleus as a whole. This begs the question as to why these structures have developed here.

It has been long established that fold initiation in multilayers requires some perturbation or irregularity within the multilayer (e.g. Ghosh, 1993). Experimental studies on sheath folding have shown that the presence of a discontinuity (slip surface) within the model is necessary to initiate sheath folding and that layer thickness and the layer viscosity contrast will significantly influence the size and shape of the folds (Reber, 2012).

Stratigraphic thickness variations incorporating marked changes in layer thickness have been argued as a locus of mega-sheath fold development in the Tauern window Austrian Alps (Gross et al., 2020). The Southern Tyennan map pattern is suggestive of a greater thickness of quartzite, and therefore quartz sand in the original continental margin setting, where a thicker wedge of sand may have been part of a channelised fan within the fluvial distributary system. In the Alps example a stratigraphic succession within an interpreted rift basin acted as a sedimentary "wedge" within the European continental margin to control the initiation, development and size of Seidwinkl mega-sheath fold (Gross et al., 2020, Figure 11).

6.2 Reversal in Litho-tectonic sequence across the Mega-sheath fold system

Utilising the younger Devonian fold-layering relationships there is an apparent change in the litho-tectonic stacking order above and below the De Witt-Propsting mega-sheath fold. The change occurs below the Nye Bay fold-nappe and above the Mulcahy Bay-Port Davey isoclinal fold stack (Figure 84) across a mylonitic high-strain zone (HSZ) at the Mulcahy River mouth (Figure 47 in Gray et al., 2022).

Unit stacking in the uppermost Nye Bay fold-nappe (Figure 84) is shown within the Mt Eleanor Anticline in the northern part of the Southern Tyennan domain and the coastal exposures from Top Rocks to Mulcahy Bay. The anticline core (lowest unit) is platy or schistose quartzite, structurally overlain by quartzite, followed and intercalated with low-grade pelite (phyllite), with the highest unit the high-grade schists of the Davey Metamorphic Complex in the core of the fold-nappe (Gray et al., 2022).

A reversal in the litho-tectonic "stratigraphy" can be seen within the Davey Creek Syncline where the structurally highest unit is the schistose or platy quartzite, underlain by quartzite with pelite (phyllite) the lowest unit or slice. The high-grade schists are only preserved on the far south coast at Red Point where the inferred Red Point macro-fold shows that they are outboard and therefore below the low-grade pelite in the core of the macro-fold (see Gray & Vicary, 2022b in prep.). The stacking order reversal and the younging changes are shown and encapsulated in Figure 84.

Limitations and Assumptions of the Geometric 2D Model (Figure 84):

1. The model assumes a simple stacking of slabs/sheets that have lateral continuity across the entire Southern Tyennan domain.

2. The model assumes a simple fold train within the "inverted" unit stack with high-grade schist at the base and the platy quartzite unit at the top. The fold train consists of the uppermost Mulcahy-Davey isoclinal fold stack transitional into the underlying De Witt-Propsting mega-sheath fold and the complementary South West Cape mega-sheath fold that is also transitional into the Red Point macro-fold.

3. Younging data are very limited and sparsely-distributed across the Southern Tyennan domain.

4. There are no younging data across the De Witt-Propsting and South West Cape mega-sheath folds to confirm the inferred younging relationships.

5. The structural stacking implied in the model is "underlain" by a structurally lower, asymmetric fold-pair that defines the structure of the entire eastern part of the Southern Tyennan domain from Bathurst Harbour to the Arthur Range.

6. This fold-pair structurally overlies dolomite and dolomitic phyllite in the far eastern part of the domain suggesting that a Central Tyennan-style Scotchfire metamorphic sheet (see Gray and Vicary, 2021) may underlie the Southern Tyennan domain.

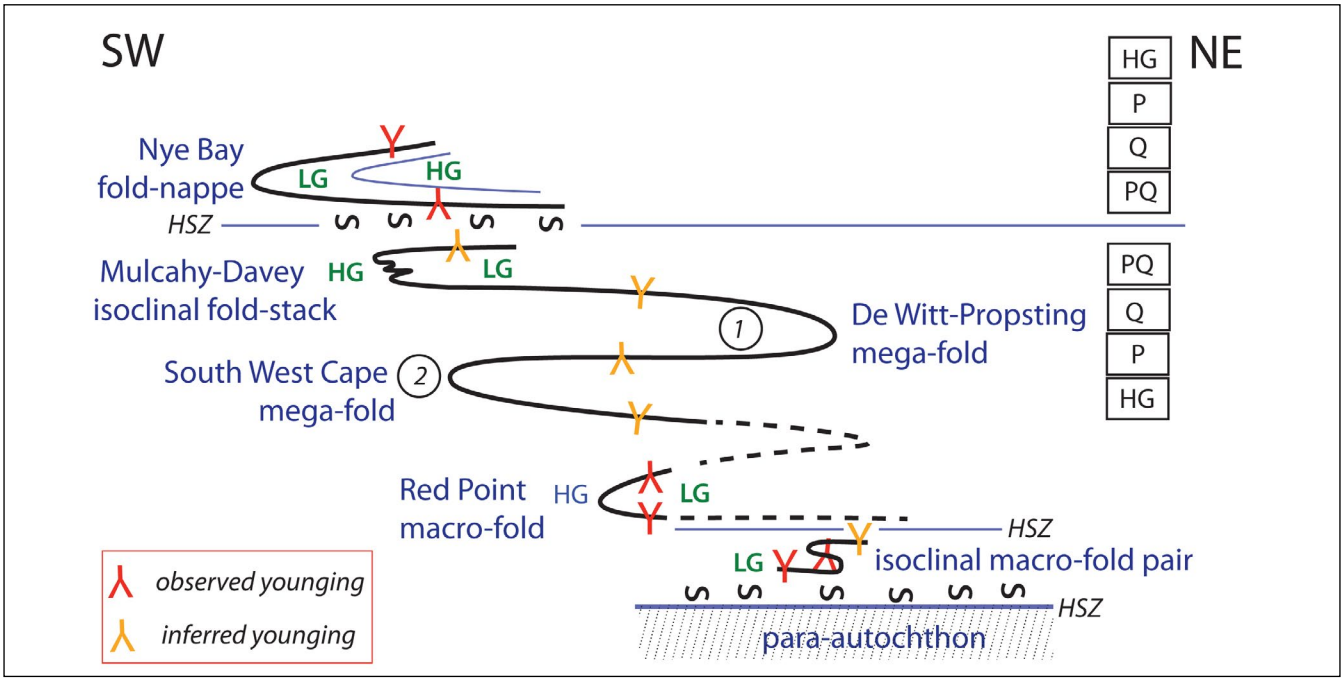

Figure 84. Structural model based on the observed stacking relationships and limited younging observations for the Southern Tyennan domain. The model shows decoupling below the Nye Bay fold-nappe linked with a change in unit stacking from that in the fold-nappe with high-grade schist as the uppermost unit, to a reversed stacking in the underlying fold stack, the underlying mega-sheath folds and the Red Point macro-fold. In these structures the high-grade schist is the structurally lowest unit. Note the De Witt-Propsting (circled 1) and South West Cape (circled 2) mega-sheath folds evolved coevally as a complementary mega-sheath fold pair. HSZ: high strain zone.
The lowest unit (hatched) is the para-autochthonous Scotchfire-equivalent metamorphic sheet.

6.3 Significance of the Inner shell (Sheath fold Core) Structural Complexity

Folding in shear (Figure 83) produces refolded folds and overprinting cleavages (Figure 85). These fold and fabric relationships (Figure 85) are typical of the De Witt-Propsting mega-sheath fold innermost shell or core (Figure 86a) and sheath-fold nose (Figure 86b), and core of the South West Cape mega-sheath fold (Figure 86c). All show early sets of isoclinal macro-folds refolded by north-trending, isoclinal macro-folds (Figure 86).

At the outcrop scale the first isoclinal fold set has a foliation (Sm1) as axial surface foliation (blue lines, Figure 85), whereas the second isoclinal fold set has a crenulation cleavage (Scc2) as axial surface foliation (pink lines, Figure 85). Both are refolded by an axial surface crenulation cleavage (Scc3) (orange lines, Figure 85). In some instances the first isoclinal fold set has an axial surface crenulation cleavage (Scc1).

These relationships show that 1) the De Witt-Propsting mega-sheath core (De Witt-Propsting part)-nose (Davey River part) and 2) the South West Cape mega-sheath fold are second-generation isoclinal fold-nappes that isoclinally refold an earlier set of macro-isoclines (Figures 85 and 86). These are designated F1 and F2 by simple refolding relationships but this is most likely an oversimplification in that the deformation and folding was progressive and part of a shear-related continuum. During the early stages sets of isoclines developed and were refolded by later-formed, and therefore younger, isoclinal fold sets (Figure 83).

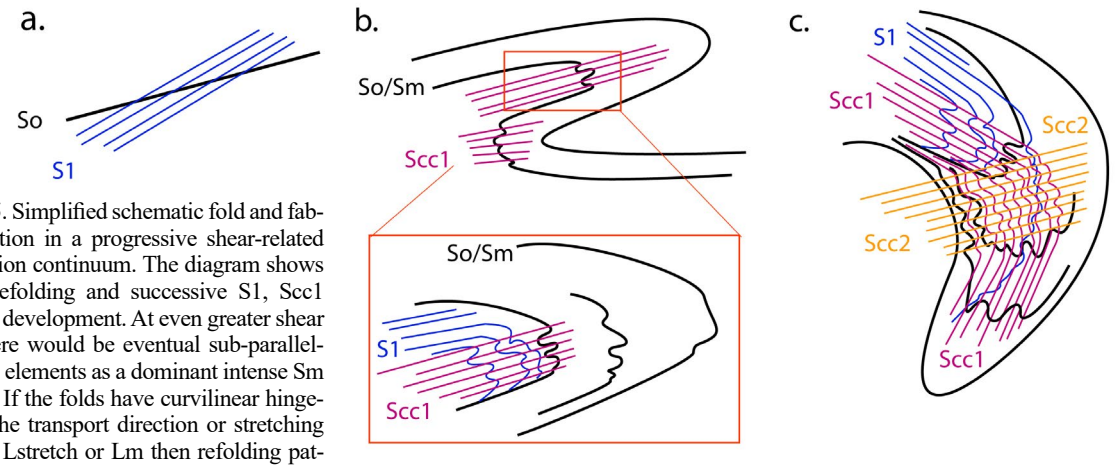

Figure 85. Simplified schematic fold and fabric evolution in a progressive shear-related deformation continuum. The diagram shows coaxial refolding and successive S1, Scc1 and Scc2 development. At even greater shear strain there would be eventual sub-parallelism of all elements as a dominant intense Sm foliation. If the folds have curvilinear hinge-lines in the transport direction or stretching direction Lstretch or Lm then refolding patterns would have banana-shaped form (compare with Figure 86).

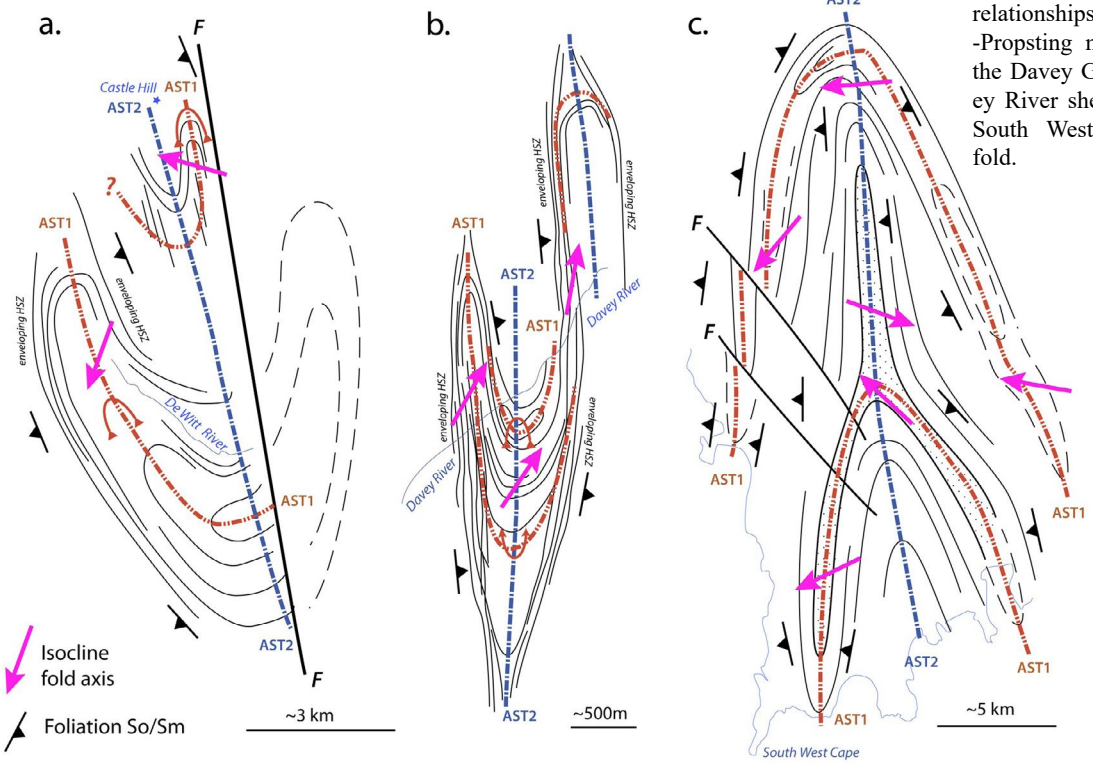

Figure 86. Simplified structural-relationships for a) the De Witt -Propsting mega-sheath core, b) the Davey Gorgepart of the Davey River sheath nose, and c) the South West Cape mega-sheath fold.

6.4 Fabric Evolution and Cannibalisation during Sheath Folding

As discussed in Section 6.3 the core and nose of the De Witt-Propsting mega-sheath fold show complex refolding and fabric evolution unlike most other parts of the Southern Tyennan domain. This complexity we suggest is linked to the inner-shell evolution during elongation of the sheath-fold nose (see Section 6.5).

This ongoing deformation within the shear-related continuum leads to a process of cannibalisation where zones of intense fabric Sm expand laterally in all directions to truncate and segment, and eventually isolate and envelop parts of the evolving structures at all scales (Figure 87). Many of these zones of intense Sm are high-strain zones with platy, schistose quartzite having mylonitic character.

This process appears important in the evolution of the Davey River sheath nose component of the De Witt-Propsting mega-sheath fold.

6.5 Decoupling within the Mega-sheath fold

Juxtaposition of the complex refolded macro-isoclines in the inner core of the De Witt-Propsting mega-sheath fold with the banded, concentric outer shells suggests that the inner part has decoupled and translated relative to the outer or shells during progressive sheath-fold development (cf. Alsop and Holdsworth, 2012).

The decoupled outer shells potentially define the outer layers (limbs) of the early, initial mega-sheath (F1 phase) reflecting the initial stages of sheath fold development. With increased shear strain decoupling of the inner part or core of this fold leads to refolding of the contained early, macro-isoclinal fold by the production of a new, macro-isoclinal hinge (F2 phase). This F2 sheath-fold hinge subsumes the existing outer shells as a nested carapace.

As part of this process the early stretching lineation Lm is also refolded across early and late formed isoclines at all scales (cf. Alsop and Carreras, 2007). Local changes in Lm orientation across the De Witt-Propsting macro-structure (see also MacLean and Bowen, 1971, Figure 4) relate to this folding and refolding process, but overall the Lm trend is at high angles to the sheath long (y) dimension (Figure 3).

This complex structure and refolding pattern is also preserved within the nose or eastern termination of the mega-sheath (see Section 4) and with the form of the sheath suggests eastwards translation of the core.

Figure 87. Axial surface fabric intensification that leads to eventual isolation of thin layers into relict isoclines and fold-pod augen (photo top left). The fold is from station DG19-22 on the ridgeline south of Davey Gorge (Figure 56).

7.0 ACKNOWLEDGMENTS

- Andrew McNeill for providing support through the 2016-2020 Geoscience Initiative, reviewing the document and providing comments.

- Mike Hall, Peter Williams and Paul Lennox for mapping and structural data collection. This compilation would not have been possible without their fieldwork.

- Chris Large for editing and formatting of the final publication.

- Parks and Wildlife Service (PWS) for access into the World Heritage Area and to allow measurement, sampling and photograph collection.

- Jason Bradbury DPIPWE for assistance with WHA and PWS permits for scientific research.

- Rodney Smith from Rotorlift for helicopter transport into the southwest.

- Rick Allmendinger and Nestor Cardozzo for use of OSX Stereonet.

8.0 REFERENCES

Alsop, G., and Carreras, J. 2007. Structural evolution of sheath folds: a case study from Cap de Creus. *Journal of Structural Geology,* 29, 1915-1930.

Alsop, G.I. and Holdsworth, R.E., 1999. Vergence and facing patterns in large scale sheath folds. *Journal of Structural Geology*, 21, 1335-1349.

Alsop, G. and Holdsworth, R.E., 2004. The geometry and topology of natural sheath folds: a new tool for structural analysis. *Journal of Structural Geology,* 26, 1561-1589.

Alsop, G. and Holdsworth, R.E., 2006. Sheath folds as discriminators of bulk strain type. *Journal of Structural Geology*, 28, 1588-1606.

Alsop, G. and Holdsworth, R.E., 2012. The three dimensional shape and localisation of deformation within multilayer sheath folds. *Journal of Structural Geology,* 44, 110-128.

Berry, R.F. 2014. Chapter 4.2 Cambrian Tectonics – The Tyennan Orogeny. In Corbett, K.D., Quilty, P.G & Calver, C.R. editors, Geological Evolution of Tasmania pp 95-110. *Geological Society of Tasmania Special Publication,* 24, Geological Society of Australia (Tasmania Division).

Berry,R.F. and Crawford, A.J. 1988. The tectonic significance of Cambrian allochthonous mafic-ultramafic complexes in Tasmania. *Australian Journal of Earth Sciences*, 35, 523-533.

Cobbold, P.R and Quinquis, H. 1980. Development of sheath folds in shear regimes. *Journal of Structural Geology*, 28, 119-126.

Ghosh, S.K., 1993. *Structural Geology Fundamentals and Modern Developments*. Pergamom Press. New York. 598p.

Goscombe, B.D., 1991. Intense non-coaxial shear and development of mega-scale sheath folds in the Arunta Block, central Australia. *Journal of Structural Geology*, 13, 299-318.

Gray, D.R. and Vicary, M. J., 2021. Structural Geology of the Central Tyennan Region, Tasmania. Mineral Resources Tasmania, *Geological Survey Paper,* 7, 69p.

Gray, D.R. and Vicary, M. J., 2022a. Structural Geology of the Arthur Range, Southern Tyennan Domain, Tasmania, *Geological Survey Paper,* 8, 79p.

Gray, D.R. and Vicary, M. J., 2022b. Structural Geology of the Red Point Metamorphic Complex, Southern Tyennan Domain, Tasmania. Mineral Resources Tasmania, *Geological Survey Paper,* 12, in press.

Gray, D.R., Vicary, M. J. and McNeill, A.W., 2022. Structure of the High-grade Coastal Belt, Southern Tyennan Domain, Tasmania. Mineral Resources Tasmania, *Geological Survey Paper,* 9, 87p.

Gross, P., Handy, M.R., John, T., Pestal, G. and Pleuger, J. 2020. Crustal-scale sheath folding at HP conditions in an exhumed Alpine subduction zone (Tauern Window, Eastern Alps). *Tectonics*, 39, 22p.

Henderson, J.R., 1981. Structural analysis of sheath folds with horizontal X-axes, northeast Canada. *Journal of Structural Geology*, 3, 203-210.

Hall, W.D.M. 1965. Unpublished Progress Report No.1-March-June 1965 for Exploration Licence 13/65 Southwest Tasmania: Geological and geochemical exploration in the area between Bathurst Channel, Cox Bight and South West Cape. Tasmanian Company Report 65_0398. 68p.

MacLean, C.J. and Bowen, E.A., 1971. Structure of the Precambrian rocks of the Port Davey area, south western Tasmania. *Papers and Proceedings of the Royal Society of Tasmania*, 105, 97-0104

Quinquis, H., Audrun, Cl., Brun, J.P. and Cobbold, P.R. 1978. Intense progressive shearin Isle de Groix blueschists and compatribility with subduction or obduction. *Nature*, 273, 43-45.

Ramsay, J.G. 1967. *The Folding and Fracturing of Rocks.* McGraw Hill.

Reber,J.E., Dabrowski, M. and Schmid, D.W., 2012. Sheath fold formation around slip surfaces. *Terra Nova*, 24, 417-421.

Srivastava, D. 2011. Geometrical similarity in successively developed folds and sheath folds in the basement rocks of the northwestern Indian Shield. *Geological Magazine*, 148, 171-182.

Stefanski, M.Z. 1957a. Progress Report on Regional Geological Survey of the Port Davey-Cox Bight Area. *Tasmanian Department of Mines Technical Report,*2, p.87-106.

Stefanski, M.Z. 1957b. Unpublished geological map of the Port Davey-Cox Bight Area. Tasmanian Department of Mines.

Williams, P.R. 1978. Digital Geological Atlas 1:50000 Series. Sheet 8011S. *Davey*. Mineral Resources Tasmania.

Williams, P.R. 1982. Geological Atlas 1:50000 Series. Sheet 91 (8011S) Davey. *Explanatory Report Geological Survey Tasmania.*

APPENDIX 1

STRUCTURAL DATA

File Download

Tasmanian Government

Mineral Resources Tasmania
PO Box 56 Rosny Park
Tasmania Australia 7018
Ph: +61 3 6165 4800

info@mrt.tas.gov.au www.mrt.tas.gov.au